Trapped Atom Collisions and Evaporative Cooling of non-S State Atoms

by

Bonna Kay Newman

Submitted to the Department of Physics
in partial fulfillment of the requirements for the degree of

Doctor of Philosophy

at the

MASSACHUSETTS INSTITUTE OF TECHNOLOGY

September 2008

Author .....
Department of Physics
August 26, 2008

Certified by .....
Thomas J. Greytak
Lester Wolfe Professor of Physics
Thesis Supervisor

Certified by .....
Daniel Kleppner
Lester Wolfe Emeritus Professor of Physics
Thesis Supervisor

Accepted by .....
Thomas J. Greytak
Chairman, Department of Physics Graduate Committee

Trapped Atom Collisions and Evaporative Cooling of non-S State Atoms

by

Bonna Kay Newman

Submitted to the Department of Physics
on August 26, 2008, in partial fulfillment of the
requirements for the degree of
Doctor of Philosophy

Abstract

Large numbers of dysprosium and holmium atoms are trapped using the technique of buffer gas (^{3}He) loading. The two-body loss rate coefficient, g_{2b}, is measured to be $(1.8 \pm 0.2) \times 10^{-12}$ cm^3 s^{-1} at 506 mK for dysprosium and $(7.2 \pm 1.5) \times 10^{-13}$ cm^3 s^{-1} at 360 mK for holmium. These are consistent with scaling of dipole relaxation rates of hydrogen and other alkalis. They are also favorable for evaporative cooling if the elastic cross section is large.

A theoretical model is developed which incorporates the effects of finite background gas densities during an evaporative cooling process. The details of the collisions with the background gas are studied as a function of trap depth and atom temperature. The large vapor pressure of ^{3}He at cryogenic temperatures (compared to that of ^{4}He) makes it more difficult to attain the background gas densities necessary for thermal isolation.

Despite this, 2×10^{11} dysprosium atoms are evaporatively cooled from 300 mK to 50 mK. The analytical model is used to estimate the background gas density and the atom-atom elastic collision cross section. The ratio of elastic to inelastic collision rates for Dy-Dy collisions is estimated to be about 50. This value may be large enough to achieve effective evaporative cooling. Plans are outlined to attempt further cooling of dysprosium atoms as well as other atomic species.

Thesis Supervisor: Thomas J. Greytak
Title: Lester Wolfe Professor of Physics

Thesis Supervisor: Daniel Kleppner
Title: Lester Wolfe Emeritus Professor of Physics

Acknowledgments

One of the great attractions of experimental atomic physics is the small team nature of the experiments. I have been fortunate to have had an excellent team of very talented physicists to work with over the last six years. My advisors, Tom Greytak and Dan Kleppner, welcomed me into a dynamic and engaging lab. The have taught me to demand a high level of experimental work and are role models for my future career. Tom has been supportive of my career both in and out of the lab; and readily available to provide advice on physics laboratory questions, as well as continuously alerting me for opportunities for development in the general physics community. Dan Kleppner is always available to help me work through difficult physical concepts and ideas. I greatly appreciate his "outside the box" suggestions when we are trying to solve difficult problems in the lab. I have learned much from engaging in scientific conversations with him and trying to mimic his approach to solving problems. I have also had the pleasure of collaborating with Prof. John Doyle at Harvard. He inspires new directions of research with excitement and his engagement in the lab and his students lives is truly unique.

I have spent most of the last six years in the company of two fantastic labmates, Nathan Brahms and Cort Johnson. This thesis has been a truly collaborative effort and I could not have finished this work without their assistance. I learned most of the atomic physics I know through the animated and engaging group discussions in front of the whiteboard. After many long days in the lab, we became close friends as well. Nathan's passion and knowledge in the world of physics are difficult to match. I have been lucky to have had him to discuss the subtle details of physical systems. I have always left these conversations with new perspective and insight. Cort Johnson, in addition to being an excellent physicist, is also an excellent father, husband, and friend. His dedication to his family and his community are truly a source of inspiration.

My research has also brought me into contact with a number of other great post docs and grad students. Both Rob deCarvalho and Chih-Hao Li were instrumental in

organizing and teaching Nathan, Cort, and I how to run a lab and get an experiment done while still having fun. Kendra Vant, Lia Matos, and Julia Steinberger welcomed me into the research group and are excellent role models as female scientists. The births of both Tycho and Clara were exciting times in the lab and great examples of female scientists getting to "do it all". Julia is a dear friend and a gifted scientist. I have also had the pleasure of working with the Doyle group at Harvard. They have been an excellent resource for lab supplies and materials, ideas, and Friday afternoon beers. Specifically, working with Yat Au Shan over the last few months was a great opportunity to get to know him and help him develop into a productive researcher.

The MIT support staff have been integral in making it possible for me to finish my PhD. I have made friends with many of the people from facilities who are always ready with a hello and a smile. Cryolabs has helped me out of a number of tight spots by going out of their way to ensure that we had enough cryogenic liquids to keep the experiment cold. The MIT physics departmental staff has also been key in getting many of my departmental projects off the ground.

I would like to thank the MIT Women in Physics group. Without this group of women, I don't know that I would have made it through the first few years of graduate school. Our benefactress, Dr. Margaret Wong has been a great supporter who has enabled us to make many MIT a better place for all women. In addition, Dave Guerrara has proved to be a surprising ally in initiating creative ways of encouraging women in the field.

When I moved to Boston six years ago, I felt that I had moved to a strange and dark land (no more 300 days of sunlight per year). I would like to thank all of my teammates on my two soccer teams Monster Balls FCU and Shockers United. You have provided me with a great deal of sports, entertainment, and excitement over the years. I'd also like to recognize Rachel, Katie, Shaina, and Devon for being my girlfriends in spite of my interest in "lasers". Thank you Wally for putting up with the long hours that this thesis required.

Being so far away from my family, the Keohanes have supported me like a surrogate child and offered me a home on the east coast. I would also like to thank the

Bijur/Montgomery family for including me so completely into their lives.

In addition I have a number of friends who have let me live vicariously through them as I was in grad school. Mary, Paul, and Tom have always been ready for an adventure when the lab became too mundane. My infrequent but greatly rewarding adventures reminded me that there are plenty of stories left to be experienced.

Nicole Head has been there for me at every turbulent turn. She is a great inspiration in her dedication to education and those less fortunate. Thank you Nicole for being such a wonderful friend.

My friend Sean Hansen is a source of strength and perseverance. In addition to being an amazing friend who has always been willing to drop anything to listen to me, Sean also dedicated seven years of his life to defend our country serving two tours in Iraq. Thank you for always being there to right my world when it was turned upside down.

Mauro Brigante has been one of my dearest friends since the first day of grad school when we met after a grueling Part I exam. We have shared many personal successes and developed together as professional physicists. I can always count on Mauro for a good laugh and an understanding ear over a pint of beer. He also introduced me to a great group of other MIT students Joe, Alejandro, Fred, and Eric. I had an awesome time exploring my inner nerd with all of you.

Finally, I would like to thank my family. Education has always been a number one priority for my family. My paternal grandmother established the precedent that has led to three generations of Dr. Newmans. My sisters have always been there as a source of loving competition. My parents always prioritized our educations in making decisions about where to move. Thank you for the work ethic, the values, and the love. I could not have done this without you. And finally to my niece, Rel, thank you for giving us all hope when it seemed lost.

For my family

Contents

List of Figures

List of Tables

Chapter 1

Introduction

In the 23 years since the first neutral atoms were confined in a magnetic trap [1], cold atomic physics experiments have made number of significant scientific advances. Among these advances are the realization of quantum degeneracy [2–6], superfluidity in dilute gases [7–9], and quantum gas insulators [10, 11]. Cold trapped atoms allow for precise control of external and internal degrees of freedom. These systems provide a platform for better precision measurements of fundamental constants [12] and atomic clocks [13].

In spite of all of these advances, the number of different systems which can be studied is limited to a small fraction of magnetic atoms. The majority of experiments use laser cooling to load magnetic traps. Laser cooling is highly dependent on the electronic configuration and level structure of the atoms. This limits many experiments to the small set of mostly alkali atoms with S ground states. Molecules and more complex atoms, with many vibrational levels or complex electronic structures, can not be trapped. Developing new methods which can expand cold temperature regime research to other systems could yield new experimental discoveries.

Buffer gas cooling and loading of magnetic traps is one alternative method that has been proposed to expand the list of species that can be trapped [14–16]. Buffer gas cooling has proven to be very good for loading magnetic traps with various species of atoms and molecules [17–25]. Specifically, it is one of the few techniques that allows trapping atoms with non-zero orbital angular momentum in their ground state

[17]. In addition buffer gas loading experiments have demonstrated further cooling if thermal isolation from the buffer gas can be achieved [20–23]

This thesis reports on experiments in which highly magnetic non-S state rare earth atoms have been trapped and loaded using buffer gas cooling techniques. We have measured the rates of spin relaxation due to atom-atom collisions in both holmium and dysprosium after the buffer gas has been mostly removed. These measurements contribute to theoretical studies of dilute dipolar gases [26–28]. The rates are also shown to be favorable for efficient evaporative cooling. Initial attempts at enhancing evaporation rates demonstrate cooling of large numbers of dysprosium atoms to 50 mK.

In addition, a model is developed of trap dynamics in the presence of finite background gas densities. This model fills a gap in buffer gas trapping theory by incorporating exothermal collisions with background gas atoms into the evolution of temperature and number of magnetically trapped atoms. We find that for cooling with a ^{3}He buffer gas, these effects are important because of the high vapor pressure of ^{3}He below 1 K.

1.1 Magnetic Trapping

An atom (or molecule) with a magnetic dipole moment, μ, in a magnetic field $\vec{B}$ experiences a potential

$$U = -\vec{\mu} \cdot \vec{B}. \tag{1.1}$$

The weak field seeking ground hyperfine states of a neutral atom can be magnetically trapped in a magnetic minimum. However, magnetic traps are relatively shallow with the deepest magnetic traps of a few Kelvin [29]. Trapping is possible only when the thermal energy $k_B T$ is smaller than the depth of the trap. To put this more concretely, I introduce a parameter η as the ratio of the trap depth to the atom temperature.

$$\eta \equiv \frac{U_{trap}}{k_B T} \tag{1.2}$$

For successful trapping in our apparatus, η must be greater than ten [25]. This requires cooling most atoms to temperatures less than one Kelvin.

1.2 Methods of Atom Cooling

The most common method for cooling atoms is laser cooling. In one dimension, laser cooling can be understood with a simple model. A laser is red de-tuned from an atomic transition such that it is resonant with atoms moving towards the beam at a specific velocity. Photons are absorbed from the beam, promoting atoms to an excited state. These atoms are slowed due to photon recoil during the absorption. When the excited state decays, the photons are radiated with equal probability in any direction (not just into the mode of the laser), with an average energy equal to the a photon absorbed by an atom at rest. The emitted photons on average have more energy then the absorbed photons resulting in cooling of the atoms [30].

There are two main limitations to laser cooling. The first is that it requires a "closed" transition; where the excited state only couples to the original ground state. If the atom decays into a different state, another laser must be used to "repump" the atom back into the cooling state. Laser cooling has been proven to work well for the alkali atoms but for only a limited number of other atoms. This technique can quickly become impractical for atoms with more complex electronic structure or for molecules with their many closely spaced vibrational and rotational levels.

The second limitation is that each photon scattering event carries away only a small amount of energy. An atom traversing the laser beam can undergo thousands of scattering events each resulting in a small amount of cooling. However, unless the atoms are pre-cooled, only a small fraction of the atoms are cooled to low enough temperatures for trapping. While the alkali metals have provided an excellent platform for atomic physics experiments, there is desire to develop techniques that expand the species that can be cooled and trapped to include more complex atoms and molecules.

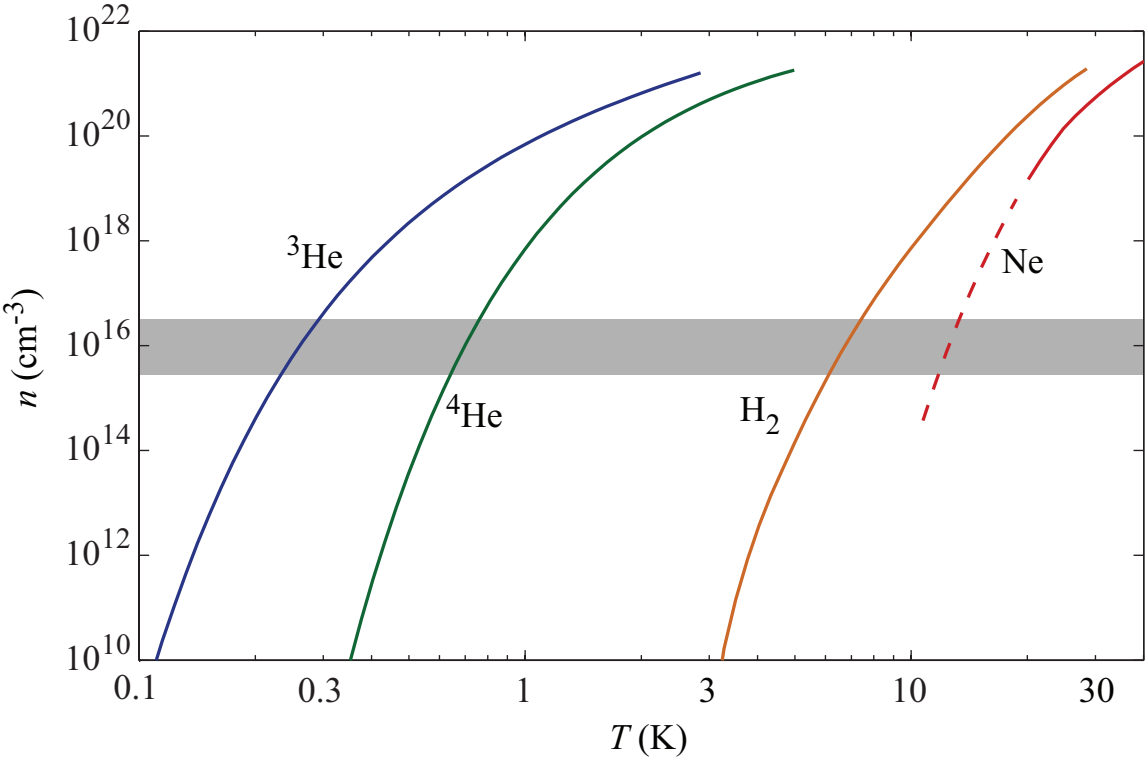

Figure 1-1: Vapor densities of various cryogenic gases [32, 33]. The shaded region indicates the typical densities necessary for buffer gas loading. The H_2 curve is approximate and the dashed line is an extrapolation. The isotopes of He are best suited for buffer gas loading into shallow magnetic traps.

Buffer gas loading is an alternative method for cooling various species without regard of their spectral properties. Magnetic atoms are introduced into a magnetic potential in the presence of a cold non-magnetic background gas or "buffer gas". The un-trapped buffer gas is kept in thermal equilibrium with a thermal reservoir (such as the mixing chamber of a dilution refrigerator). Elastic collisions with the buffer gas remove energy from the atoms, cooling them to temperatures low enough for trapping. To date, 17 atoms and 4 molecules have been successfully trapped from various families of the periodic table [17–25, 31].

For successful buffer gas loading, each atom must undergo ∼100 collisions with the buffer gas atoms before it leaves the trapping region [14]. If we assume an elastic collision cross section of 1×10^{-14} cm^2 and a 10 cm long cell, the buffer gas density needs to be 1×10^{15} to 10^{16} cm^{-3}. This requires that the buffer gas have an adequate

vapor pressure at low temperatures. Figure 1-1 shows the vapor densities of various cryogenic gases. Only ^{3}He and ^{4}He have vapor pressures sufficient for buffer gas loading below 3 K. In addition helium, as a noble gas, has no valence electrons. As we will see in the next section helium's closed shell structure is ideal for minimizing inelastic collision rates.

All of the experiments in this thesis use a ^{3}He buffer gas. This facilitates loading at the lowest temperature for a given buffer gas density; corresponding to the largest possible value of η for a given trap depth.

Removing the Buffer Gas

At the temperatures where the trap is loaded, typically 200 to 500 mK, cold collision studies of atoms with the helium gas have yielded insight into the physical mechanisms at work in the collision and into some aspects of atomic structure [17, 24]. However, to reach the ultracold temperature regime where the deBroglie wavelength is on the same order as the atom separation, the atoms need to be cooled further.

The presence of the buffer gas in the trapping region continues to connect the temperature of the atoms to the cell walls. For further cooling, thermal isolation of the atoms must be achieved through removal of the buffer gas atoms. This can be achieved in one of two ways. In the first method, the bulk of the buffer gas is physically removed from the trapping region into another chamber. The second method is to cool the whole system to a temperature where the helium vapor density is very small. In the experiments discussed in this thesis, both techniques are used in combination. We physically remove the buffer gas by opening a valve in the trapping chamber connecting it to another chamber maintained at high vacuum. At the same time, we cool the cell, decreasing the equilibrium background gas densities.

Once the buffer gas has been removed we are left with a magnetically confined sample of atoms. This sample is suitable for studying atom-atom collisions. Furthermore, thermal isolation of the atoms opens the way for attempting further cooling of the sample.

1.3 Atom-Atom Collisions

Atom-atom collision studies in the cold temperature regime have so far been mostly limited to atoms with no orbital angular momentum in the ground state. This is due to the difficulty of achieving long lived cold samples. In this thesis, I will present measurements of atom-atom collisions between two lanthanide atoms. The lanthanide series is composed of the atoms in the periodic table with atomic numbers from 57 to 71. These atoms are also called rare earth atoms. In addition to certain transition metal atoms [18], rare earth atoms offer an interesting atomic system for study because of the complex electronic structures. The lanthanides have unfilled d- and f- valence shells (see Table 1.1). Outside of these highly anisotropic valence shells, there are filled s-shells which have larger average radii than the unfilled valence shells. The filled symmetric s-shell has been found to suppress anisotropy in the interatomic potentials and as a result the inelastic collision rates with helium atoms are much smaller than naively expected [17, 34]. Our apparatus is ideally suited to extend the study of shielding and anisotropy of collisions involving rare earth atoms.

1.4 Evaporative Cooling

Evaporative cooling has proven to be the key to reaching temperatures and phase space densities necessary for quantum degeneracy of magnetically trapped samples. The cooling mechanism at the atomic level is the same process that is familiar from everyday experience; more energetic particles are lost to the environment resulting in a lower equilibrium temperature for the remaining system. In atomic physics, this process is enhanced by manipulating trap geometries and collision processes [12, 35].

Evaporative cooling of a non-S state atom to quantum degeneracy would expand the study of ultracold phenomena to new atomic and molecular systems. In addition to the possibility of exploring a new regime of physics with ultracold samples of non-S-state atoms, a trapped sample of highly magnetic rare earth atoms has been proposed as a platform for quantum computing [36]. It has also been predicted that

the relativistic corrections to the transition frequencies for atoms with large open shells such as dysprosium and holmium could reveal variations in the fine structure constant [37–40]. Cold, long lived atom samples could increase the precision of these measurements.

After a hot atom "evaporates" from the trap, collisions rethermalize the remaining atoms to a new equilibrium temperature. The time that this takes depends on the rate for the atoms to undergo these collisions, the elastic collision rate. At the same time, inelastic collisions and trap losses are decreasing the atom population and in some cases increasing the equilibrium temperature of the sample. Successful evaporative cooling requires that the rate of "good" elastic collisions be much greater than the rate of "bad" inelastic collisions.

S-state atoms have spherically symmetric electron density distributions. The electronic interaction of two colliding S-state atoms does not effectively drive spin relaxation from the weak field seeking Zeeman levels. The inelastic (Zeeman state changing) collision cross section of S-state atoms with other S-state atoms is usually small while the elastic cross section is high. The ratio of good to bad collisions is favorable for evaporation. For non S-state atoms, the electronic interaction of two colliding atoms is strong due to the interaction of the magnetic dipole moments during the collision. The electronic angular momentum can be strongly coupled to the rotational angular momentum of the collision. The resulting interaction is anisotropic [28] and is very effective at spin relaxing the trapped Zeeman levels making evaporation in these systems more difficult [36, 41–43].

Four atomic species have been evaporatively cooled from a buffer gas loaded magnetic trap – chromium, europium, molybdenum, and meta-stable helium [20, 22, 23, 44]. All of these atoms have magnetic dipole moments greater than 3 μ_B and have were loaded using ^{4}He. Our system uses ^{3}He as the buffer gas. This is done because of a parallel experimental goal of expanding buffer gas cooling and loading to weakly trapped 1 μ_B species. As mentioned earlier, ^{3}He permits loading at colder temperatures and larger η. However, the larger vapor density of ^{3}He at cryogenic temperatures also makes it more difficult to remove the buffer gas to levels accept-

Atom	$\mu(\mu_B)$	M_{at}(amu)	Ground State	Isotopes
Dy	9.94	162.5	4f10.6s2	5 (160,161*,162,163*,164)
Ho	8.97	164.9	4f11.6s2	1 (165)

Table 1.1: Basic atomic properties of species studied in this thesis. *Designates isotopes with non-zero nuclear angular momentum. All data is from the NIST Atomic Spectrum Database [45].

able for evaporative cooling. Removing enough ^{3}He can not be done by lowering the cell temperature alone, as it is done in a ^{4}He experiment. Bulk removal of the gas is needed.

1.5 Thesis Overview

This thesis presents the results of experiments with two highly magnetic rare earth atoms, holmium and (multiple isotopes of) dysprosium. The basic atomic properties of these atoms can be found in Table 1.1.

Much of the most of the effort in the research described here was in building a robust and versatile buffer gas loading apparatus that provides the flexibility required to magnetically trap a variety of species with different electronic structures and atomic properties. Chapter 2, provides an overview of the experimental apparatus and I describe the general methods and procedures used to create and study the atomic ensembles. In addition, this chapter outlines the various parameters we can tune and adjust in our system for different types of experiments.

Chapter 3 presents measurements of atom-atom collisions in dilute gases of holmium and dysprosium. We find that the rate of inelastic collisions suggest that further evaporative cooling may be possible for these non-S state atoms.

Chapter 4, describes a theoretical model I developed to assist our pursuit of evaporative cooling. Many evaporation models have been developed in other work [46, 47], but our model is different because it includes effects of small densities of background gas. The model shows us that to fully isolate the atoms, the background gas densities must be decreased to lower levels than previously believed.

Chapter 5 will present data which demonstrate cooling of dysprosium atoms from 200 mK to less than 50 mK. I will use the model developed in Chapter 4 to understand the mechanisms of cooling. In addition, I will outline experimental improvements which are currently underway to attempt further cooling of dysprosium.

Finally, Chapter 6, discusses other possible future evaporation experiments that might be pursued in our experimental apparatus.

Chapter 2

Apparatus and Methods

This thesis describes experiments involving several atomic species and addresses a variety of experimental goals. All experiments were performed in the same buffer gas cooling apparatus and employed a common experimental procedure. The apparatus has an adaptable setup that can be modified for different experiments. In this Chapter, I will describe the procedures to produce, cool, and load a generic dilute atomic gas into a magnetic trap. It is a general procedure that applies to a variety of different atomic species. The specifics of times, temperatures and atom numbers will vary from species to species. The procedures outlined here are intended to be used as a reference for future experiments. More detailed information about the apparatus can be found in the theses of Brahms [25] and Johnson [48]. Modifications made for a specific experiment will be detailed wherever they are appropriate.

2.1 Overview of the Apparatus

A diagram of the apparatus is shown in Figure 2-1. The atoms are buffer gas loaded and studied in the "collision chamber" that is attached to the mixing chamber of an Oxford Kelvinox 400 dilution refrigerator [49]. The refrigerator cooling power has been measured as 31 mW/K^2 and reaches a base temperature of 16 mK when no external heat loads are attached. The refrigerator and experiment are contained within a triple walled cryostat. We extended the internal vacuum chamber around the

refrigerator to contain an experimental cell (described below). The vacuum chamber extension is inserted in the bore of the magnet.

Optical access is through the bottom of the apparatus. Light is passed through a series of three BK-7 windows that are located at each shield of the cryostat and maintained at progressively lower temperatures. The window on the 77 K shield is sealed to a steel welded bellows attaching the bottom of the inner vacuum chamber to the cryostat base. This seal maintains separation between the outer cryostat vacuum and the inner vacuum chamber around the refrigerator and cell.

Magnet

The magnet is made by American Magnetics Inc. [50] according to the designs of the "Mark V" magnet described in [29]. It consists of two coils aligned along a vertical axis. Each coil can be controlled independently. In the Helmholtz configuration – both currents in the same direction – the field is roughly uniform across the cell. In the anti-Helmholtz configuration – currents in opposite directions – there is a point of zero field near the center of the cell. For all of the experiments in this thesis the magnet is run in the anti-Helmholtz configuration that produces a ellipsoidal quadrupole magnetic trap.

The super-conducting magnet is located in the ^{4}He bath space of the cryostat. Vapor cooled leads with copper/superconductor bus bars deliver current from room temperature. A maximum current of 101 A in the anti-Helmholtz configuration creates a field at the cell walls of 4.0 T. For safety, the magnitude of the currents in each coil should not differ by more than 80 A.

A bucking coil is secured to the top of the magnet cask and is wired in series with the top coil but configured such that the current runs in the opposite direction. The bucking coil was designed to cancel the magnetic field at the mixing chamber and cell top, minimizing eddy current heating when the magnetic field is changed quickly. The specifics of this design are described in Appendix B.

A diagram of the alignment of the magnet and cell is shown in Figure 2-2 along with contour plot of the magnet potential inside the cell dimensions. The magnetic

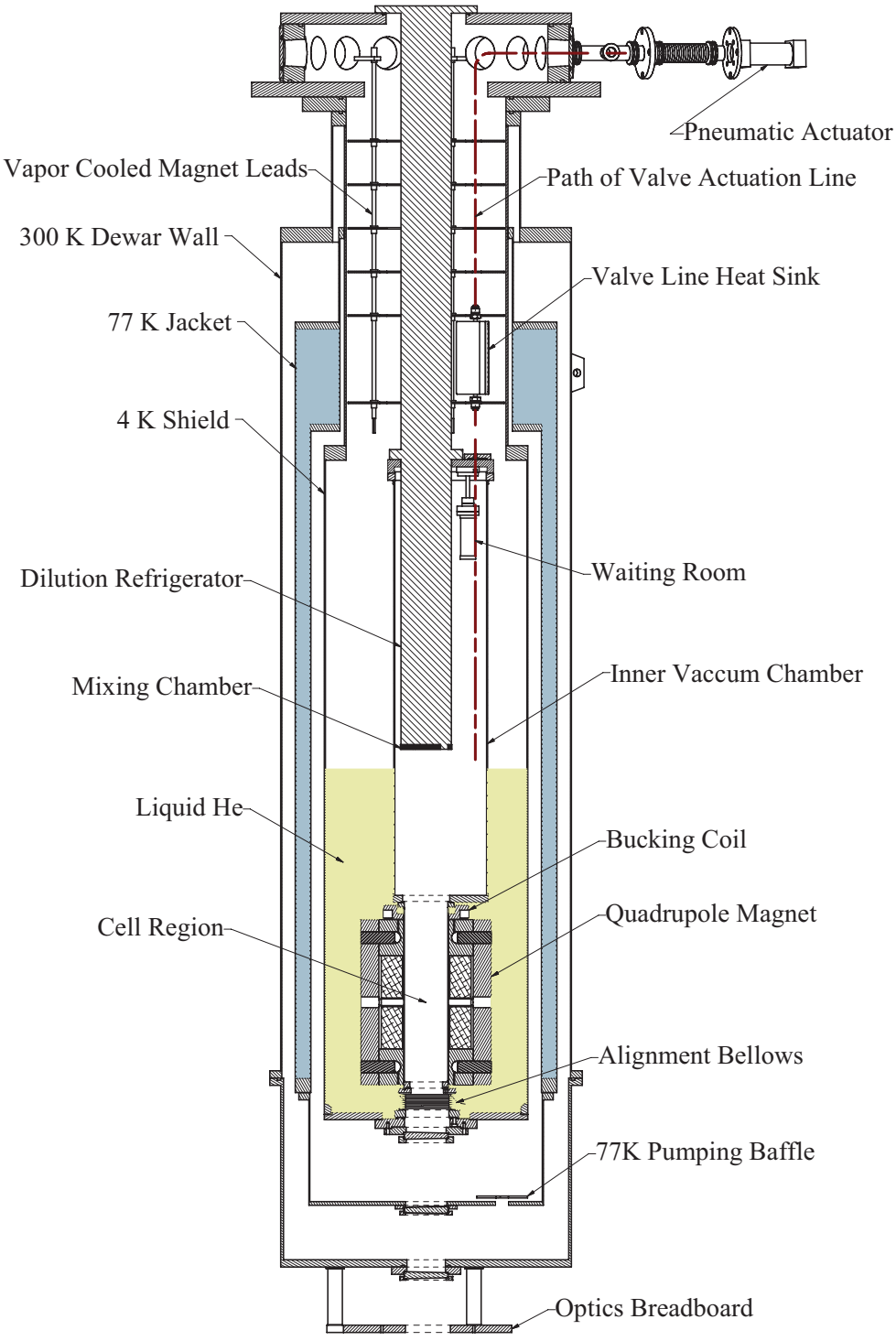

Figure 2-1: A cross sectional view of the cryostat. The valve itself is not shown as it is inside of the cell. However the pneumatic actuation system, controlled at room temperature using a "string and spring" method, can be seen on the right side of the diagram. Both the ablation and detection lasers enter the apparatus from the bottom. The cell (not shown here) fits inside the core of the magnet.

field has been modeled using Biot-Savart Software designed by Cirrus Software [51]. Good agreement has been found between the modeled fields and measured fields of the magnet.

Cell

A cut-away view of the cell is depicted in Figure 2-3. The cell used in the experiments for this thesis is a wire-wrapped plastic cylinder. There are about one thousand, 10 mil diameter insulated OFE copper wires, lining the exterior of a thin G-10 cell wall. These extend the length of the cell and are bound at the top and clamped to the mixing chamber of the refrigerator. The wires provide thermal contact along the entire cell wall in order to decrease cell cooling time and thermal variations. The thin diameter minimizes eddy current heating while the magnetic fields are changed.

The cell is composed of two chambers. The bottom chamber is centered in the bore of the magnet such that the magnetic field minimum with the magnet in anti-Helmholtz configuration is about 5 cm above the bottom of the cell. The bottom of the cell is sealed with a sapphire window, chosen for good thermal conduction. The sample holder is located 5 cm above the trap minimum. Pieces of solid metal of each species to be studied are glued to the underside of the sample holder. The samples are easily targeted by the ablation laser entering from the bottom of the cell.

The upper chamber of the cell, or "pump chamber", is separated from the bottom chamber by a fast cryogenic valve. The walls of the pump chamber are lined with an activated charcoal sorb. At low temperatures, the sorb effectively pumps helium, reducing the vapor pressure to an extremely low value [32]. The valve consist of a 2 inch diameter teflon boot that seals against a ring of highly polished alumina. The valve is sealed with $\sim$20 lbs of force from slight compression of a large phosphor bronze spring manufactured by Southern Spring [52]. It is actuated pneumatically at room temperature by pulling on a wire rope to further compress the spring. The valve boot can be displaced vertically by 2 inches in 30 ms. Varying the pressure in the room temperature actuator allows the valve to open more slowly to minimize the number of trapped atoms swept out with the buffer gas. Considerable experimental effort was

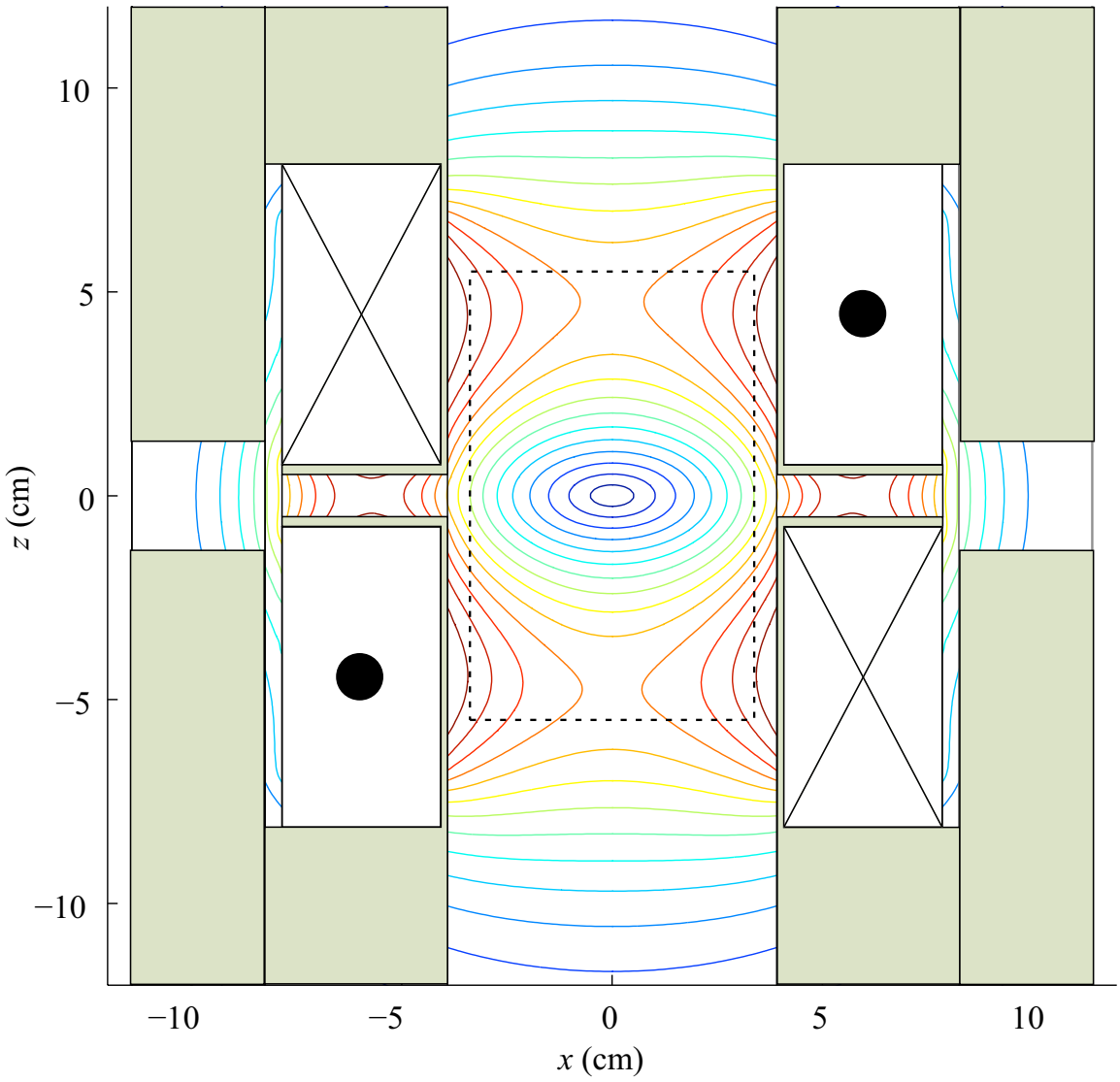

Figure 2-2: A diagram of the cell and magnetic field alignment. In addition to coaxial alignment, the height of the magnet is carefully adjusted to put the trap minimum roughly equidistant between the mirror and the window when the currents in the two coils is equal.

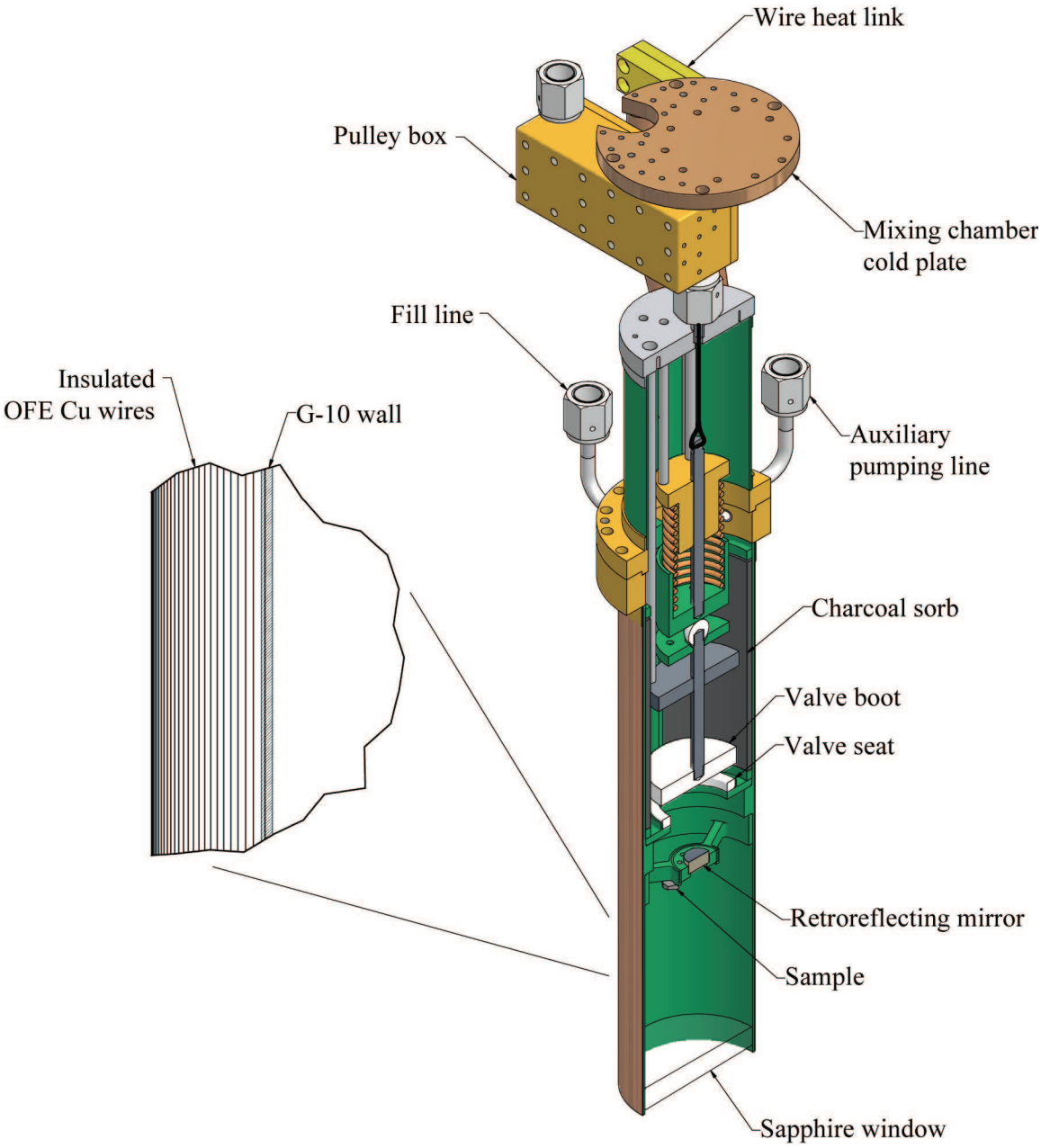

Figure 2-3: A cut-away view of the plastic cell used in all evaporation experiments. The cell is constructed of thin G-10 tubing lined on the outside with thin copper wires. This allows for good thermal conduction along the cell walls but very little eddy current heating during fast magnet ramps. The bottom end is sealed with with a sapphire window attached to the cell with epoxy.

Atom	Ground State		Excited State				λ	A
	Term	g_J	Term	J'	g'_J	Level (cm^{-1})	(nm)	(10^8 s^{-1})
Dy	$^5I_8$	1.24	^5H	7	1.26	24708.99	404.7	1.92[a]
Ho	$^4I_{15/2}$	1.2	(15/2,1)*	17/2	unknown	24360.38[b,c]	410.5	1.8[b,c]

Table 2.1: Atomic level information for the optical transitions used for absorption spectroscopy in this thesis. The last column, A, is the line strength. All data from Ref. [45], except Ref. [55][a], Ref. [56][b], Ref. [57][c]. *(J_1,J_2) coupling.

expended in the design and implementation of the valve. A complete description of the valve and actuation can be found in [25].

The top part of the cell is thermally anchored to the mixing chamber through a flexible copper heat link manufactured by Janis Research [53]. The base temperature of the cell has varied from 100 - 130 mK depending on the force supplied by the screws which bolt the heat link to mixing chamber.

Optical Detection of the Atomic Sample

The atoms in the trap are detected by absorption spectroscopy. The method is shown schematically in Figure 2-4. For experiments on dysprosium (holmium), the light source is an external cavity stabilized 405 nm (410 nm) laser diode centered on a frequency resonant with an atomic transition. Optical properties of the atomic transitions used in this thesis are listed in Table 2.1. The laser is swept across an interval centered on the transition frequency using a triangle or sine wave sweep. The sweep is controlled by a Stanford Research Systems DS345 function generator [54] that outputs a control voltage to a piezo which varies the external cavity length. Details of the specific laser diodes used can be found in Chapter 3.

The resonant laser light is split into two beams. One beam remains on the optics table and is passed through a Coherent Wavemaster wavemeter [58], and then into a Fabry-Perot cavity (fsr = 750 MHz). This setup provides a rough measure of optical frequency with the wavemeter and a determination of the frequency offset from the free spectral range of the Fabry-Perot cavity.

The other beam is either coupled into a fiber or passed through air to the optics

board hung from the bottom of the dewar. Once the beam is on the board, it is again split into two beams. The first beam goes into a "reference" photomultiplier tube (PMT). The second "probe" beam is directed into the cryostat, through the atom cloud, and retro-reflected by a small 1 cm diameter mirror in the center of the sample holder (see cell description above). The retro-reflected "signal" beam is separated from the incoming probe beam with another beam splitter and aligned into a second detector that is closely matched to the reference detector. Care is taken every day to check that the ingoing probe beam is hits the center of the cell mirror and that the retro-reflected beam overlaps it on the mirror at the bottom of the cell. This procedure ensures that the beam passes through the center of the cell (the trap minimum) twice. The PMTs used for 400 nm detection are Hamamatsu R2557 photomultiplier tubes [59]. All of the alignment optics are attached to the bottom of this board. Consequently, the optical alignment is done upside down and must be carried out while lying on one's back beneath the apparatus.

Data Acquisition

The experiment is run with a program written for National Instruments Labview 7.1 that was later upgraded to Labview 8.5. It controls the timing sequence, data acquisition, and records the operation parameters of the refrigerator. Data acquisition is carried out using an internally buffered NI-6070E DAQ board [60]. The signals from the signal and reference PMTs, one cell thermometer, driving voltage for the probe laser, and the currents in both coils are recorded with a time stamp stored in a general format text file.

2.2 General Experimental Procedures

Almost all of the experiments reported in this thesis were done using the basic experimental procedures outlined here. Each "data acquisition" cycle consists of some or all of the following basic steps. Below is a list and basic description of each step. Each step is further explained (when necessary) in greater detail below.

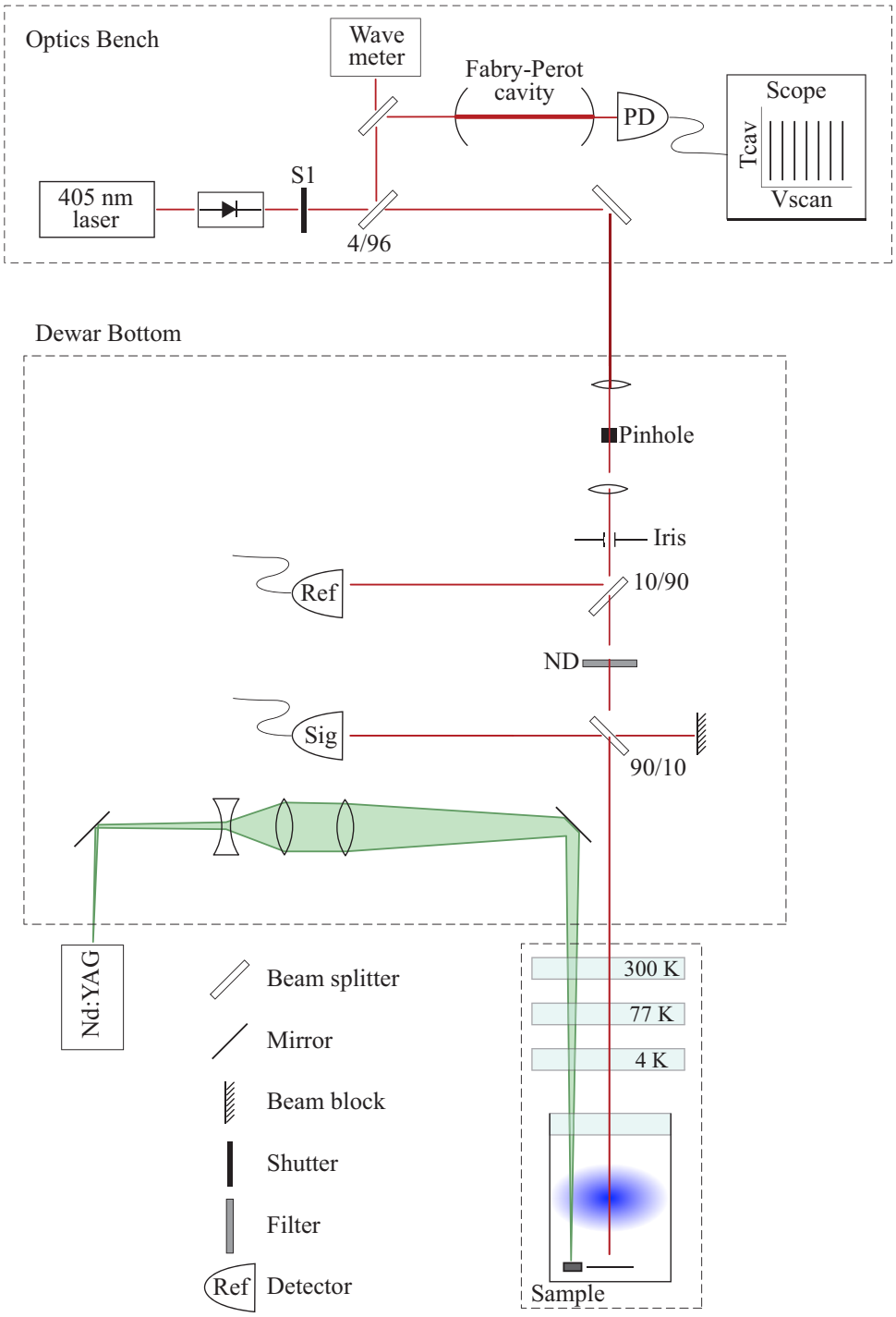

Figure 2-4: Optical detection setup for both dysprosium and holmium.

Step 1. Load buffer gas into experimental chamber to desired density by applying a heater pulse to the waiting room. The amount of buffer gas loaded depends on the power of the heater pulse as described below.

Step 2. Raise magnet currents to attain desired trapping field.

Step 3. Start scanning laser across the transition with desired frequency and begin data acquisition to get a zero absorption signal.

Step 4. Heat the cell walls to desorb enough buffer gas to load the magnetic trap. This is explained in greater detail below.

Step 5. Ablate atom precursor to introduce hot atoms.

Step 6. Wait 20 - 100 ms for initial thermalization. If there is no magnetic trap, the buffer gas density can be determined from lifetime of the lowest order diffusion mode of the atoms in the trap. See Chapter 3 for a more detailed explanation.

Step 7. Open valve for evaporation or two-body collision rate measurement.

Step 8. Lower the magnet currents (for evaporative cooling).

Step 9. Heat cell to empty trap of atoms in order to establish an empty cell baseline with the valve open.

Step 10. Close valve and ramp down magnet.

If the valve is not opened during the experiment (i.e. for measurements of collisions with buffer gas), Step 1 does not have to be repeated for each subsequent data acquisition cycle. Small modifications can be made at each step for optimization for a given experiment.

The timing is controlled by a NI-6534 High Speed Digital I/O board by National Instruments [60] with 1 ms resolution. The entire sequence (with the exception of buffer gas loading) is programmed for each acquisition prior to execution. The following descriptions add more detail to the steps outlined above.

Loading the Buffer Gas

The buffer gas needs to be loaded into the bottom chamber of the cell after each data acquisition cycle if the valve has been opened. It is stored in a small "waiting room" maintained at 4 K. The waiting room contains an activated charcoal sorb that is saturated with He at the beginning of each experimental run. The waiting room is connected to the bottom chamber of the cell by a large impedance. A heater attached to the waiting chamber can be pulsed for 90 sec periods to heat the sorb to around 12 K in order to desorb a gas of He. This builds enough pressure behind the impedance to load ∼20 monolayers of gas on the colder cell walls. The voltage of the pulse changes the buffer gas pressure in the waiting room so that various amounts of buffer gas are loaded into the cell. We can vary the buffer gas density from 10^{15} to 10^{18} cm^{-3}. The lifetime of ^{3}He buffer gas in the cell at 150 mK with the valve closed is about 1 day.

Ablation: Atom Gas Production

For all of the experiments described in this thesis, the atom gas is created through ablation of a solid precursor attached to the sample holder in the cell. Ablation is done using a Continuum Minilite II 532 nm Nd:YAG laser [61] capable of 5 ns pulses. The delay between the flashlamp and the Q-switch triggers can be varied to generate pulse energies from 5 to 25 mJ.

The ablation beam enters the refrigerator through the windows on the bottom of the cryostat near the path of the probe beam. A separate mirror setup is used for alignment. The beam passes through a telescope for beam shaping. The circular beam is then passed through a 1 m focusing lens before entering the apparatus. The

focus is adjusted to maximize production from each target.

The ablation pulse heats the cell by approximately 50-100 mK. The cell top thermometer peaks about 100 ms after ablation.

Loading the Trap

To load atoms into the trap, we need to create densities of buffer gas in the trapping region on the order of 10^{16} cm^{-3}. This can be done one of two ways.

Hot Loading. A ∼1-5 J heater pulse is applied to the cell top 1.5 seconds before the ablation pulse. This heats the cell by about 300 mK which desorbs enough buffer gas for loading.

Cold Loading. Only the ablation pulse is used to heat the cell. ^{3}He frozen on the cell walls is desorbed by the ∼50 mK temperature rise (as measured by a thermometer at the top of the cell). This can create densities large enough to load atoms. The cell is heated less and the atoms are trapped at a lower temperature. However, this loading scheme is not successful with all species.

Each of these techniques has benefits and drawbacks. Hot loading results in a warmer cell that takes a longer time to cool to base temperature. However it can result in better removal of buffer gas atoms (see Appendix A). Cold loading heats the cell less but leaves more ^{3}He atoms adsorbed to the cell walls rather than fully removed from the system. Small swings in the cell temperature (i.e. induced by magnet ramps) can then desorb more ^{3}He from the cell walls decreasing trap lifetime.

Opening the Valve

The valve can be opened at any time after the ablation pulse. In general we aim to have the valve open at peak optical absorption (∼100 ms after ablation). While the minimum valve opening time is 30 ms, the electronic relay and pneumatic cylinder system takes about 50ms to begin opening the valve. Thus we assume 80ms from the

point of the trigger to valve fully open. We can change the speed at which the valve opens by partially closing a valve on the exit chamber of the pneumatic cylinder. For lighter atoms such as lithium, or for lower trap depths, this can be utilized to minimize "wind" effects during buffer gas removal [62].

Ramping down the magnet (for evaporation)

As will be discussed in more detail in Chapter 4, enhanced cooling from evaporation is achieved by lowering the trap depth, $U_{max} = \mu B_{max}$. This can be done one of two ways: by ramping the current in the magnet coils down together or ramping one current relative to the other. In the former configuration, the maximum trap depth is determined by the field at the walls $B_{max} = B_{walls}$. We call this evaporation against the walls. In the latter configuration, the trap minimum is actually translated along the vertical axis. If the current in one coil is less than ∼69% of the current in the other coil the trap depth is determined by an axial surface – the window or the mirror at the cell ends – such that $B_{max} = B_{surf}$. In practice, the trap can be ramped towards either axial surface. This is known as evaporation against the window (or mirror).

The coils of the magnet are controlled with separate four-quadrant power supplies. One is a Cryomagnetics CS-4 [63] and the other a Lakeshore 622 [64]. These supplies are controlled programmatically through voltage controls from the computer. However, internal protection circuitry prohibits the Cryomagnetics power supply from ramping at rates greater than -1.7 $\mathrm{A\,s^{-1}}$. Systems for faster ramping will be described in Chapter 5

2.3 Signal Processing

Throughout each data acquisition cycle, the probe laser is scanned across the spectral lines of an atomic transition at a rate from 10 to 500 Hz. As the laser center frequency approaches resonance we observe increased absorption of the probe beam. We are able to resolve spectral features of our atoms by detecting the change in absorption as a function of frequency.

The transmission signal, T, is calculated by dividing the measurement of the signal intensity, S, by the reference intensity, R. This allows us to calculate a quantity of optical depth defined as

$$OD = -ln(\frac{I}{I_0}) = -ln(1 - T). \tag{2.1}$$

According to this definition, in the absence of absorption, T = 1. In our experiment, the intensities of light entering the signal and reference PMTs are not matched. To account for this, we record a 500 ms baseline at the beginning of each data acquisition cycle. We normalize the transmission signal by this baseline. For acquisitions when the valve is opened, this can cause a shift in this baseline. Often on these scans we take a late baseline by removing atoms from the trap with a heater pulse.

This method of data processing automatically divides out any noise in the system that is common to both the signal and reference beams, such as intensity fluctuations of the laser. Other sources of noise include physical vibrations of the mirror at the top of the cell, electronic noise, or shot noise. By looking at the variation in the baseline scans we are able to verify that these sources of high frequency noise in our system are less than 2%.

Once we have measured the optical density as a function of laser frequency, we can perform a fit to the spectrum. The fitting procedure employs a model that accounts for all parameters affecting absorption including position dependence of the atom density, probe beam radius and position, light polarization, and magnetic broadening. The spectrum modeling software was developed by Brahms and deCarvalho [25, 65].

Chapter 3

Collisions in the Low Buffer Gas Density Regime

Collisions play a central role in any atom cooling and trapping experiment. As a general rule, elastic collisions, in which the internal states of the atoms are unchanged, lead to thermal equilibrium of the translational motion of the atom ensemble. In the buffer gas loading method, atoms are cooled through elastic collisions with a cold helium buffer gas to a temperature at which they can be magnetically trapped. Inelastic collisions with the buffer gas lead to trap losses, as they change the spin state of the atoms to an un-trapped state. After the buffer gas is removed, collisions between trapped atoms determine the lifetime and temperature of the sample.

In addition to their relevance for magnetic trapping of atoms, studies of collisions, especially at low temperatures, reveal details of fundamental atomic properties and interactions. The rate of spin relaxation in a trapped atom sample can probe anisotropy of the interatomic potential or the effects of higher order processes (such as spin-orbit coupling). For atoms with complex asymmetric electronic configurations this is very difficult to analyze theoretically. For these atoms measurements of collisions are useful for testing theory and to model collisions of atoms (and molecules) with non-S state ground states [28].

The experimental apparatus described in Chapter 2 is well suited for collision studies of various atomic species. In a series of earlier experiments, we have used

the apparatus to investigate collisions of atoms with helium. A study of collisions of noble metal (Cu, Ag, Au) atoms with ^{3}He revealed an anomalous loss process that could not be explained by currently understood atom collision models [24]. In addition, attempts were made to buffer gas load transition metal atoms; cobalt, nickel, and iron [48]. These attempts at trapping were unsuccessful, although they made it possible to place limits on the rates of inelastic collisions with helium.

In addition to being able to study collisions of atoms with the helium buffer gas, the valved chamber construction of the cell permits removal the buffer gas and the study of the subsequent atom-atom collisions. In this chapter, I will report on measurements of inelastic collision rates between two rare earth atoms, dysprosium (Dy) and holmium (Ho). These measurements build on the work done by Hancox, *et al*, studying the collisions of rare earth atoms with helium. Her research, performed in a similar buffer gas cooling apparatus, found smaller inelastic collision rates than expected [17]. Our measurements help to extend the model proposed by Krems and Buchachenko [34], that the filled s-state shields valence electrons in the f- and d-shells, decreasing the anisotropy of the interatomic potential. First, I will give a brief overview of the physics of collisions at cold temperatures as it applies to buffer gas cooling and loading (atoms colliding with helium), as well as evaporative cooling (atoms colliding with atoms).

3.1 Trap Loading: Collisions with the Buffer Gas

Elastic collisions with a cold buffer gas thermalize the ablated atoms to the temperature of the cell walls. This reduces the kinetic energy to a value where the atoms may be trapped in a laboratory-realizable magnetic field.

To load the trap through buffer gas collisions, the mean free path of the atoms traveling through the buffer gas, $\lambda = 1/\sigma_{bg} n_{bg}$ must be much smaller than the radius of the trap. Here σ_{bg} is the elastic cross section of the atoms with the buffer gas and n_{bg} is the buffer gas density. In addition, the atoms must undergo enough collisions

to be cooled from the hot temperatures at which they are produced[1] to the cell wall temperature. Experiments have shown that this is on the order of 100 collisions for atoms being loaded through ablation at starting temperatures around 1000 K [14]. If we assume a collision cross section of atoms with helium, σ_{bg} $\sim 10^{-14}$ cm^2, and a trap length of 10 cm, buffer gas densities on the order of 10^{16} cm^{-3} are necessary for loading[2]. At high buffer gas densities, the atoms are at approximately the same temperature as the buffer gas within a few milliseconds.

At these densities, the motion of the atoms through the cell is diffusive. The temporal evolution of the atoms density, n, is determined by the diffusion equation

$$\frac{\partial n}{\partial t} = D\nabla^2 n. \tag{3.1}$$

D is the diffusion constant defined as [66]

$$D = \frac{3\pi}{32}\frac{\overline{v}_\mu}{n_{bg}\,\sigma_d}. \tag{3.2}$$

Here n_{bg} is the buffer gas atom density and σ_d is the diffusion cross section[3]. $\overline{v}_\mu$ is the thermally averaged relative velocity. For two particles with different masses, m_1 and m_2, and temperatures, T_1 and T_2,

$$\overline{v}_\mu = \sqrt{\frac{8k_B}{\pi}\left(\frac{T_1}{m_1} + \frac{T_2}{m_2}\right)}. \tag{3.3}$$

If the particles are in thermal equilibrium then $T = T_1 = T_2$, and Equation 3.3 reduces to the average thermal velocity of a particle with the reduced mass.

Solutions to the diffusion equation can be described as a series of eigenmodes of the form

[1] In our experiments, the atoms are produced through ablation. Other buffer gas loading schemes use a discharge or beam of particles. The production temperature for ablation or discharge is on the order of 10^3 K. Beams are usually pre-cooled to $\sim$ 4 K [19].

[2] This is consistent with observations in the experiment.

[3] In general for distinguishable particles, the diffusion cross section is smaller than the elastic cross section σ_{el} by order unity. In this thesis we will assume them to be equal.

$$n(\vec{r},t) = \sum_i n_i(\vec{r}) e^{-t/\tau_i}. \tag{3.4}$$

Each $n_i(\vec{r})$ is a spatial eigenfunction determined by the boundary conditions of the problem. We solve for only the lowest order mode in this problem as the higher order modes decay more rapidly.

If the trapping field is off, Equation 3.1 is easily solved for simple geometries. For a cylindrical cell of length, L and radius, R, and $n = 0$ at the cell walls, the solution is

$$n(\vec{r}) = n(0) J_0\left(\frac{j_{01}\, r}{R}\right)\ cos\left(\frac{\pi\, z}{L}\right). \tag{3.5}$$

$$\tau_{diff} = \frac{n_{bg}\, \sigma_{bg}}{g_{cyl} \overline{v}_\mu}. \tag{3.6}$$

$$g_{cyl} = \frac{3\pi}{32}\left(\frac{j_{01}^2}{R^2} + \frac{\pi^2}{L^2}\right). \tag{3.7}$$

$J_0(r)$ is the zeroth-order Bessel function and j_{01} is the location of its first zero.

If the trapping field is on, the atoms feel a retarding force that can be approximated with a drift velocity term on the right hand side of Equation 3.1. This will have the effect of increasing the lifetime of the trapped atoms. For an ellipsoidal quadrupole trap, in a cylindrical cell the diffusion lifetime can be approximated by [25]

$$\tau_{cyl} = \frac{n_{bg}\sigma_d}{g_{cyl}\overline{v}_\mu}\, e^{0.31\eta + 0.018\eta^2}. \tag{3.8}$$

In the high buffer gas density regime, necessary for loading, the lifetime of the atoms in the trap increases linearly with the buffer gas density.

Not all collisions with the buffer gas are elastic. Inelastic collisions between atoms and buffer gas can change the internal state of the atoms. Trapped atoms are in the weak field seeking m_F states. A collision which changes the projection of the total spin to a high field seeking m_F state will result in the loss of an atom from the

trap. This is known as "Zeeman relaxation". The rate of atom losses due to Zeeman relaxation can be described by

$$\dot{N}_{at} = -\Gamma_{ZR} N_{at}. \tag{3.9}$$

Where,

$$\Gamma_{ZR} = n_{bg} \sigma_{ZR} \overline{v}_{\mu}. \tag{3.10}$$

We call this a "one-body" loss mechanism, as each collision involves only one trapped atom. The lifetime due to Zeeman relaxation is $1/\Gamma_{ZR}$ and is inversely related to the buffer gas density. For most atoms, the inelastic cross section with helium, σ_{ZR}, is much smaller than the elastic cross section, σ_{bg}. However, if there is enough buffer gas in the cell, the Zeeman relaxation time limits the trap lifetime. A more rigorous discussion of the physics of Zeeman relaxation is given in Johnson's thesis, Ref. [48].

The loss processes we have described so far occur in the high buffer gas density regime necessary for loading. All of the experiments in this thesis will take place after the atoms have been loaded and the buffer mostly removed. To isolate the atoms inside the trap, there must be a range of buffer gas densities for which the lifetime of the atoms is long enough that we can open the valve, or about 100 ms.

We will define a parameter γ to describe the ratio of the rates of elastic to inelastic collisions with the buffer gas

$$\gamma_{bg} \equiv \frac{\Gamma_{el}}{\Gamma_{in}}. \tag{3.11}$$

The 100 ms lifetime requirement places an empirically derived minimum on this ratio for successful buffer gas loading[4].

$$\boxed{\gamma_{bg} \geq 10^4}$$

[4]I will derive a similar limit for γ corresponding to atom-atom collisions later in this chapter.

Collisions in the Low Buffer Gas Density Regime

In the low buffer gas density regime, there is no diffusion. The trap lifetime due to interactions with the buffer gas is inversely proportional to the buffer gas density. After removal of the buffer gas, any residual background gas couples the trapped atoms to the temperature of the cell walls. In this regime, increasing the buffer gas density couples the temperature of the atoms to the cell walls, increasing the heat load on the atoms and decreasing the trap lifetime. The details of this interaction will be important for attempting evaporative cooling. I will quantify the interaction of the atoms with low densities of background gas in the next chapter, and derive a limit for the maximum background gas density which can be tolerated. Typically it is on the order of 10^{11} cm^{-3}.

We have been successful in removing the buffer gas below the level where the trap lifetime is dominated by collisions between the atoms. Appendix A discusses the removal of the buffer gas. The rest of this chapter is concerned with the interaction of trapped atoms with other trapped atoms assuming the low buffer gas density limit.

3.2 Atom-Atom Collisions

Once the buffer gas is removed, collisions between atoms are responsible for the thermal equilibrium and most of the losses from the trap. Similar to the helium-atom collisions described above, elastic collisions with other trapped atoms bring the ensemble into thermal equilibrium and can cause losses near the trap edge. Inelastic collisions result in atom losses from any location in the trap.

At any point $\vec{r}$ in the trap, the local loss of atom density, n, due to intra-atomic collisions will vary as the atom number density squared

$$\dot{n} = -g_{2b} n^2. \tag{3.12}$$

Here, g_{2b} is the two-body rate constant with units of cm^3 s^{-1}. The rate constant for any process can be related to the cross section by the thermally averaged velocity,

$g \equiv \sigma \overline{v}_{\mu}$. For a homogenous gas Equation 3.12 has a unique solution

$$n(t) = \frac{n(0)}{1 + n(0) g_{2b} t}. \tag{3.13}$$

However, the local density, n, is not a measurable quantity in our experiment as we can only measure bulk atom cloud behavior. In a spherical quadrupole magnetic trap, the local number density is weighted by the Boltzmann distribution.

$$n(\vec{r}) = n_o \, e^{-U(\vec{r})/k_B T} \tag{3.14}$$

Here n_o is the peak density of atoms found at the center of the trap where the atoms are coldest and the density is largest. We can define an effective volume such that $N = n_o \, V_{eff}$, where N is the total number of atoms in the trap.

$$V_{eff} \equiv \int_0^{\vec{r}_{max}} e^{-U(\vec{r})/k_B T_{at}} dV \tag{3.15}$$

If we insert Equation 3.14 into Equation 3.12 and integrate over the actual trapping volume, we find

$$\dot{n_o} = -\frac{g_{2b}}{8} n_o^2. \tag{3.16}$$

Solving Equation 3.16 we find an equation similar to 3.13 but for the observable quantity, n_o.

$$n_o(t) = \frac{n_o(0)}{1 + n_o(0) g_{2b} t/8} \tag{3.17}$$

3.2.1 Elastic Collisions

General quantum mechanical elastic scattering is treated in most quantum mechanics textbooks [67, 68]. A useful discussion of atomic collisions can be found in Ref. [66].

At room temperature elastic cross sections are typically in the range of 10^{-15} to 10^{-14} cm^2 [69]. The elastic collision cross section depends strongly on the interference of scattering paths when the incoming atoms are in a superposition of total orbital

Atom	(F, m_F)	σ_{el} (cm^2)	Source
H	(1,1)	1×10^{-15}	[72]
^{7}Li	(2,2)	3×10^{-13}	[73]
^{23}Na	(1,-1)	6×10^{-12}	[74]
^{39}K	(2,2)	1×10^{-13}	[75]
^{52}Cr	(3,3)	5×10^{-14}	[20]
^{87}Rb	(1,-1)	5×10^{-12}	[76]

Table 3.1: Elastic collision cross sections in the cold to ultracold limit for various atoms. While all of these atoms are S-state, their elastic cross sections at low temperature vary greatly.

angular momentum states. The difference between interatomic potentials from these states introduces a phase shift in the scattering amplitude with a finite probability of a spin change during a collision. As the atoms are cooled, higher order angular momentum partial waves are "frozen out" because the atoms do not have enough energy to tunnel through the angular momentum barrier of the interatomic potential. We call this the limited partial wave or "cold" regime. Further cooling brings the atoms into the near zero-energy limit, or the "ultracold" regime. In these collisions only the s-wave contributes to the scattering amplitude and the elastic cross section approaches a constant. Extensive treatment of atomic collisions in the cold and ultracold collisions can be found in review articles [70, 71]. The ultracold elastic cross sections for various species of atoms are shown in Table 3.1.

Elastic Losses

While elastic collisions are mostly thermalizing, they can also lead to atom loss in a magnetic trap. A more rigorous discussion of this process will be given in the next chapter, but I will provide a brief discussion of it here for completeness. Although the total energy is conserved, the atoms can exchange momentum during the collision; one atom exits the collision with greater energy and one with less than before the collision. If such a collision occurs near the edge of the trap, this can excite one atom to an orbit that will cause it to leave the trap. This atom will carry away the extra energy gained in the collision, leaving its collision partner still in the trap. This is

the basic idea behind evaporative cooling.

Unlike the inelastic collisions discussed below, not every elastic collision leads to trap loss. Only some small fraction of collisions will result in an atom attaining enough energy to leave the trap. However, closer to the trap edge, the probability increases. We will see in the next chapter that this probability will scale roughly as $\sqrt{\eta}e^{-\eta}$. For very deep traps ($\eta > 10$) this process will account for a very small fraction of atom losses.

3.2.2 Inelastic Collisions

Three types of inelastic collisions affect magnetically trapped atoms: spin exchange, dipolar relaxation and three-body recombination. In most traps, three-body recombination rates are very low due to the relatively low densities [47, 77]. The first two types of collisions are binary collisions involving only two atoms. Both of these types of collisions lead to spin relaxation from a trapped state to a magnetically un-trapped state of one or both atoms.

Spin Exchange

Spin exchange collisions preserve the total spin angular momentum of the two colliding atoms and occur frequently in a magnetically trapped sample. In the case of spin 1/2 particles, the molecular interaction of a spin up and spin down particle introduces a phase shift in the scattering amplitude during the collision. Depending on the length of the interaction, the atoms can exchange spin states.

In collisions involving particles with spins greater than 1/2, the molecular potential couples the input state to output channels with the same total angular momentum projection. For simplicity consider two atoms with no nuclear spin. The electronic spin state is represented by $|\mathbf{S}_1, m_1; \mathbf{S}_2, m_2\rangle$, such that $\mathbf{S}_t = \mathbf{S}_1 + \mathbf{S}_2$ and $\mathbf{M}_t = m_1 + m_2$. As the atoms approach each other, the total spin projection $\mathbf{M}_t = m_1 + m_2$, remains a good quantum number and couples the state of the incoming atoms to outgoing interatomic states with the same total spin projection. There is a finite

probability the atoms will leave the collision in any state $|S_1, m_1'; S_2, m_2'\rangle$, such that $\mathbf{M}_t$ is conserved.

If both atoms are in the most-weak-field-seeking state (or the most-high-field-seeking state), meaning that $m = \pm$S, the molecular potential can only couple to the same outgoing states; thus spin exchange is forbidden. For atoms trapped by a potential minimum, atoms in any spin state other then the most "stretched" state can end up in an un-trapped state and immediately leave the trap.

A similar argument can be made for atoms with non-zero nuclear spin in fields where m_F is a good quantum number. In this case, the molecular potential will couple exit states that maintain total $|m_F\rangle$ in the collision, resulting in all of the atoms quickly decaying into the most-weak-field-seeking state, $|m_F\rangle = F$ for each hyperfine level. Once the system is fully polarized, further spin exchange is forbidden because of angular momentum conservation [47, 78, 79]. Consequently, spin exchange has the effect of "purifying" the spin state of the samples into the most-weak-field-seeking state.

For alkali atoms, spin exchange rate constants are typically 10^{-12} cm^3 s^{-1} [47]. If we assume similar rates for the rare earth atoms, at the densities in our trap, the sample will be spin polarized in each of the hyperfine levels in about one second. After that, spin exchange no longer plays a role in trap population evolution.

Dipolar Relaxation

Dipolar relaxation couples the internal spin angular momentum to the orbital angular momentum of the colliding atoms. This can cause spin relaxation out of the trapped state during a collision of two spin polarized atoms. The Hamiltonian for this collision is simply the classical expression describing the interaction of two magnetic dipole moments.

$$H_{dip}(r) = \frac{4\mu^2}{r^3}[\mathbf{J_1} \cdot \mathbf{J_2} - 3(\mathbf{J_1} \cdot \mathbf{n})(\mathbf{J_2} \cdot \mathbf{n})] \tag{3.18}$$

n is the unit vector connecting the two magnetic moments and r is the distance between the two atoms. Since H_{dip} varies as r^{-3}, dipole relaxation is a long range interaction. Classically, when two colliding atoms approach to a distance r_o, they feel a perturbation $H_{dip}(r_o)$ for a characteristic time τ_c. In the classical approximation, $\tau_c = r_o/v$ where v is the velocity during the collision. The inelastic dipole cross section varies as the probability that the spin is changed, squared.

$$\sigma_{dip} \propto \left(\frac{\mu^2}{v r_o^2}\right)^2 \tag{3.19}$$

The cross section will scale as μ^4 and as r_o^{-4}. The velocity, v, in this expression (unlike most other velocities in this thesis) is not simply the average thermal velocity. Instead this velocity will depend on the interatomic potential of the collision. As temperature approaches zero, the cross section will tend to zero too. This is due to higher order partial waves being "frozen" out of the interaction (see the section on Elastic Collisions above). I will assume for the atom temperatures in this thesis (40-500 mK, well above the s-wave limit) that the dipole cross section is constant and the two-body rate constant will vary as the $\sqrt{T}$. For alkali atoms ($\mu = 1\mu_B$) dipolar rate constants have been calculated to be typically 10^{-15} cm^3 s^{-1} [80, 81]. Unlike spin relaxation, dipole relaxation can occur between two fully polarized atoms. After spin exchange has polarized the samples, dipole relaxation dominates the inelastic processes.

3.2.3 Limits on γ_{2B}

As I will discuss in detail in the next chapter, in order to cool by evaporation or to achieve long lifetimes in the trap, the losses due to inelastic atom-atom collisions must be small compared to the rate of thermalization. Assume that if an ensemble of atoms is not in thermal equilibrium with its surroundings, each atom needs to undergo n collisions to effectively thermalize to equilibrium. We introduce a ratio of the coefficients of elastic to inelastic collision rates for two-body collisions similar to that for one-body collisions.

$$\gamma_{2b} = \frac{g_{el}}{g_{in}} \tag{3.20}$$

If γ_{2B} is too small, the atoms never rethermalize to a new thermal distribution. Instead, the sample size is simply decreased. For successful evaporative cooling,

$$\boxed{\gamma_{2b} \gg 1}$$

Buffer gas loading, which is capable of attaining large initial trap populations, is well suited for attempts to achieve evaporation even in the case of small γ_{bg}.

3.3 Rare Earth Atoms

The rare earth atoms are interesting for cold atom research because they are non-S state atoms that can be loaded into a magnetic trap using buffer gas cooling. This presents the intriguing possibility for loading, and perhaps cooling to degeneracy, atoms or molecules with orbital angular momentum.

In 2005 Hancox *et al.* studied collisions of a variety of rare earth atoms with ^{3}He [17]. The result of their research is summarized in Table 3.2. The rare earth atoms have γ_{bg} large enough to allow for buffer gas trapping and lifetimes long enough for removal of the buffer gas. This comes about because the unfilled valence shell (f or d) is partially shielded by filled shells (including a filled 6s-shell) with average radii greater than the unfilled valence shell. These filled shells decrease the anisotropy of the interaction of the rare earth atom with helium [28, 82]. The atom-He elastic collision cross sections were all found to be large, on the order of 10^{-14} cm^2.

According to Krems *et al.*, similar suppression of anisotropy might also increase the elastic collision cross section for atom-atom collisions [34, 83]. The filled s-shells repulse each other so that the average interaction radius is greater than it would be for unshielded f- valence shells. For dipolar spin relaxation, the rate varies as r^{-4} and could be sensitive to the repulsive forces that increase the radius of interaction.

Our apparatus is ideally suited to measure the inelastic rates of rare earth intra-atomic collisions as well as to attempt evaporative cooling. The fast-opening cryogenic

Atom	Term	μ (μ_B)	Number Trapped	γ_{bg} (10^4)
Tm	$^2F_{7/2}$	3.99	2×10^{11}	2.7±1.4
Er	$^3H_6$	6.98	2×10^{11}	4.3±2.3
Nd	$^5I_4$	2.41	1×10^{12}	8.7±4.9
Tb	$^6H_{13/2}$	9.94	2×10^{11}	12±0.6
Pr	$^4I_{9/2}$	3.29	3×10^{11}	13±0.8
Ho	$^4I_{15/2}$	8.96	9×10^{11}	28±1.6
Dy	$^5I_8$	9.93	2×10^{12}	45±2.4

Table 3.2: Ratio of elastic to inelastic cross sections for the various rare earth atoms as measured by Hancox *et al*, Ref. [17]. For all of these atoms unfilled f- and d- shells are shielded by filled 6s shells giving rise to suppressed anisotropy of the interatomic potential.

valve, low cell temperature, and the ability to do fast magnetic field changes were all designed with the intent to carry out evaporative cooling of various species.

Considering that the dipole-dipole interaction scales with μ^4, holmium and dysprosium with μ equal to 9 and 10 respectively, might seem less than ideal lanthanide species for evaporative cooling. However, we chose these atoms because their large values of γ_{bg} is efficient for loading and cooling the atoms with a helium buffer gas. We initially attempted to measure the two-body relaxation rate of praseodymium. Problems with the low signal-to-noise ratio, short trap lifetime in the presence of buffer gas, and low production thwarted our efforts.

3.4 Two-body Collision Rate Measurement

Our apparatus allows us to remove the buffer gas atoms quickly and measure atom-atom collision rates. To determine collision rates we measure the lifetime of atoms in the trap. The lifetime is determined by both losses of atoms due to evaporation (an elastic process) and losses due to inelastic collisions that result in an un-trapped atom as explained above. If the lifetime due to background gas collisions is longer than 100 ms, we can decrease the buffer gas density in the trapping region to approximately 10^{11} cm^{-3} by opening the valve. At these buffer gas densities, the lifetime of the atoms is dominated by the atom-atom collisions. By measuring this lifetime and the

temperature, we can derive the inelastic collision rate constant.

We load atoms into a magnetic quadrupole trapping field using buffer gas densities of approximately 10^{16} cm^{-3}, trapping more than 10^{11} atoms at 500 mK. The exact temperature depends on the magnetic moment and the mass of the atoms as well as the temperature of the cell after ablation.

Once the atoms are cooled to temperatures where η is greater than ten, we open the valve in less than 200 ms. This removes the majority of the buffer gas and isolates the atoms.[5]

After the buffer gas has been removed, we can measure the decay of the atoms in the trap and fit it to Equation 3.17 to determine the two-body rate constant. The losses account for all atoms that leave the trap due to any two-body process, whether elastic or inelastic. For the reasons mentioned in Section 3.2.1, the elastic loss rate is highly suppressed for a trap with η greater than ten. Additionally, we fit the data only for times greater than one second, after spin exchange has purified the sample.

The procedure for taking two-body measurements is simple. We start by recording a spectrum at zero field. After verifying the buffer gas density in the cell, laser alignment, and frequency centering, we establish an ellipsoidal quadrupole trap geometry with the gradient in the axial direction being twice that in the radial direction. We record a spectrum in the trapping field before opening the valve, to check that nothing has changed during the magnet ramp. Finally, we take a scan across the transition frequency while the valve is opened but and the magnets are maintained at constant current maintaining a constant current in the magnet coils. Opening the valve often introduces a new offset into the signal. In order to account for this, at the end of the data acquisition cycle we heat the cell to remove any remaining atoms and get a new baseline of the empty cell signal.

Both dysprosium and holmium atoms are ablated using a 10 mJ pulse. For both atoms we used a similar laser setup. In dysprosium, the 404.71 nm transition between the $^5I_8$ state and the $^5H_7$ state can be reached with a standard blue laser diode

[5]Removal of the buffer gas can sweep out some of the atoms due to "wind". For highly magnetic atoms the loss is insignificant for most trapping geometries. The losses are estimated with Monte Carlo in much greater detail in Brahms' thesis [25].

Atom	Isotope	Abundance	Isotope Shift[c] (MHz)
Dy	164	0.282	0
	163	0.249	130
	162	0.255	370
	161	0.189	510
	160	0.0234	810

Atom	Isotope	Ground State		Excited State	
		A[a](MHz)	B[a](MHz)	A(MHz)	B(MHz)
Dy	163	162	1152	190±10[c]	1000±200[c]
	161	-116	1091	-140±10[c]	1700±200[c]
Ho	165	800.583	-1688	653±2[b]	-500±200[b]

Table 3.3: Data used for spectrum fitting of Dy and Ho spectra. [a]Ref. [85], [b]Ref. [86], [c]Best fits to zero field data.

centered near 405 nm. Similarly, we used a second blue diode centered around 410 nm to reach the 410.5 nm transition between the ${}^4H_{15/2}$ ground state and the (J_1,J_2) = (15/2,1) excited state for holmium atoms.[6] The diodes were installed in a Toptica Photonics DL100 laser head [84].

3.4.1 Fitting the Data

We use a similar process to fit the spectral data for both dysprosium and holmium.

Dysprosium

Figure 3-1 shows the zero-field dysprosium spectrum. There are 5 isotopes of dysprosium with populations greater than 2%. Two of these isotopes have I = 5/2 with hyperfine structure. The energy levels of two isotopes of dysprosium are shown in Figure 3-2. Details of the transition, including the isotope shifts and hyperfine constants we used to fit the data, are in Table 3.3. At zero-field, with typical loading buffer gas densities, the Dy has a diffusion lifetime of approximately 100 ms. We have

[6]The laser diodes were harvested from a Sony Playstation HD-DVD player bought at Best-Buy. As the HD-DVD technology lost out to Blu-Ray, HD-DVD players became very inexpensive. With minimal effort, the laser diode was removed and the lasing frequency determined. Using a diffraction-grating stabilized external cavity allows precise tuning and scanning of the laser frequency for spectroscopy.

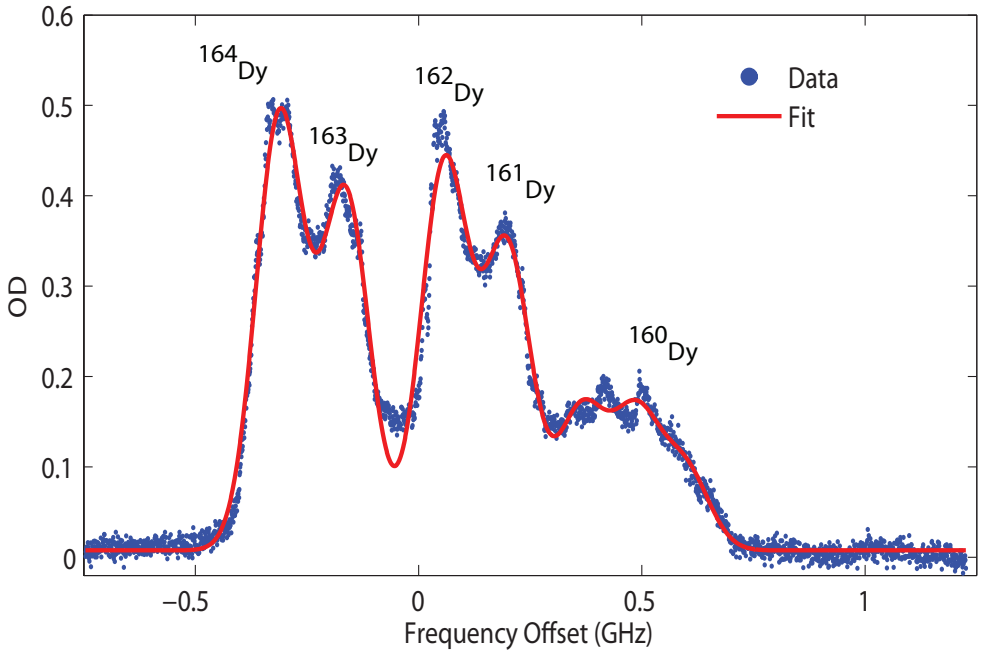

Figure 3-1: Dy spectrum at zero field on the transition ${}^5I_8 \rightarrow {}^5H_7$ at 404.7 nm[45]. There are five isotopes of Dy with occupation greater than 2%. From the spacings of the isotope peaks for ^{165}Dy, ^{163}Dy, and ^{161}Dy at zero field, we can estimate the hyperfine constants (A, B) for the excited state (see Table 3.3). Finite residual magnetic fields broaden the zero field spectrum slightly so temperature information can not be found from this spectrum.

good production of atoms with maximum optical depths of about 0.5, (about 60% absorption of the beam).

Most of the data were taken with the magnet ramped to 30A in each of the coils creating a magnetic field at the cell walls of 1.25 T. We load approximately 10^{11} dysprosium atoms at 500 mK with buffer gas densities of 9×10^{15}, for an initial trap depth, $\eta = 16.5$. Trap lifetimes before opening the valve are about 500 ms. We optimized the valve opening time to 100 ms after the ablation pulse to give maximum signal at late times.

To extract the value of g_{2b}, we convert the optical depth spectrum profile into meaningful numbers. We can fit the averaged atomic spectrum to a spectrum model that accounts for atom number, atom temperature, hyperfine state populations, magnetic trap parameters, and the detection laser beam profile at various times after

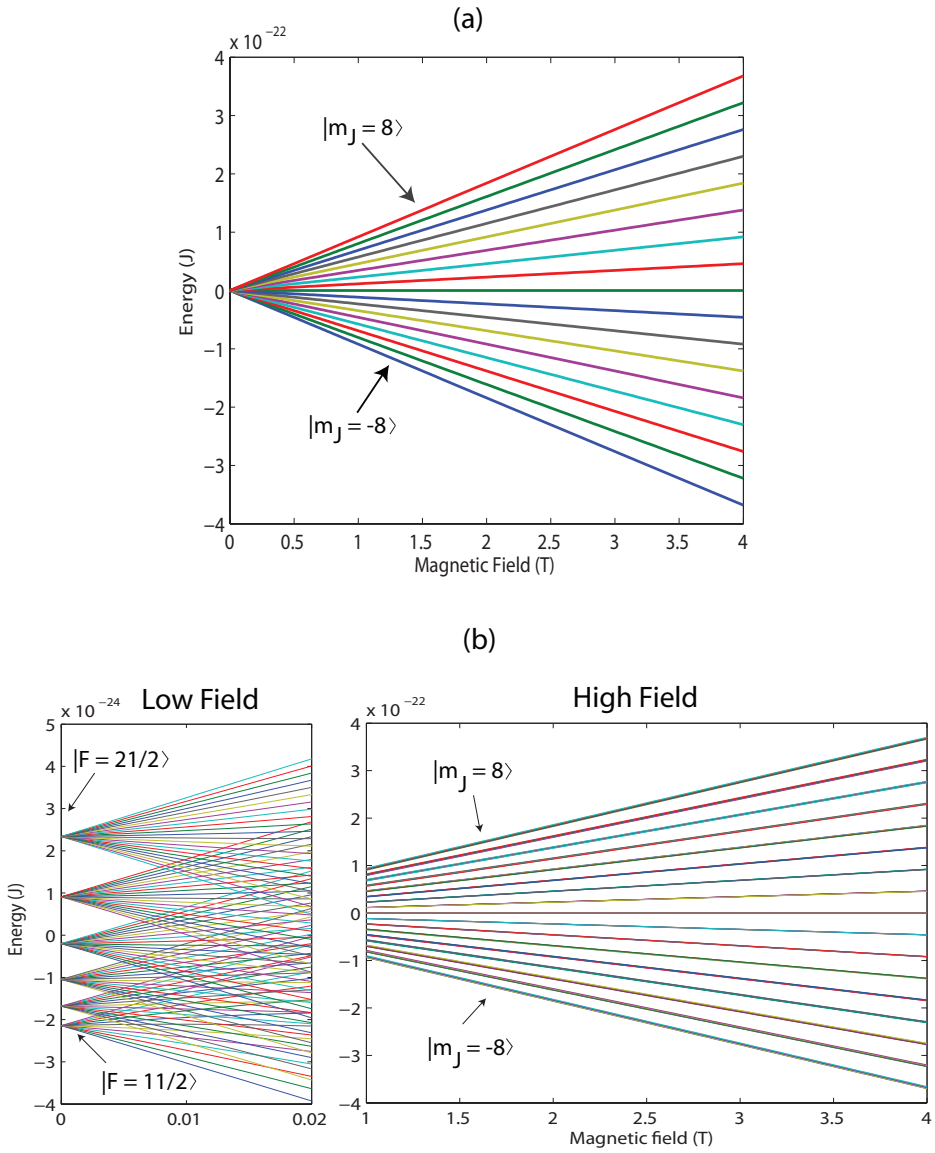

Figure 3-2: Energy levels of the $^5I_8$ ground state Dy. We magnetically trap the weak field seeking states of each isotope. (a) ^{164}Dy: I = 0. J is always a good quantum number. (b)^{163}Dy: I = 5/2. At high field m_J is a good quantum number. Each m_J manifold has 6 states corresponding to each m_I state.

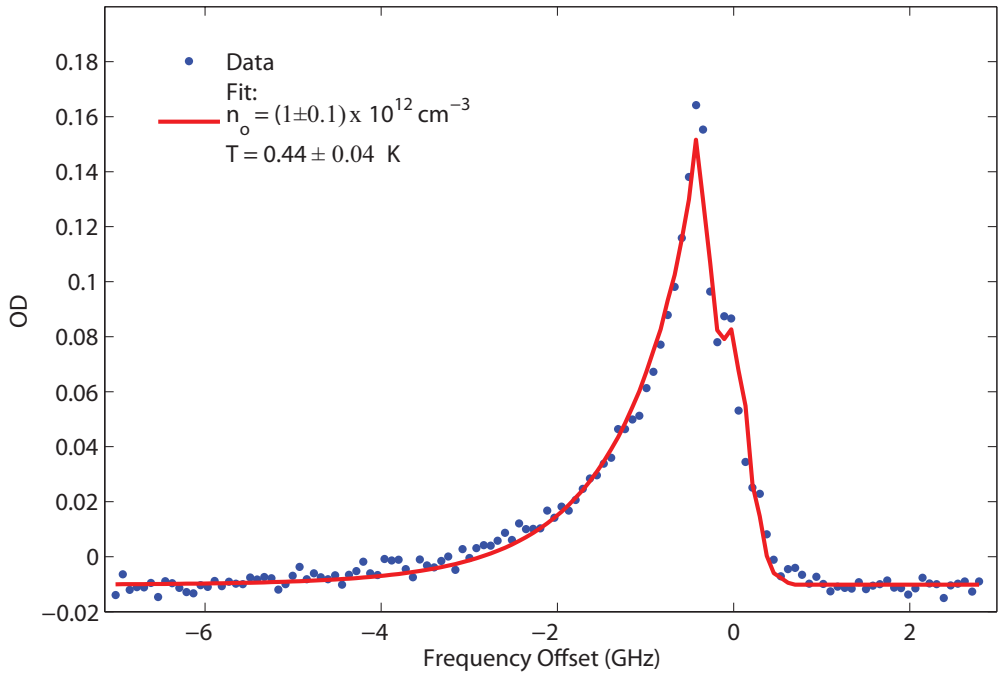

Figure 3-3: The spectrum of dysprosium trapped in an 8.5 K deep trap, taken 4.5 seconds after the valve is opened. The fit shows atom densities of $(1\pm0.1)\times10^{12}$ cm^{-3} at 440±40 mK with $\tilde{\chi}^2 = 0.38$.

ablation. The beam profile and magnetic trap parameters can be estimated from the experimental setup. The populations of the different hyperfine levels are estimated by assuming a thermal equilibrium distribution based upon the energy splittings. The atom number density, n_o, and temperature of the atoms can be adjusted for the best fit. An example of one of these fits for Dy is shown in Figure 3-3. The atom fitting model is described in detail in Brahms' thesis [25].

The standard deviation in the spectrum fitting is on the order of ±10% of the fit parameter for both temperature and atom density. We also extract $\tilde{\chi}^2$ value for each spectrum fit. Each fit is adjusted until $\tilde{\chi}^2$ is less than 5 to ensure a smaller systematic error in the model fit to the data.

After attaining atom number and temperature information for various times after ablation, the atom density is plotted versus time and fitted to a one-body or two-body curve. Figure 3-4, is a comparison of a one-body fit – Equation 3.9 – and a

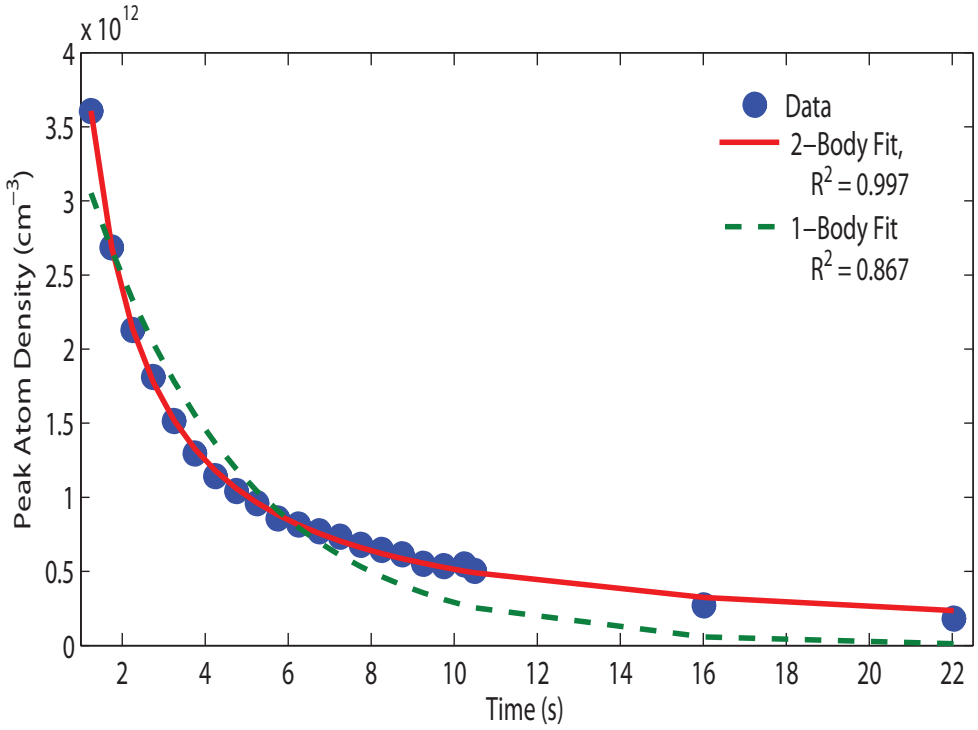

Figure 3-4: A comparison of a one-body decay model and a two-body decay model fit to the atom number density of dysprosium evolving in time. Each point on the plot was found by fitting to an average spectrum. The better agreement of the two-body fit ($R^2 = 0.997$) implies that the loss mechanism is primarily due to intra-atomic collisions. We uncertainty in the atom number fit is $\sim 10\%$. We estimate the uncertainty in the rate constant measurement by averaging the fits from many different experimental runs.

two-body fit – Equation 3.17 – to the atom number as a function of time. The quality of the two-body fit verifies that the mechanism behind the population decay in our trap, once the valve is opened, is due to primarily to atom-atom collisions rather than collision with the buffer gas. The two-body fit gives values for g_{2b} and the initial atom number density. We extract a number for g_{2b} for each data file. To extract a final value, we average g_{2b} for thirteen different files and use the standard deviation of the values to estimate the uncertainty of the measurement.

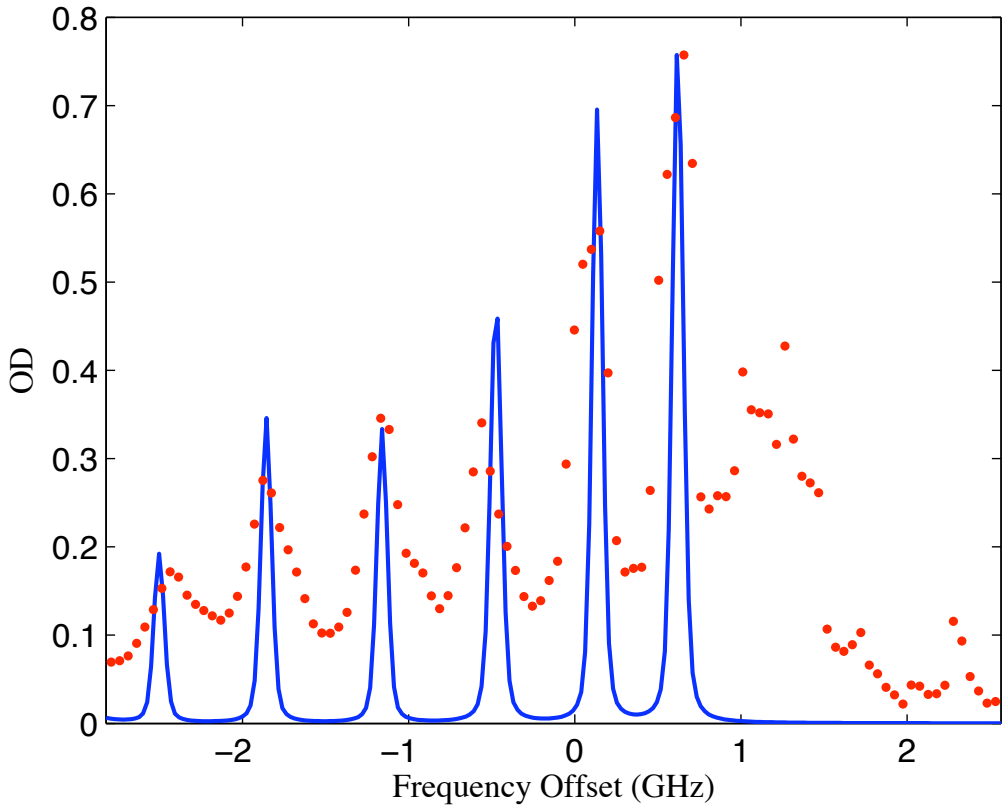

Figure 3-5: Holmium spectrum at zero field on the transition ${}^4I_{15/2} \rightarrow (15/2, 1)$ at 410.5 nm. For fitting purposes we only use transitions to the ${}^4H_{15/2}$ state.

Holmium

We followed the same basic fitting procedure for the holmium data as for dysprosium. The transition used in holmium for detection is from the ${}^4I_{15/2}$ ground state to the $(J_1, J_2) = (15/2, 1)$ state, at 410.5 nm. The exact configuration of the excited state in the L,S basis is unknown. A fit for the transition to the ${}^4J_{17/2}$ state was done at zero field. This transition accounts for the largest peaks in the spectrum as seen in Figure 3-5. At zero field and loading buffer gas densities, we see lifetimes of about 100 ms. Production of atoms is good, giving peak optical depths greater than one.

We load 5×10^{11} holmium atoms into a 12.4 K deep trap with about 8×10^{15} cm^{-3} buffer gas density at 330 mK. Unlike dysprosium, holmium has only one isotope. However, because I = 7/2, there are 7 hyperfine levels in the ground state and 9 in the

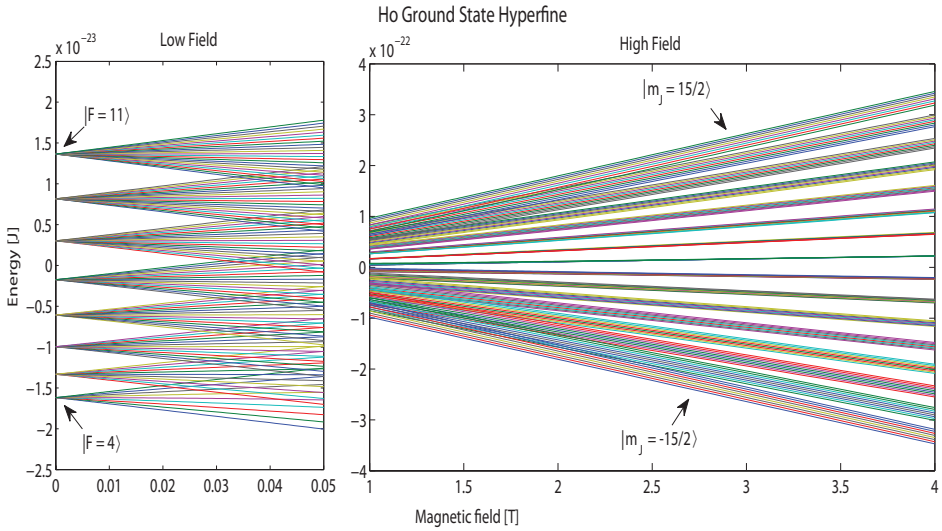

Figure 3-6: Energy levels of the $^4H_{15/2}$ ground state of ^{165}Ho as a function of magnetic field. We magnetically trap weak field seeking states. I = 7/2 and at high field J is a good quantum number. Each m_J manifold has 8 states corresponding to different m_I states.

excited state (see Figure 3-6). The spectrum is Zeeman broadened at high magnetic fields so that only the most populated hyperfine levels are resolvable. The separation of these states along with thermal broadening provide the necessary information for a reasonable fit. An example of a fit to a trapped spectrum is shown in Figure 3-7. The details of the spectrum are are not resolvable in the data. The spectrum is broad (about 12 GHz wide) and is difficult to scan across quickly.

In spite of complications with fitting the spectrum, the holmium data also supports a two-body loss model better than a one-body loss model. Figure 3-8 shows a typical fit to the data. We averaged over nine similar fits to attain the final value and uncertainty of g_{2b}.

3.4.2 Results

The results of our study of two-body collisions in holmium and dysprosium are summarized in Table 3.4. The uncertainty reported is the standard deviation of the two-body rate constant averaged from multiple data acquisition cycles. It does not

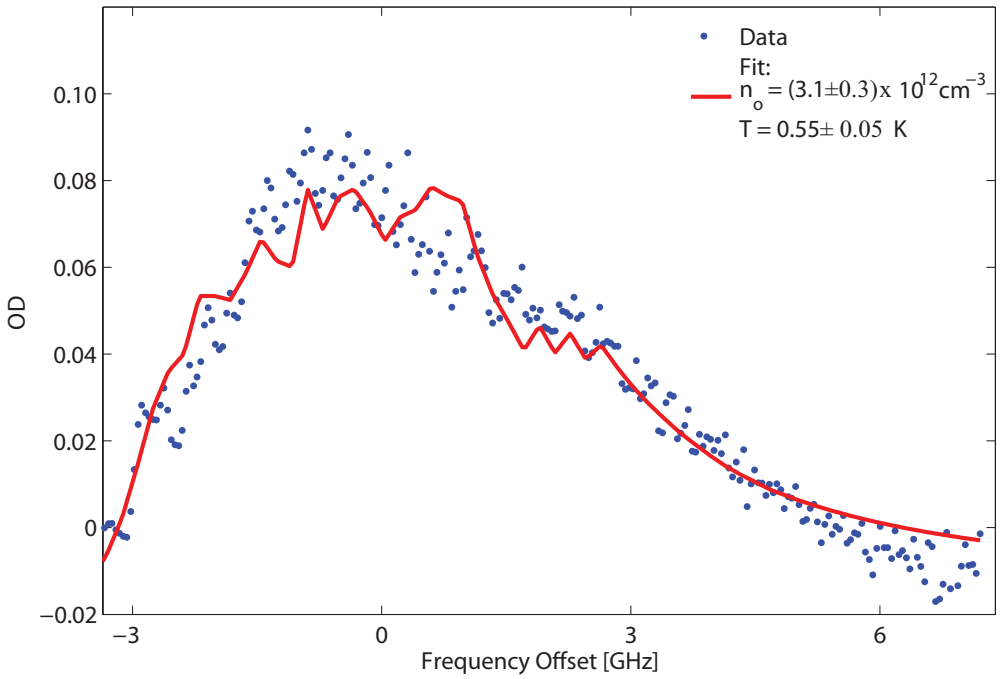

Figure 3-7: The spectrum of holmium trapped in an 12.4 K deep trap, taken 2.5 seconds after the valve is opened. The fit gives atom densities of $(3\pm0.3)\times 10^{12}$ cm^{-3} at 330±30 mK with $\tilde{\chi}^2 = 0.66$.

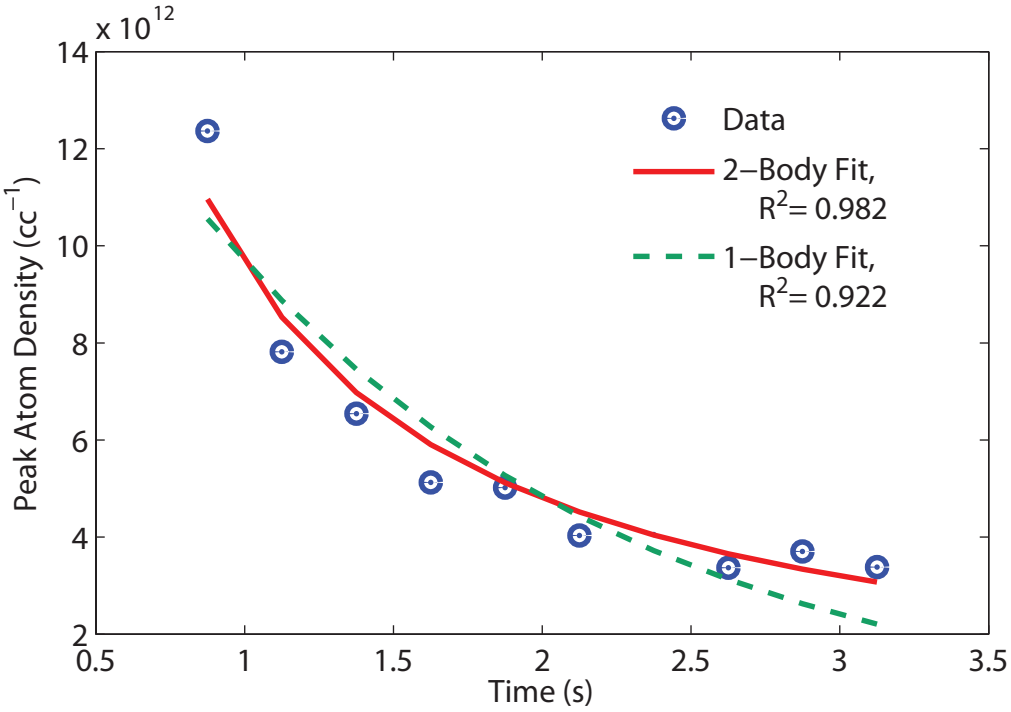

Figure 3-8: A comparison of a one-body decay model and a two-body decay model fit to the atom number density of holmium evolving over time. Each point on the plot was found by fitting the an average spectrum. The better agreement of the two-body fit implies that the loss mechanism is primarily due to atom-atom collisions.

	g_{2b} (cm^3s^{-1})	Temp. (mK)	σ_{dip} cm^2
Dy	$1.8(0.2)\times10^{-12}$	516(26)	$1.6(0.2)\times10^{-15}$
Ho	$0.72(0.14)\times10^{-12}$	403(57)	$0.7(0.2)\times10^{-15}$

Table 3.4: Final results from the study of Ho and Dy trap losses due to intra-atomic processes.

include systematic uncertainty in the spectrum model fitting. As seen above, the two-body rate constant is related to the collision cross section by the velocity of the collision.

$$g_{2b} = \sigma_{dip}\overline{v} \tag{3.21}$$

We assume that the rate of collisions is determined by the average thermal velocity and $\overline{v} = \sqrt{16k_BT/\pi m}$. In the absence of a shape resonance or Feshbach resonance the two-body rate constant should depend on temperature (through the velocity), but not on the average magnetic field. To check our that our measurements were not due to some other process that looked two-body, we performed the measurement at two different fields. We found good agreement within the uncertainty of our measurements at various fields.

If we assume that different species of atoms have similar interaction lengths, r, the dipolar cross sections should scale as μ^4. We can compare our results to similar measurements on hydrogen atoms, which found g_{2b}=$(1.2\pm.5)\times10^{-15}\,cm^3\,s^{-1}$ at 43 mK [87–89]. This corresponds to $\sigma_{dip}(H) = 3.5\times10^{-19}\,cm^2$. We estimate that σ_{dip} for rare earth atoms to be 10^4 times larger than the hydrogen cross section at a similar temperature. The collision cross sections we have measured are only 3×10^3 times larger hydrogen. This could be due to a slight suppression of the anisotropy of the interatomic potentials due to shielding from the filled s-shells [83].

In addition, we can compare the dysprosium and holmium measurements to each other. We expect for cross sections to scale such that σ_{dip}(Dy)= 0.66 $\sigma_{dip}(Ho)$. We measure the ratio to be 0.44, in reasonable agreement with the expected value. These comparisons uphold the hypothesis that the two-body decay rates is dominated by

dipolar relaxation.

In addition, these rates are favorable for evaporation. If the elastic atom-atom cross section is large (as found in collisions with He), γ_{2b} will be large, easily satisfying the requirement of 50 elastic collisions per inelastic loss, and evaporation will be feasible with these non-S state atoms. We report in Chapter 5 on successful adiabatic cooling of dysprosium atoms to 50 mK, and progress towards further evaporation. First, I will discuss the details of evaporative cooling in a buffer gas apparatus in the context of a model designed to take into account the affects of background gas. This model will be used to understand the data collected during evaporating.

Chapter 4

A Model of Evaporative Cooling

The technique of evaporative cooling has been key in the development of ultracold atomic physics and generally essential for cooling to the degenerate regime. Evaporative cooling refers to a variety of experimental techniques that preferentially remove more energetic atoms from a trapped sample. As these atoms are removed, the remaining trapped atoms rethermalize to a lower energy state, thus cooling the entire ensemble. It is similar to the mechanism through which a cup of coffee cools. This technique has been used in most experiments that have achieved degenerate dilute gases. The fundamental physics of evaporative cooling is now well developed. It is covered in many sources, such as Ref. [35, 47]. However, evaporative cooling in a buffer gas apparatus is a unique situation because of the more pronounced effects of background gas collisions.

Collisions with a background gas of un-trapped atoms lead to additional heating and loss during the evaporation process. In this chapter, I will develop a model of evaporative cooling in the presence of a background gas. This model is built upon previous work done in both this group at MIT and at Harvard by Doyle, *et al* [20, 46, 90, 91]. Previous success of evaporative cooling in a buffer gas apparatus has been achieved with ^{4}He as the buffer gas. The vapor pressure of ^{4}He at our loading temperatures is orders of magnitude less than that of ^{3}He , and too small to be used for trap loading. We have found that even with the removal of most of the buffer gas with the valve, there is still some small density of ^{3}He in the cell. This residual ^{3}He

is enough to affect the evaporative cooling process. Building on previous work, the model presented here expands our understanding of collisions with background buffer gas. Specifically, it incorporates a more realistic model of background gas collisions in the range where the background gas stops cooling and begins to heat the trapped sample. This model shows the need to reduce the background gas density to lower levels than previously believed necessary to achieve efficient evaporative cooling of the sample. In the remainder of the thesis, the model will expand our understanding of what is happening in the system at low background gas densities, temperatures, and trap depths.

In this chapter, I assume that the majority of the buffer gas has been removed from the trap region. I will refer to any residual buffer gas as the "background gas" and use the subscript bg. In addition, the background gas is non-magnetic and is unaffected by the trapping potential. Similarly, "atoms" (and the subscript at) will refer the trapped neutral atom that is being evaporated. For numerical calculations, I will assume that the background gas is ^{3}He. In addition, we will use the the elastic cross section of He with Dy as 1.4×10^{-14} cm$^-2$ [86], and with Li as 3×10^{-15} cm$^-2$ [16].

4.1 Methods of Evaporative Cooling

Today in cold physics, evaporative cooling is a term used to describe a variety of experimental techniques designed to cool trapped atom samples. In 1986, following the first observation of trapped of neutral atoms, Hess proposed a technique of decreasing the magnetic field at one point in the trap to allow atoms to escape and enhance cooling [35]. Hess made this proposal while working with the ultracold hydrogen group here at MIT. The group put the proposal to work in a high aspect ratio Iöffe-Pritchard trap, which they "opened" at one end. In this approach the confining radial gradient at the center of the trap remained constant during the evaporation. As the atoms cooled, they settled into the center of the trap, building up a density so high that the two-body dipolar decay became prohibitive. This problem was ad-

dressed by simultaneously lowering the radially confining magnetic field, though at a different rate optimized to achieve the most efficient cooling path. In 1988 Hess's theory was realized when hydrogen was evaporatively cooled to 1mK using this method [87]. A decade later, in 1994, the idea was combined with laser cooling techniques, as proposed first by Pritchard [12] in 1983, to evaporatively cool other alkali atoms. Using a radio frequency optical excitation, known as an "RF-knife", atoms are excited from trapped hyperfine levels to un-trapped hyperfine levels at a specific trap depth. In 1995, this technique was used in the first realizations of a Bose-Einstein condensate (BEC). It is now a standard experimental technique in the atomic physics community.

If the atom position in the trap is determined by total energy, then evaporative cooling can also be achieved by introducing a surface, such as a wall or window, into the trapping region. If an atom's orbit intersects a surface, it is removed from the trapping region. This is usually done by translating the trap minimum.

In our experiment we control the shape and magntitude of the magnetic potential by manipulating the currents in the two magnet coils. Evaporative cooling is achieved by lowering the overall trap depth at the walls or moving the atom cloud toward a surface like the window or mirror as described in Chapter 2. RF evaporation is not practical in our apparatus because the high magnetic trapping field requires impractically high frequencies of microwave power.

4.2 Collisions and Losses

Both thermalization and losses result from collisions between atoms in the trap, with other atoms and with the background buffer gas. Atom loss is either exothermic (cooling) or endothermic (heating). If the energy of the atom lost is greater(less) than the average trapped atom energy, the loss contributes to cooling(heating). In addition, collisions with hot(cold) background gas atoms, can add(subtract) energy from the atom cloud. Most evaporation models do not take into account the effects of background gas because these are negligible for most experimental setups. In a ^{3}He

buffer gas cooling apparatus however, the background buffer gas plays a much larger role. With this in mind, a number of phenomena need to be considered.

1. Collisions between two trapped atoms: These collisions can be both elastic or inelastic. However, both cause losses from the trap as described in Chapter 2. Inelastic collisions result in an un-trapped state. Inelastic collisions are most common in the high density low temperature region of the trap. These losses increase the equilibrium temperature of the cloud. Elastic collision cross sections determine the rate of cooling, as evaporation is due to elastic collisions bringing the system into thermal equilibrium.

2. Collisions with the background gas atoms: Background gas collisions can lead to heating of the trapped atoms because the background gas in is in thermal contact with the cell walls and can conduct heat to a cold atom sample. In addition, background gas atoms with enough energy lead to atoms being lost from the trap. For the purposes of this model, we assume that our buffer gas density is small compared to the necessary loading density of 10^{16} cm^{-3}. In this regime, the collisions with the buffer gas can cause atoms to be removed from the trap. Collisions with background gas that do not cause atom loss can either add or remove heat from the sample, depending on the temperature of the buffer gas.

3. As the magnetic field is ramped down, some atoms are removed from the trap before any thermalization can occur, as the tail of the Boltzmann distribution is effectively removed. We refer to these losses as forced evaporation.

4. Majorana losses due to the geometry of the trap minimum in a quadrupole trap: At the minimum of a quadrupole trap the magnetic field goes to 0 and then changes direction. If the gradient of the field at the trap minimum is so large that the atoms, precessing at the Larmor frequency, cannot follow the change in the magnetic field, the atoms can be lost from the trap. In general, this loss process plays a minor role.

5. Changes in the trap volume and geometry can lead to adiabatic heating and cooling with no atom losses.

In the next few pages, we will review each of these processes and give specific functional forms to atom number loss and the average energies involved.

4.2.1 Changing Trap Volume

The rate of all collisional atom loss processes depends on the density of atoms. As the trap shape is changed, the effective volume of the trap which an atom will explore, also changes. To understand how this volume evolves, we will start with the definition of the V_{eff} previously introduced in Equation 3.15 and restated here for clarity.

$$V_{eff} \equiv \int_0^{\vec{r}_{max}} e^{-U(\vec{r})/k_B T_{at}} dV$$

Such that $\mathrm{N} = n_o V_{eff}$ as defined in Chapter 3.

The volume integral extends over all $\vec{r}$, where $U(\vec{r})$ is less than or equal to the trap depth, U_{max}. As the magnet is ramped $U(r)$ changes, thus changing the effective volume. In our experiments the magnetic trapping field can be approximated by an ellipsoidal quadrupole field. Thus we can write a functional form of $U(\rho, z)$ where ρ and z are the radial and axial distances from the trap minimum.

$$U(\rho, z) = \mu\sqrt{(\beta_r \rho)^2 + (\beta_a z)^2}. \tag{4.1}$$

Here, β_r is the gradient in the radial direction and β_a is the gradient in the axial direction. When the magnitude, I, of the currents in each coil are equal, the trap depth is defined by the cell wall (radial surface) such that , $\beta_r = B_{max}/r_{wall}$. As can be seen in Figure 4-1, near the trap minimum $\beta_a = 2\beta_r$.

The trap volume changes if we evaporate against an axial surface. Figure 4-1 shows the changing trap potential and position as one magnet is ramped down while the other is held constant. As the trap depth is lowered, the trap minimum is translated towards the surface and the gradients also change. For the purposes of modeling the

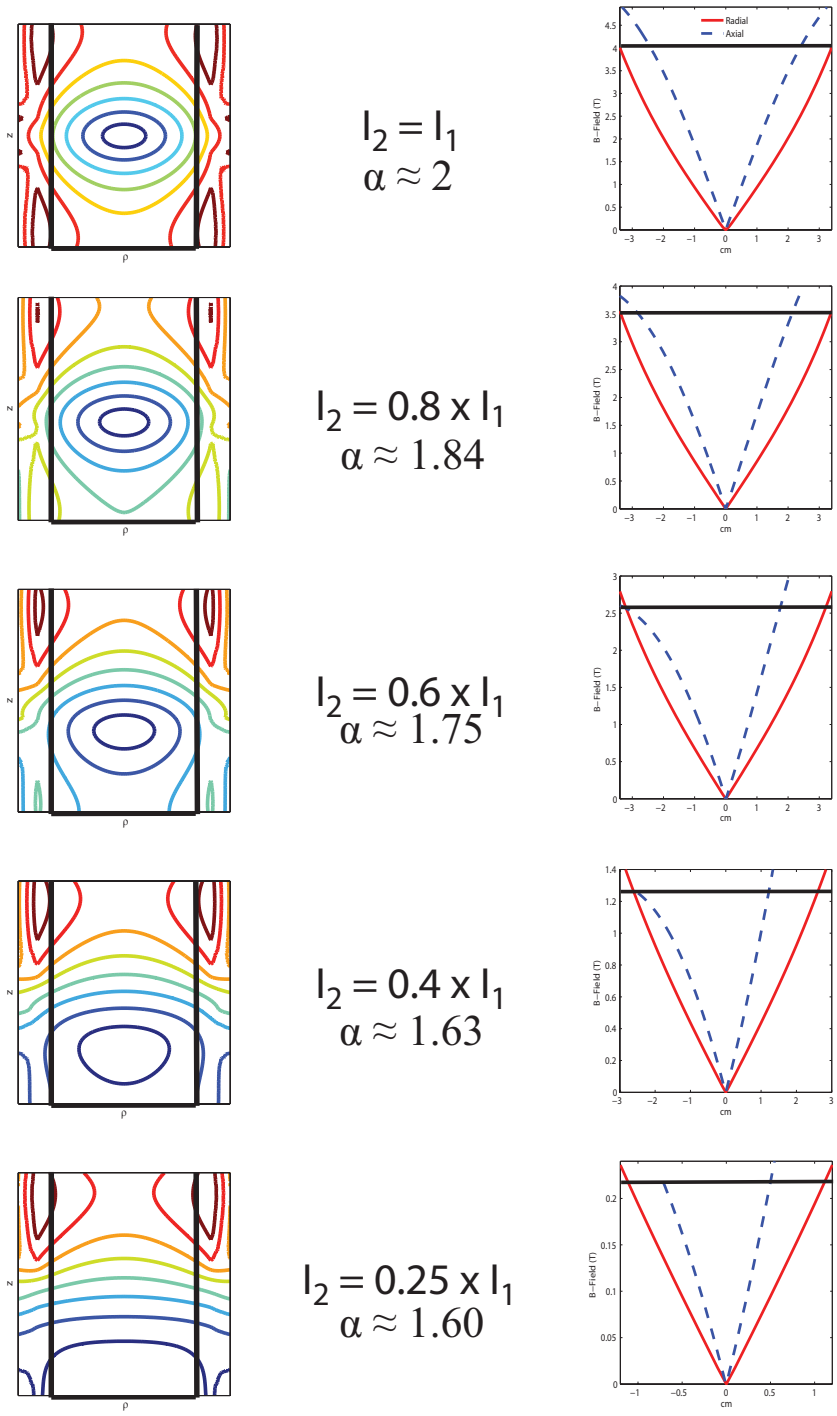

Figure 4-1: Simulations of the magnetic trapping potential during the ramp [51]. The solid lines on the contour plots are the outline of the cell. Contours are spaced every 1 T and assume $I_1 = 100$ A. Below $I_2 \approx 69\%$ I_1 the maximum trap depth is located on the axial window surface. α is the ratio of the gradients in the axial and radial directions. The right side panels show the magnitude of the magnetic field as a function of distance from the trap center in the radial (solid line) and axial (dashed line) directions. The solid line at the top of each plot defines B_{max}.

effective volume of the trap, we will assume that the trap is linear in both the axial and radial directions and define the parameter $\alpha \equiv \beta_a/\beta_r$. In the radial direction we can continue to estimate, $\beta_r = B_{wall}/r_{wall}$. In the axial direction, we can see from Figure 4-1 that the trap is not actually linear out to the evaporation surface. However, near the trap minimum, where the atom density is largest, its potential approaches linearity. We numerically calculate the trap gradient using Biot Savart [51].

In terms of α, the effective volume (for η greater than three) is approximated by

$$V_{eff} = \frac{8\pi}{\alpha}\left(\frac{R}{\eta}\right)^3. \tag{4.2}$$

Here R is the distance to the evaporation potential surface. Figure 4-2 is a plot of V_{eff} as the trap minimum is moved toward the window at constant η.

Implicit in this treatment is the assumption that the evaporation surface limits the trap at U_{max} in all directions. In reality, the evaporation surface occupies only a fraction of this potential space. At the edge of the trap, the density of trapped atoms is very low. The average time between collisions increases exponentially with the distance from the trap center, but the orbital period only increases linearly with distance. For a trap with η greater than four, an atom with energy greater than U_{max} will most likely encounter the evaporation surface before encountering another atom. Throughout the following discussion, we will use the assumption that atoms with energy close to the trap depth will orbit many times before interacting with other atoms.

4.2.2 Atom Loss from Atom-Atom Collisions

The physics of atom-atom collisions is discussed in Chapter 3. Here I will consider these collisions as they affect evaporative cooling. Elastic atom-atom collisions, while conserving total energy and the internal states of the atoms involved, can change each atom's kinetic energy. Imagine two atoms colliding near the edge of the trap. One atom is scattered into a lower energy orbit, while the other is scattered into a higher

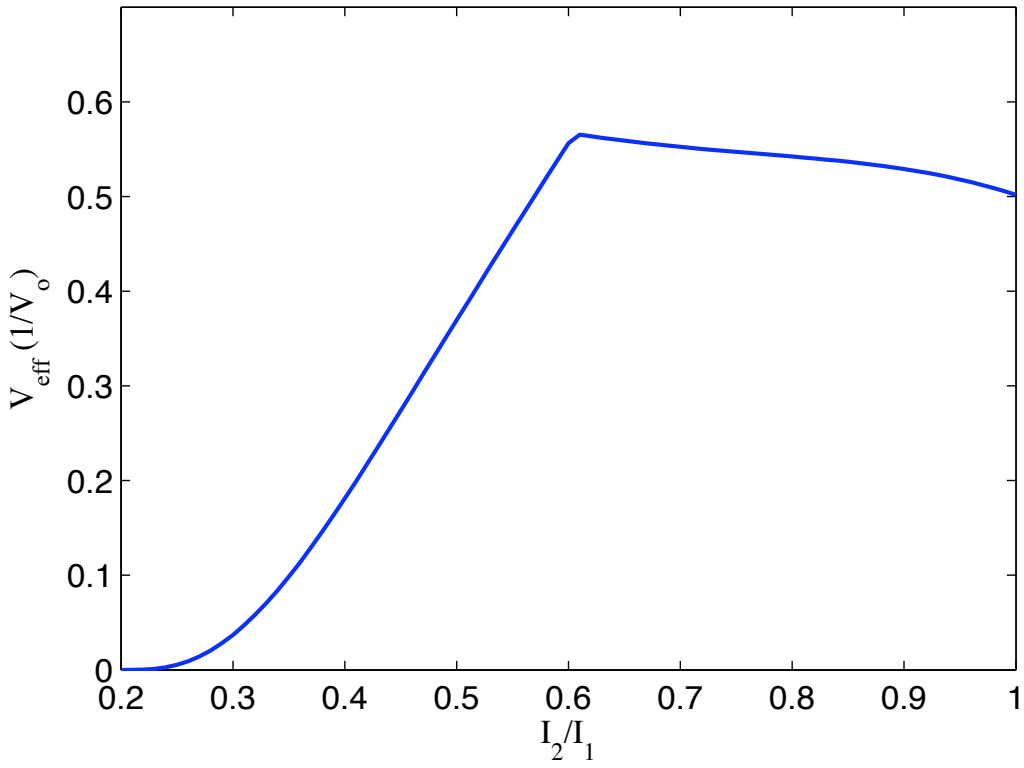

Figure 4-2: Simulation of the effective volume as a function of the ratio of currents in the two magnet coils for constant η. The vertical axis is normalized by the effective volume of a spherical quadrupole trap, $V_0 = 8\pi r_{wall}^3/\eta^3$. Around $I_2/I_1 = 20\%$, the trap minimum moves through the axial surface and all atoms would be lost.

energy orbit. If the energy of that new trajectory is larger than the trap depth and the atom does not encounter any other atoms, the atom will quickly be lost from the trap. On average atoms lost through this process carry energy larger than the average energy of the trap leading to cooling of the trapped sample. This is known as "evaporation" over the trap edge and is the physical process we aim to make most efficient by changing the trap depth.

We can write an equation describing the loss of atoms due to elastic evaporation as a function of trap depth η. We start by considering the atom loss at a position $\vec{r}$ in the trap.

$$\dot{n}_{ev}(\vec{r}) = -g_{el} n_{at}^2(\vec{r}) \tilde{f}_{ev}(\eta, \vec{r}) \tag{4.3}$$

As in Chapter 3, the loss of atoms is dependent on n_{at}^2 and is a two-body loss process. For atoms in thermal equilibrium, $\tilde{f}_{ev}(\eta, \vec{r})$ is the fraction of collisions in which one atom emerges with energy greater than the trap depth, $\eta k_B T_{at}$.

To calculate the total number of atoms lost we have to integrate equation 4.3 over the entire trapping volume.

$$\dot{N}_{ev} = -g_{el} \frac{V_{ev}}{8} \left(\frac{N}{V_{eff}} \right)^2 \tag{4.4}$$

Where [46, 47],

$$V_{ev} \xrightarrow[\eta \geq 4]{} 4\sqrt{2}\, \eta\, e^{-\eta}\, V_{eff}. \tag{4.5}$$

V_{ev} has units of volume and can be thought of as the fraction of trap volume which is evaporated from the trap in a single collision. .

In the case of inelastic collisions, the definition of the rate constant g_{in} assumes that every collision results in an atom loss. Following a similar process of starting with the local loss rate of $n(\vec{r})$ and integrating over the entire trapping volume, for all traps of the form given in Equation 4.1, we find

Loss Process	Evaporation (elastic)	Inelastic Collision	Majorana	Background Gas Collisions
Avg. Energy ($k_B T_{at}$)	(η +1)	3	9/2	0
Average Trapped Atom Energy $\langle E_{at} \rangle = 9/2 k_B T_{at}$				

Table 4.1: Average energies carried away by atoms lost from the trap by different processes for deep traps $\eta \geq 4$. Evaporation is a cooling process. Majorana and inelastic collisions cause heating. Losses due to buffer gas cause either heating or cooling. Detailed calculations can be found in Ref. [46]

$$\dot{N}_{in} = -g_{in} \frac{N_{at}^2}{8\, V_{eff}}. \tag{4.6}$$

For both of these types of losses $g = \sigma \overline{v}_{\mu}$. Changes in temperature affect the loss rate through the velocity.

To calculate the average energies of the trap and the atoms lost from the trap, we will assume a spherical quadrupole trap distribution[1]. deCarvalho calculated the average energies for atoms in an infinite spherical quadrupole trap for all η [46]. For large η, these are good approximations of the energies in the trap. For η less than four, the average energies begin to significantly decrease with decreasing η. This is because of the distortion of the normal Boltzmann distribution for small trap depths. However, at these low trap depths, evaporation is very inefficient. For most evaporation trajectories, the large η limit is sufficient.

The average energies of different loss mechanisms in the trap, for large η, are summarized in Table 4.1. Inelastic losses effectively heat the sample because they occur most frequently at the trap minimum where the density is the highest but the atoms are the coldest. Meanwhile elastic collision losses cool as they occur most frequently at the trap edges.

[1]To first order variations from the symmetric spherical quadrupole to a slightly elongated ellipsoidal geometry will affect the energy density of states by a factor, but will preserve the power law dependence on energy.

4.2.3 Collisions with the Background Gas

Buffer gas cooling experiments are especially susceptible to the effects of the background gas during evaporative cooling. Prior models of evaporative cooling in a buffer gas experiment have assumed that the residual background gas only causes atom losses, but does not affect the thermal equilibrium of the sample. In an experiment with ^{3}He , it is difficult to remove the buffer gas to densities where the thermal effects on the trapped atoms is negligible. To understand the full evolution of the trapped samples in our trap we have developed a model that includes these effects.

For an atom at any point, $\vec{r}$, in the trap, the rate of elastic collisions between atoms and background gas density and is proportional to the background gas density.

$$\Gamma_{bg} = n_{bg}\sigma_{bg}\overline{v}_{\mu} \tag{4.7}$$

Here, $\overline{v}_{\mu}$ is an average thermal velocity defined by Equation 3.3, and n_{bg} is the density of the background gas, and σ_{bg} is the cross section of the atom with the background gas.

The amount of energy transferred during the collision depends on the kinetic energy and mass of the atoms.

To treat this problem, we need to calculate the probability that an elastic collision between a trapped atom – with mass, M_{at}, and in equilibrium with a thermal reservoir at temperature, T_{at} – and a background gas atom – with mass, m_{bg}, in thermal equilibrium with a thermal reservoir at temperature, T_{bg} – will result in the trapped atom increasing its kinetic energy above a certain reference amount. Calculating this probability is further complicated by the distortion of the trapped atom energy distribution, limited by the finite trap depth. We will make the following simplifying assumptions:

- The spatial distribution of atoms in the trap is $n(\vec{r}) = n_o\, e^{-U(\vec{r})/k_B T_{at}}$ for $r \leq r_{max}$ and 0 elsewhere. r_{max} is the radius of the trapping potential.

- At each point $\vec{r}$, the atoms are in thermal equilibrium with the other trapped

atoms, and the average kinetic energy of any atom is $(3/2)\,k_B T_{at}$.

- The background gas density is constant throughout the trap.
- The background gas is in thermal equilibrium with the cell walls so that $T_{bg} = T_{cell}$. The average thermal kinetic energy of the background gas is $3/2\,k_B T_{bg}$.
- The average energy transport cross section will be weighted by a unitless factor χ related to the masses of the atoms. This factor is separated from any statistical averaging of the trapped ensembles. This is described in more detail below.
- Finally, we will assume that a collision with background gas atoms can result in either an immediate atom loss or heating of the total atomic sample, but not both. This continues the assumption used previously that once an atom is excited to an energy greater than the trap maximum, it leaves the trap before interacting with other atoms.

Armed with these assumptions, we developed a model to account for collisions with a low density of background gas atoms in a finite magnetic trap.

In her thesis, Kim [92] shows that in a single collision between two atoms at and bg, with masses M and m respectively, the average energy transferred from atom at to atom bg, integrated over all scattering angles, can be described by

$$\langle \Delta E \rangle = \chi(M, m)(K_{bg} - K_{at}). \tag{4.8}$$

Here $K_{at,bg}$ is the kinetic energy of each atom respectively, $3/2 k_B T_{at,bg}$ in this case, and $\chi(M, m)$ describes the efficiency of energy transfer of two particle of different masses for any collision.

$$\chi(M, m) = \frac{2Mm}{(M+m)^2}. \tag{4.9}$$

An atom at position $\vec{r}$ in the trap has total energy E_{at}, with potential energy $U(\vec{r}) = \mu B(\vec{r})$, and kinetic energy K_{at}. After a collision with a background gas atom, the total energy of the trapped atom is $E_{new} = E_{at} + \langle \Delta E \rangle$. If E_{new} is greater than

the trap depth, $U_{trap} = \mu B_{max} = \eta k_B T_{at}$, the atom will leave the trap. For collisions where $E_{new} < U_{trap}$, the atom does not leave the trap but instead redistributes energy, $\langle \Delta E \rangle$, to the other atoms. If the background gas is hotter than the atoms, this causes heating of the entire sample.

The rate at which the atom number decreases due to collisions with the background gas is just the collision rate scaled by the fraction of collisions which result in E_{new} greater than U_{trap}. The rate at which atoms are lost due to collisions with the background gas, $\dot{N}_{at \cdot bg}$, is

$$\dot{N}_{at \cdot bg} = -\Gamma_{bg} N F_{bg} = -n_{bg} \sigma_{bg} \overline{v}_{\mu} N F_{bg}. \tag{4.10}$$

Here F_{bg} is the volume averaged fraction of background gas collisions which result in E_{new} greater than U_{trap} causing the loss of an atom from the trap. All other background gas collisions cause heating. Any atom with potential energy greater than $U_{max} \equiv U_{trap} - 3/2 k_B T_{at} - \langle \Delta E \rangle$ will leave the trap after a collision with a background gas atom. Using the distribution of atoms in the trap from the first assumption above, we find the fraction of collisions which will cause an atom to leave the trap, F_{bg}.

$$F_{bg} = \frac{\int_{U_{max}}^{U_{trap}} e^{-U/k_B T_{at}} U^2 dU}{\int_{0}^{U_{trap}} e^{-U/k_B T_{at}} U^2 dU} \tag{4.11}$$

Figure 4-3 plots F_{bg} with η of 7 and $T_{bg} = 200$ mK, as a function of atom temperature. For large mass ratios ($M_{at} \gg m_{bg}$), the background gas removes fewer atoms out of the trap once the atoms are colder than the buffer gas. This means that heavier atoms are in thermodynamic contact with the background gas atoms to lower temperatures. This would make it difficult to get effective cooling during evaporation. For smaller mass ratios on the other hand, the sample is very sensitive to background gas losses once the trap depth has been lowered.

We can also look at the lifetime due to background gas collisions versus atom temperature, shown in Figure 4-4. We set $\eta = 7$ and $T_{bg} = 200$ mK and the buffer

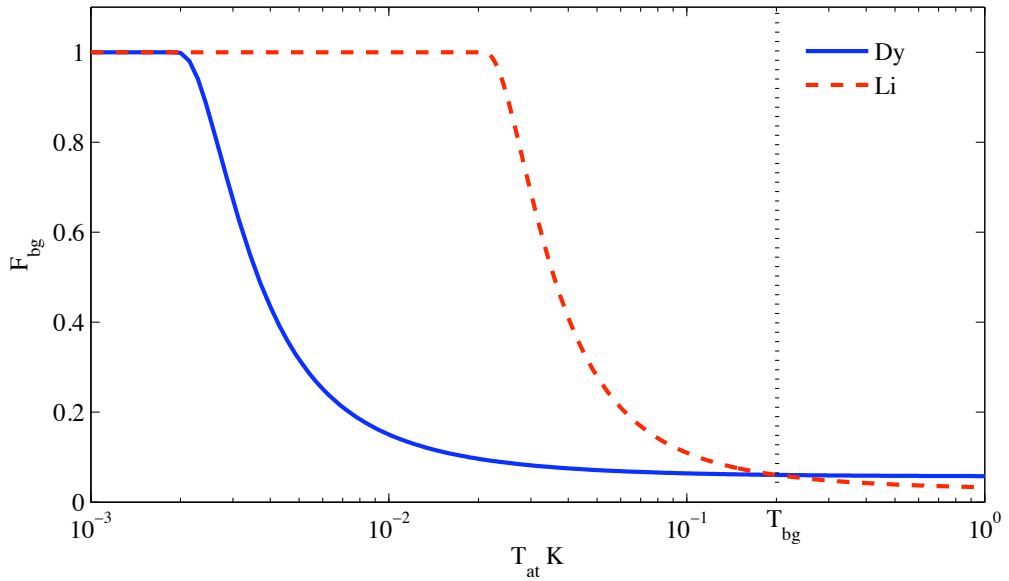

Figure 4-3: Fraction of collisions with a background gas of ^{3}He that result in an atom immediately leaving the trap as a function of atom temperature. The model assumes evaporation on the walls (radial) with constant $\eta = 7$ and $T_{bg} = 200$mK. Even at high temperatures, the kick fraction does not go to zero for a finite trap; some collisions will still cause losses. As the temperature of the atoms decreases below the temperature of the background gas the fraction of collisions leading to atom loss will increase. Eventually, for very cold atoms, all collisions will lead to losses.

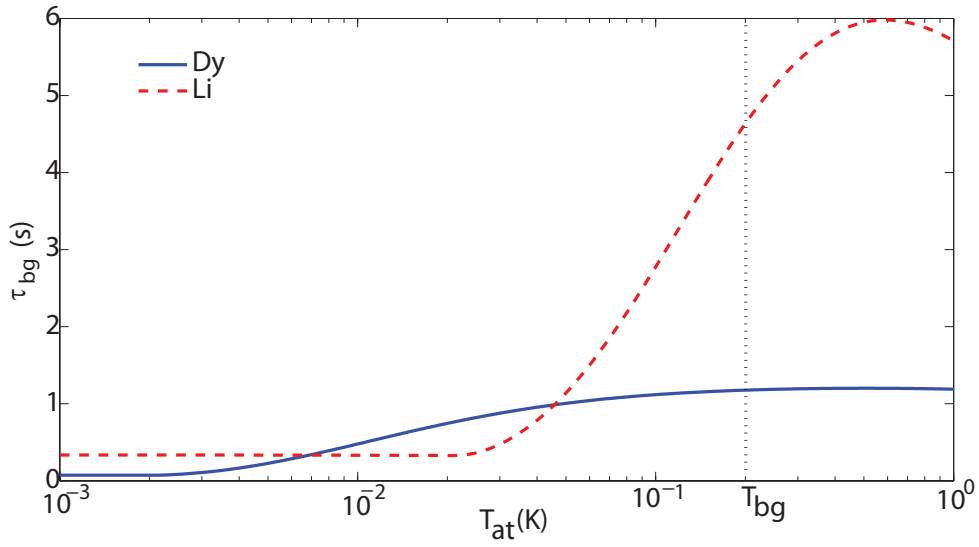

Figure 4-4: The lifetime due to atoms being energized into an un-trapped orbit and then lost from the trap ($\eta = 7$) due to background gas collisions. This process only decreases the atom number. The background gas is at constant density of 10^{11} cm^{-3} throughout the trapping region at T_{bg}.

gas density is set to 10^{11} cm^{-3}. To understand this plot, we start on the far right of the figure where the atoms are hotter than the background gas. As the atoms cool the lifetime increases because the rate of collisions is decreasing as the atoms slow down. At the same time, very few of these collisions will remove atoms from the trap. If the atoms are significantly colder than the background gas, a larger fraction of background gas collisions remove atoms from the trap. For very cold atoms, almost all collisions result in atom losses the lifetime approaches the collision rate.

Background Gas Heating

Interactions with background gas atoms thermalize the atoms to the temperature of the environment, in our case the cell walls. In our model, the background gas collisions that do not result in immediate atom loss add energy $\langle \Delta E \rangle$ to the ensemble. $\langle \Delta E \rangle$ is either positive or negative depending on whether the background gas is hotter or colder than the atoms.

Using the assumptions outlined above, we write an equation for the heating due

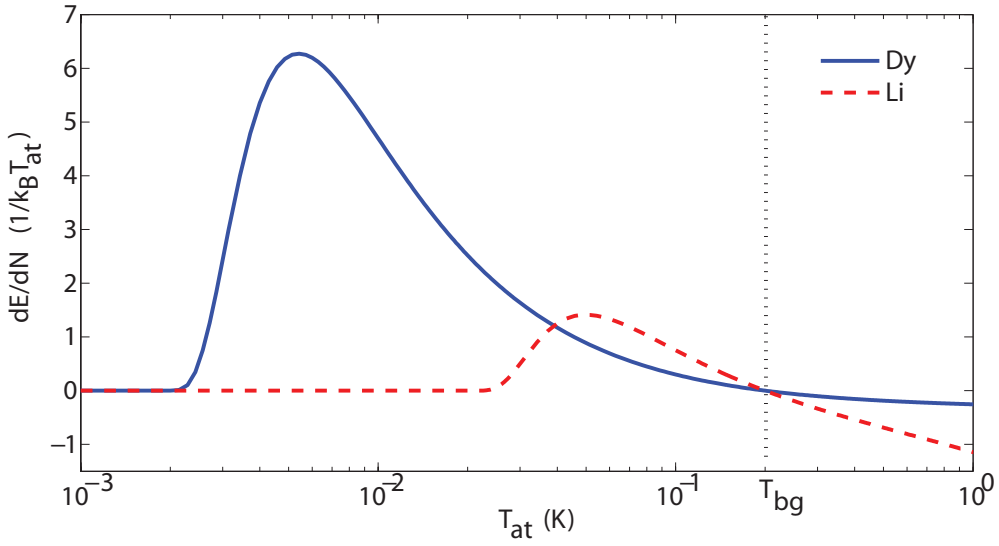

Figure 4-5: Energy absorbed per atom due to background gas collisions during evaporation at $\eta = 7$, as a function of atom temperature. Background gas density is 10^{11} cm^{-3}and $T_{bg} = 200$ mK. When the atoms are hot, interactions with the background gas cool the sample. As the atoms cool below the temperature of the background gas, the collisions start to heat the system. Finally, at low enough temperatures, atoms are removed from the trap by most collisions and cause no extra heating.

to buffer gas for the entire trapped volume.

$$\dot{E}_{bg} = \Gamma_{bg} N (1 - F_{bg}) \langle \Delta E \rangle \tag{4.12}$$

Figure 4-5 shows total heating of atoms due to background gas for a constant $\eta = 7$. For larger atoms, we see that they are thermally affected by the buffer gas for a larger range of temperatures. Not until the atoms are very cold are they fully disconnected from the cell walls. In Section 4.4, we will put a limit on the buffer gas density that can be tolerated in the cell during evaporation. But first let us finish considering the other loss processes occurring in our trapped sample.

4.2.4 Other Loss Processes

Other physical phenomena contribute to the dynamics of the system during evaporation. These include losses due to the immediate "forced" evaporation of any atoms

with energy greater than the trap maximum; Majorana losses due to the zero field at the trap minimum; and adiabatic cooling as the trap volume changes as the magnetic field changes.

As the magnet is ramped down, atoms with total energy greater than the trap depth will be immediately removed from the trap. In the limit of large η, the fraction of atoms in a ergodic trap with energy greater than the threshold energy, $\eta k_B T$ is $2\sqrt{\eta/\pi}e^{-\eta}$, independent of trap geometry [47]. At a given temperature, the rate of atom loss due to "forced" evaporation, N_f, is determined by the rate of ramping [91].

$$\dot{N}_f = 2\sqrt{\frac{\eta}{\pi}}e^{-\eta}\frac{\mu\dot{B}}{k_B T}N. \tag{4.13}$$

This loss is in addition to the loss due to continued evaporation at a constant trap depth described by Equation 4.4. On average each of the atoms removed has energy $E_{ev} = (\eta + 1)k_B T$. This is greater than the average trap energy and leads to cooling.

Majorana losses occur in the minimum of the trap. These losses are due to the zero-field minimum of the trap where the magnetic field direction changes direction in such a way that the atoms can not adiabatically follow. An atom aligned with the magnetic field in the positive z hemisphere crossing through the origin will now see a magnetic field pointing in the opposite direction. If the atom crosses the zero field point faster than it can precess about the magnetic field, then it will be in an un-trapped state and leave the trap. For a quadrupole trap, N_{maj} scales as [79],

$$\dot{N}_{maj} \propto 4\frac{\hbar}{m}\frac{N}{V_{eff}}\frac{k_B T}{\mu B' \Delta m_F}. \tag{4.14}$$

Where B' is the absolute value of the gradient of the trap at the minimum and Δm_F is difference in spin projection which would take the atom from a trapped spin state to an un-trapped spin state. The expression is not exact. Defining an exact expression requires summing over transitions into each of the lower Zeeman levels. These losses scale roughly as η^2 as the magnetic field changes. Not only do these atoms decrease the eventual sample size, they are also the coldest atoms in the trap, with potential energy approaching zero. Each atom loss increases the average energy

in the trap. In larger atoms, like dysprosium, with relatively high inelastic collision rates, the lifetime due to Majorana losses, τ_{maj}, is greater than 10^4 s and should not play a major role in evaporation [93]. Majorana lifetimes can be limiting however for smaller mass atoms with small inelastic cross sections, like lithium.

Finally, there is adiabatic cooling due to the changes in trap volume during evaporation. In our experiment, we change the absolute magnitude of the magnetic field as well as the trapping geometry during evaporation. This changes the volume of the trap causing a change in the internal energy and cooling of the system, according to

$$\dot{E}_{ad} = 3k_B T \frac{\dot{B}}{B} N. \tag{4.15}$$

4.3 Assembling the Pieces

Combining all of the processes described in the previous sections, we can develop a model to predict atom number as a function of time.

$$\dot{N}_{at} = \dot{N}_{ev} + \dot{N}_{in} + \dot{N}_{a\cdot bg} + \dot{N}_f + \dot{N}_{maj} \tag{4.16}$$

For each atom lost, the heating or cooling that occurs in the trap is determined by amount of energy it carries away compared to the average energy of an atom in the trap. For large η, the average energy per atom can be shown to be

$$\overline{E} = 9/2 k_B T_{at} \tag{4.17}$$

We can use this to find the evolution of the atom temperature as a function of time.

$$\begin{aligned} \dot{T}_{at} = \quad & \tfrac{2N}{9k_B}[(E_{ev} - \overline{E})\dot{N}_{ev} + (E_{in} - \overline{E})\dot{N}_{in} \\ & + \dot{E}_{bg} + (E_f - \overline{E})\dot{N}_f + (E_{maj} - \overline{E})\dot{N}_{maj} + \dot{E}_{ad}] \end{aligned} \tag{4.18}$$

We solve these differential equations for a set of initial conditions and set of parameters using a first order differential solver in Matlab [94]. We define $g = \sigma \overline{v}_\mu$ and incorporate the change in collision rate through the thermal velocity. We assume the cross sections for each collision process (elastic, inelastic and background gas) to be constant in the temperature ranges discussed in this thesis. In addition, we assume the background gas temperature decays exponentially with the same time constant of the cell walls. We calculate the evolution of the buffer gas density as discussed in Appendix A. Finally, we specify the currents of the two magnet coils as a function of time to calculate the trapping potential during the evaporation.

4.3.1 Evaporation Efficiency

To gauge the success of evaporation, we can look at the kinetic energy lost per atom. We define a parameter χ_e as the efficiency of evaporation [47].

$$\chi_e \equiv \frac{\dot{T}/T}{\dot{N}/N} \tag{4.19}$$

In other words, we can compare the fraction of energy removed from the trap to the fraction of atoms removed from the trap. If $\chi_e > 0$, the atom sample is cooling overall. If $\chi_e < 0$, the atom sample is actually being heated. Previous successful attempts at evaporative cooling achieved $\chi_e \geq 1.5$. For efficient evaporation, we would like to maximize χ_e.

In the absence of significant background gas, χ_e is a function of η. We could define η_{opt} to achieve the best evaporation that we could attain by continually changing the currents in the magnets to maintain constant η_{opt} in the trap. However, in the presence of background gas, χ_e is also a function of T_{bg}. This will change η_{opt} as we lower the trap depth and lead to a more complicated evaporation trajectory.

4.4 Thermal Isolation

The atoms become thermally isolated from the buffer gas when the cooling rate from evaporation (ie. atom-atom elastic collisions) exceeds the heating due to buffer gas collisions[2]. As seen in above, the amount of heating due to the background gas varies depending on the trap depth, the cell temperature, and the atom temperature. Using equations 4.4 and 4.12, and the average energy of an evaporated atom (Table 4.1), we can write an equation for the isolation buffer gas density as a function of η.

$$n_{iso}(\eta) = n_{at}\frac{\sigma_{el}}{\sigma_{bg}}\left(\frac{2\,T_{at}}{T_{at}+\frac{M}{m}T_{bg}}\right)^{1/2}\frac{V_{ev}}{V_{eff}}\frac{(\eta-3.5)}{(1-F_{bg})\,\langle\Delta E\rangle} \tag{4.20}$$

In the range where the background gas is hotter than the atoms, we plot Equation 4.20 in Figure 4-6. For thermal isolation of the atom sample, the background buffer gas density must be removed below the minimum of the curve in Figure 4-6. For a density of 10^{11} cm^{-3} dysprosium atoms, $n_{iso} \sim 10^{10}$ cm^{-3}. Below this buffer gas density, the cooling from the evaporation will dominate. For more efficient evaporation, the background gas density should be at least ten times smaller than the minimum. For colder atom temperatures, n_{iso} increases because background gas collisions simply remove atoms from the trap.

Decreasing η moves the curve in Figure 4-6 up and narrows the range of temperatures that cause heating. Evaporation at a lower η might be more successful. However, lowering η also makes evaporation less efficient, in that each evaporated atom carries less relative energy. Increasing the density of the trapped atoms would also increase n_{iso}. However, losses and heating due to inelastic collisions increase as n_{at}^2, making evaporative cooling very inefficient. Finally, one can imagine first adiabatically cooling the atoms into a regime where the buffer gas is mostly causing atom loss but no heating. If this could be done, the atoms would be thermally isolated from the background gas. However the lifetime would be limited by these collisions.

[2]We can neglect the other processes if we assume constant η. Adiabatic cooling will be zero, as will forced evaporation. The other processes lead to heating of the sample, but independent of the cell temperature.

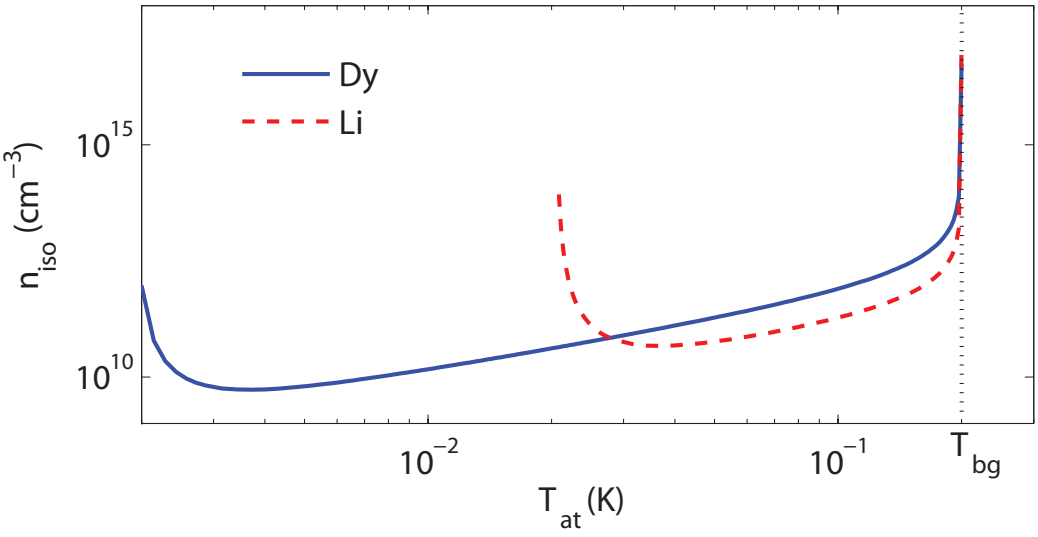

Figure 4-6: The maximum background gas density tolerable for thermal isolation of the trapped atoms, as a function of T_{at} for an $\eta = 7$ and $n_o = 1 \times 10^{11}$ cm^{-3}. Plot assumes σ_{el}(Li) $= 1.3 \times 10^{-13}$ cm^2 [73] and σ_{el}(Dy) $= 8 \times 10^{-14}$ cm^2, which is estimated in Chapter 5.

4.5 Applications of the Model

Evaporation is a dynamic process. The decrease in atom number, necessary for cooling, can also decrease signal making it difficult to make measurements. Until cooling is observed, which will increase the optical depth due to increased density of atoms at in the cold center of the trap, it is hard to monitor the changing physical properties of the atoms in the trap. In the next chapter, we will use the model described in this chapter to help understand the data taken during magnet ramps. The model accepts variations in the atomic species, the starting temperature, the initial number of trapped atoms, the buffer gas density, and the ramp trajectory. In addition to these input parameters, we can vary the rates of elastic and inelastic collisions. By fitting to the data available during the ramp process, we can make educated guesses about the changing dynamics of the atom sample.

Chapter 5

Evaporative Cooling of Dysprosium

Successful evaporative cooling has been limited to atoms with no orbital angular momentum, or S-state atoms. The electron density distribution of an S-state atom is spherically symmetric. The electronic interaction of two colliding S-state atoms does not strongly drive spin relaxation from the most weak field seeking Zeeman level and the ratio of elastic to inelastic collisions, γ_{2b}, is large.

For non-S-state atoms, the interaction of the atoms' magnetic dipoles during the collisions can cause rapid decay from the trapped spin state. Previous attempts made by other groups have found it to be virtually impossible to evaporatively cool other non-S-state atoms such as strontium [41–43].

The measurements of the two-body rate constants for dysprosium and holmium described in Chapter 3 suggest that these rare earth atoms may have slightly suppressed inelastic collision rates. If the elastic collision rates are similar to alkali-alkali atoms ($\sim 10^{-}15$) then about 100 elastic collisions could occur for every inelastic collision, large enough to permit efficient evaporative cooling. The large magnetic dipole moments of dysprosium and holmium atoms increase the dipolar relaxation rate but allow for trapping in that we can use much smaller currents to trap the atoms. This makes ramping much easier as there is much less power to dissipate.

Armed with the model developed in the last chapter, we can try to understand what is going on inside of the system during the dynamic process of lowering the trap depth. In this Chapter, I will describe two experimental runs where we attempted

evaporative cooling of dysprosium atoms. In the second attempt, we demonstrated successful adiabatic cooling from 300 mK to 50 mK. In the last section I propose future experimental plans to enhance this cooling.

5.1 Initial Attempt: Slow Ramp with Rapid Atom Loss

We made a series of initial attempts to evaporatively cool dysprosium by ramping the magnets such that the atoms moved toward the window at the bottom of the cell. For atom densities of about 1×10^{12} cm^{12}, the 1/e time of the trapped atoms due to inelastic collisions is about 10 seconds. In the first run, the ramp was controlled using the magnet power supplies which are internally limited to -1.7 A s^{-1} ramp rates for the inductive loads of our coils. The slow ramp rate means that the time necessary to ramp to an η sufficient for evaporation is on the same order as the inelastic collision loss lifetime.

We started by loading into an asymmetric trap with 30 A and 20 A in the top and bottom coils respectively. At this ratio of currents the magnetic field at the wall and the window is approximately the same and corresponds to a trap depth of 0.94 T or 6.25K. Cooling was attempted by decreasing the current in the lower coil. As the current in the lower coil is decreased, the trap minimum moves toward the window and the trap depth becomes determined by the field strength at the window, allowing the atoms to evaporate against this surface.

We load about 10^{11} dysprosium atoms at 350 mK into the asymmetric trap, through a hot loading scheme where the cell is heated to approximately 350 mK before the samples are ablated. The valve is opened 100 ms after the ablation pulse. The lower coil is ramped from 20 A to 14 A in about 5 seconds. We expect to observe initial cooling due to adiabatic expansion as the trap volume is increased of about 35 mK, followed by evaporation of atoms and possible cooling. Instead, we see an initial increase in the temperature as seen in Figure 5-1.

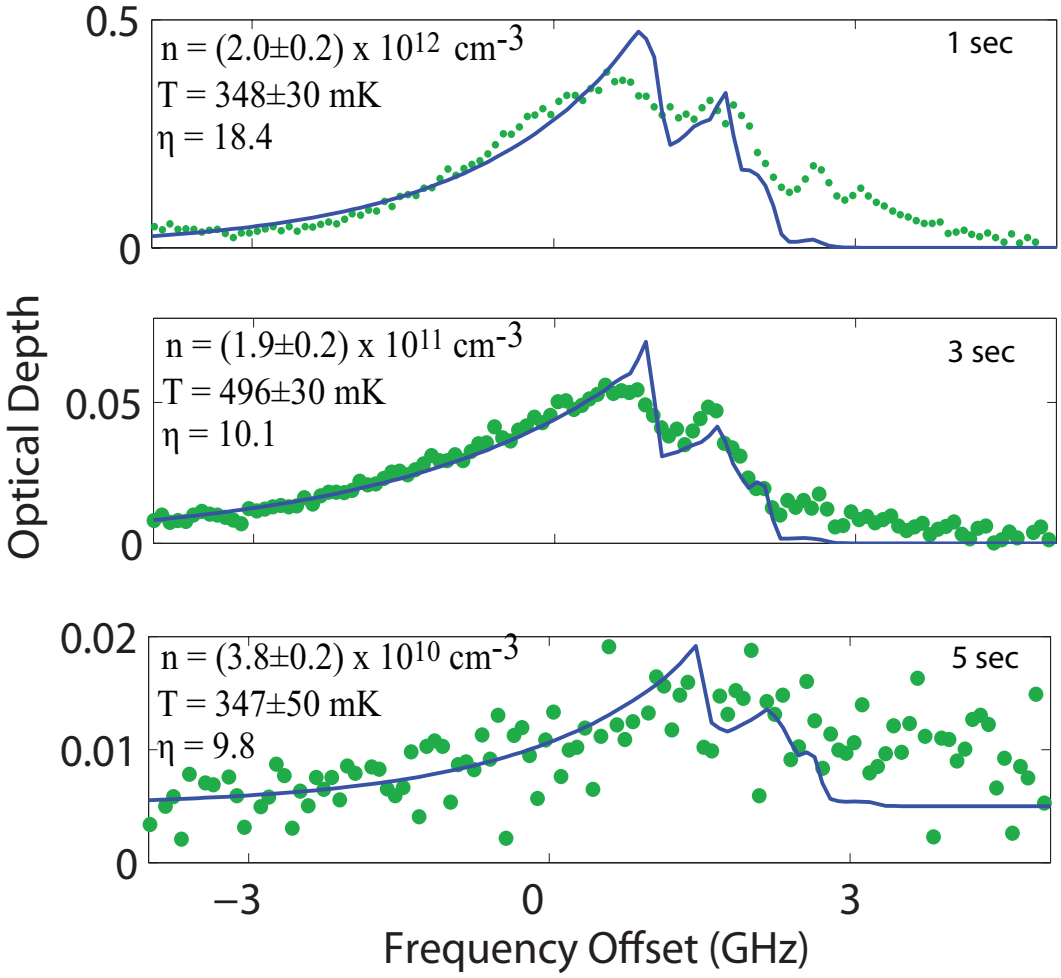

Figure 5-1: The first attempt to cool dysprosium. It was determined that the magnet ramp was too slow and we lost all atoms before the magnet ramp ended.

We also see a large decrease in signal during the ramp. This could be because of either atom loss or a decrease in density due to the changing volume. At the beginning of the magnet ramp η is approximately 18. With no cooling during the ramp, η is only decreased by a factor of two by the end of the ramp. As the effective volume scales as η^{-3}, we would expect to see the density to decrease by a factor of 6. Instead the peak density drops by a factor of 100. From this we conclude that we are observing atom number loss.

To explain this loss, we return to the different loss mechanisms described in the last chapter. For large η, the fraction of the atoms lost due to evaporation over the trap edge is very small. Therefore the atom loss must be due to inelastic collisions and/or collisions with the buffer gas. However these two losses are distinguishable. We fit the number density as a function of time and find that it fits well to a one-body curve decay curve with a time constant of 1.5 s, Figure 5-2. From this we conclude that there are significant losses due to buffer gas during this ramp.

If the culprit is indeed buffer gas, we need to accomplish two things. The first is to ramp faster in order to finish the ramp before buffer gas collisions destroy the sample. The second is to decrease the background gas as much as possible.

5.2 Modifications

To increase the ramp rate, we installed large shunt resistors which allow us to ramp down the magnets at a rate of 10 A/s.

To increase the signal-to-noise ratio when loading a large volume trap, we removed the lens that focused the probe beam onto the atom cloud. Additionally, the beam radius was increased to 0.5 cm – the width of the retro-reflecting mirror at the top of the cell – in order to see as much of the cloud as possible.

As these changes were being made, the apparatus was warmed up and it was discovered that the heat link from the cell wires to the mixing chamber was not well attached. This connection was tightened. Upon cool down, the time constant for cell cooling had decreased by a factor of 2 and the minimum base temperature dropped

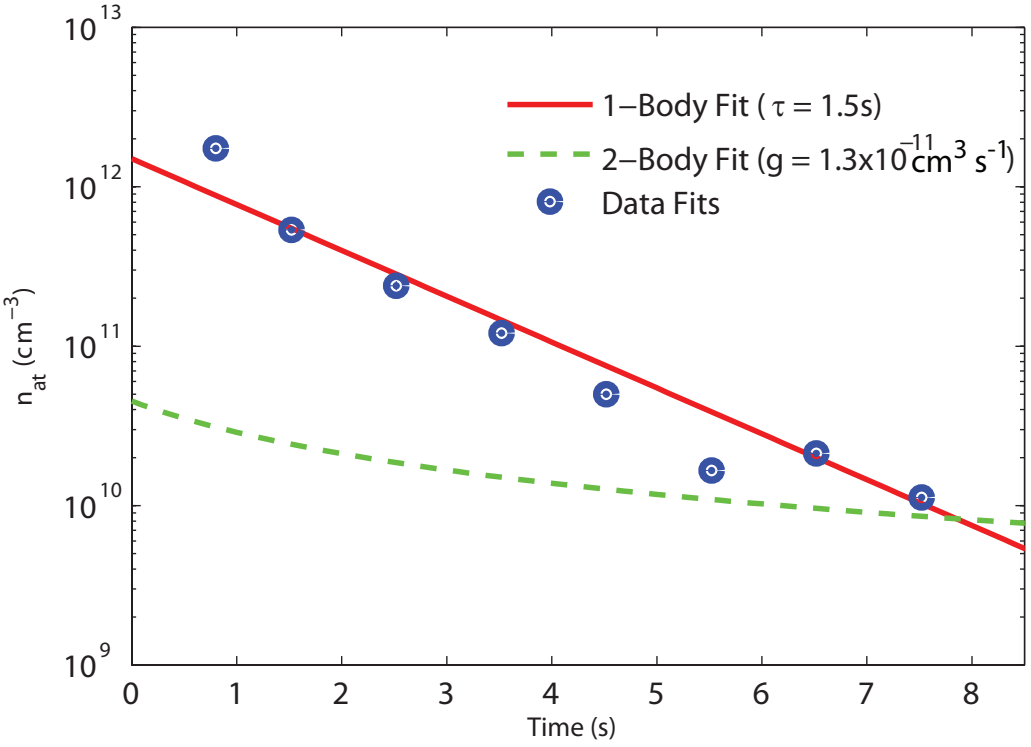

Figure 5-2: The first attempt to cool dysprosium. It was determined that the magnet ramp was too slow and we lost all atoms before the magnet ramp ends.

by 30 mK. The lower cell temperature allowed us to use the YAG ablation pulse to desorb enough buffer gas from the cell walls to load the trap while placing a minimum heat load on the cell. This procedure is well suited for loading atoms into the cell at a colder starting temperature. In addition it makes it easier to cool the cell to lower temperatures more quickly after the ablation pulse.

5.3 Evaporative Cooling

Once the new magnet ramping system was in place, the first experimental ramp, which ramped both magnets to zero, showed cooling of trapped dysprosium atoms to 50 mK. During this experiment, the atoms were loaded using the "cold loading" method described in Chapter 2. The valve was never opened. Approximately 100 ms after the ablation pulse, a switch that bypasses the shunt resistors was opened and the current was allowed to fall to zero amps in both coils simultaneously. This procedure maintains the relative gradients in both the axial and radial directions and aims to evaporate against the cell walls.

Before the ramp, we loaded 1×10^{12} dysprosium atoms at 300 mK in a 5.6 K deep trap. We fit to the spectrum to get specific information about atom number and temperature. Figure5-3 shows the evolution of the temperature of the atoms. The After eight seconds there was about 0.2 A of current in the coils. This corresponds to a 56 mK deep trap. We fit the atomic spectrum here for 7×10^{10} atoms at 54 mK.

We fitted the data using the model developed in the last chapter. The input parameters for the model are the currents in each coil at each time, the starting temperature and density of the buffer gas atoms, and the starting temperatures and density of the trapped atoms. In addition, we input the calculated spectrum the cross sections for each collision process. To achieve a better fit, the starting buffer gas density and the atom-atom elastic cross section are varied.

The model begins just after the ablation pulse or about 0.5 seconds before the coils are ramped down. We assume a exponential decay of the currents from 20 A to 0 A with a time constant of 2.2 seconds. The first data point is one second after the

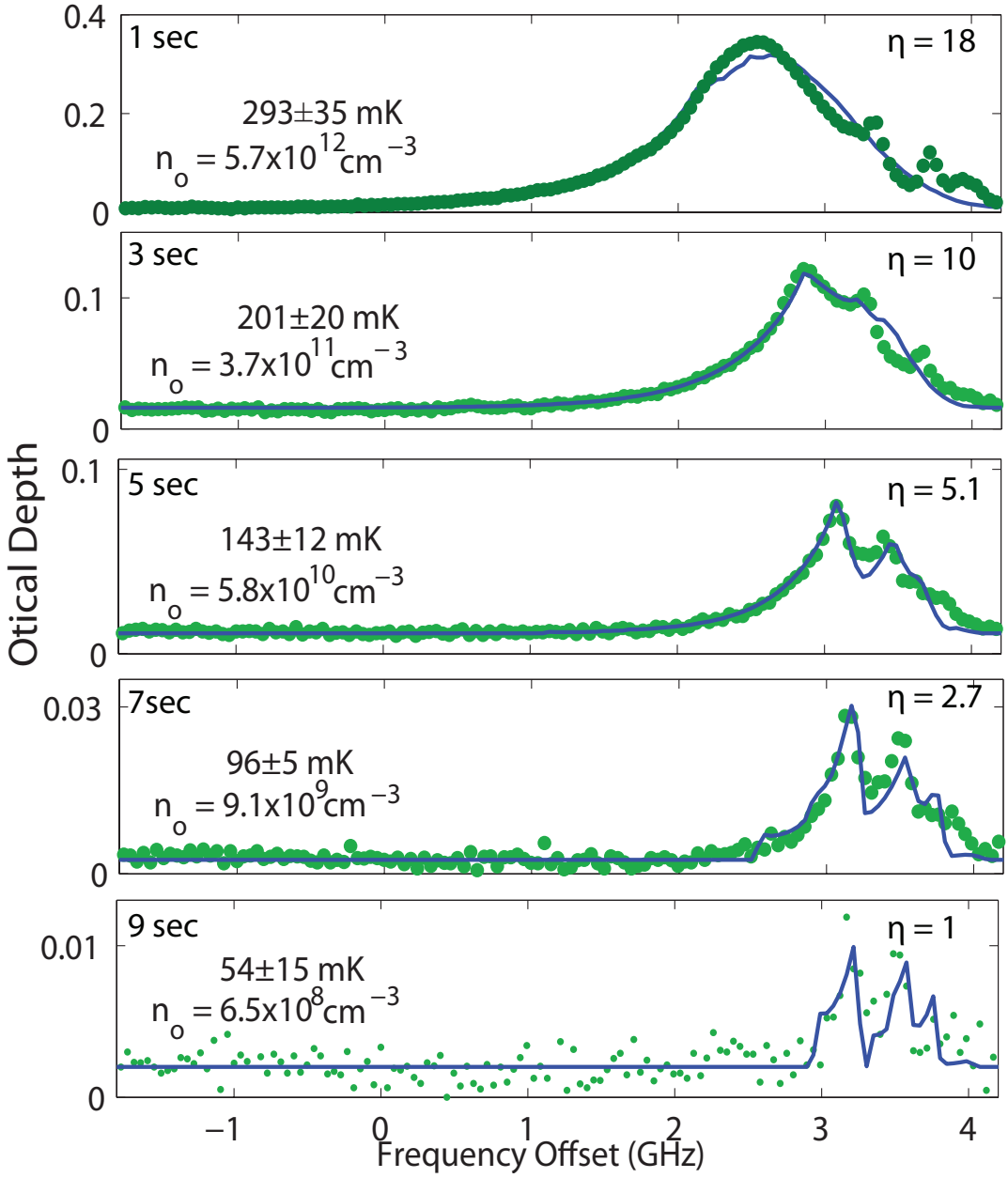

Figure 5-3: Evidence of cooling of dysprosium atoms from 300mK to 50mK.

ablation pulse. We assume the initial atom temperature of 320 mK just after the ablation pulse. The initial atom temperature and buffer gas temperature are assumed to be equal at this point. The buffer gas temperature will decrease exponentially with a 10 second time constant which mimics the behavior of the cell temperature measurement. The atom temperature is allowed to evolve according to the model. For these temperature ranges the cross sections are assumed to be temperature independent. However the collision rates will depend on thermal velocities and $\sqrt{T}$. The cross section for dysprosium-helium collisions, σ_{He}, is taken to be 1.4×10^{-14} cm^2 [17]. The inelastic Dy-Dy collision cross section is 1.6×10^{-15} cm^2, from Chapter 3. We find good agreement with the data for an initial n_{bg} of 2.4×10^{12} cm^{-3} and an elastic Dy-Dy collision cross section of 8×10^{-14} cm^2. The data and the model are shown in Figure 5-4. The model and data are in good agreement until very late times when η is smaller than 4, in accordance with the assumptions made in the modeling for high η. Uncertainties have not yet been estimated as this is only one set of data and is very preliminary.

The assumed Dy-Dy elastic collision cross section (8×10^{-14} cm^2) corresponds to a γ_{2b} of 50. However, it is only a single data point and the uncertainty can not yet be determined. However, by varying the model we find a systematic uncertainty of $\pm$ 50. Further experimentation is necessary check this measurement. If it is correct, evaporation of dysprosium atoms will be more difficult, but could be possible with the right experimental setup.

We can use the model to gain insight into what is happening as the trap is ramped down. Figure 5-5 shows the contributions to the atom losses and the cooling for collisions with the buffer gas, intra-atomic collisions, and adiabatic cooling. This shows that the heating due to interactions with the background gas is mostly canceled by cooling from evaporation. The actual temperature change of the atoms is due to adiabatic cooling. However, adiabatic cooling alone does not account for the atom number loss. In this model, buffer gas collision seem to be dominating the loss mechanisms. If this is true, reducing background gas density more, might help evaporative performance.

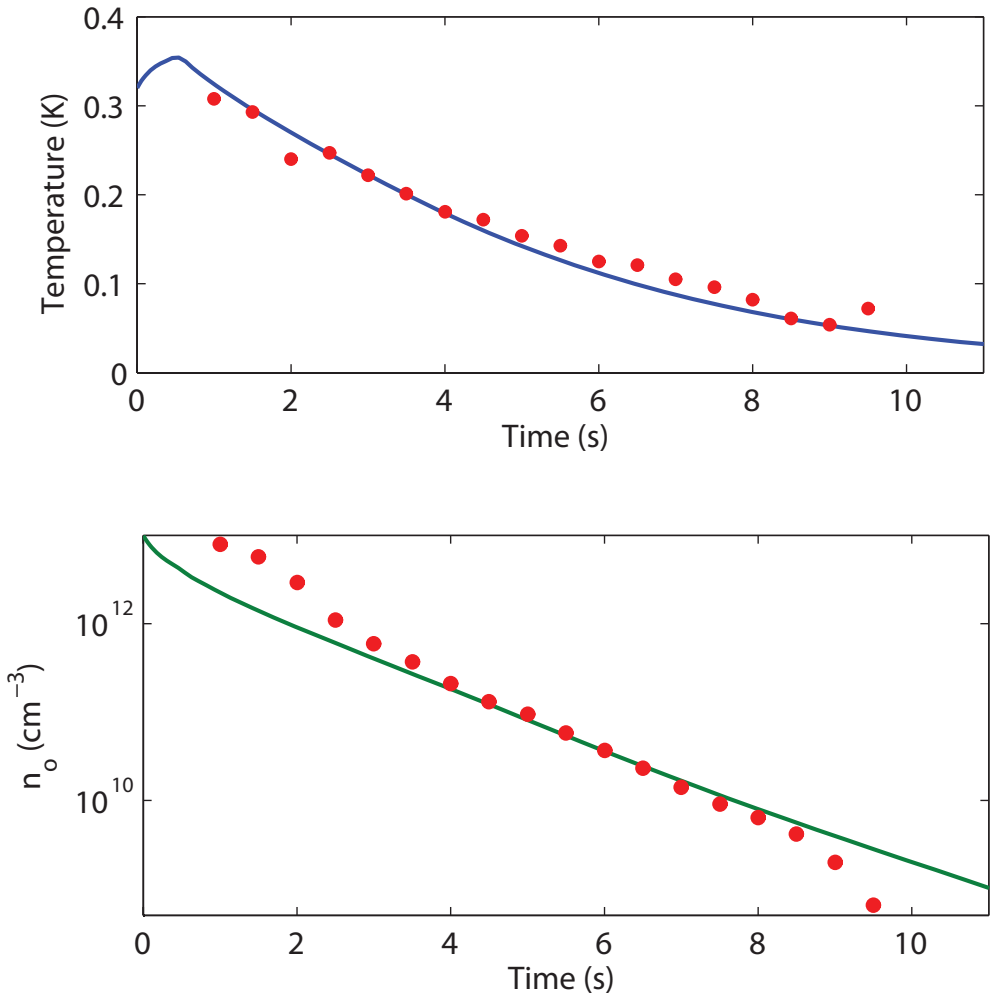

Figure 5-4: The evolution of temperature and peak density of the Dy atoms during the evaporation ramp. The solid line is the model fit for best agreement to the data with an initial buffer gas density of 2.4 $\times$ 10^{12} $cm^{-3}$and an Dy-Dy elastic collision cross section of 8 $\times$ 10^{-14} cm^2. Error bars have not been place on the figure as it is from only one datum and there is no statistical basis yet. Systematic uncertainties on the temperature and number data are estimated at $\pm 10\%$.

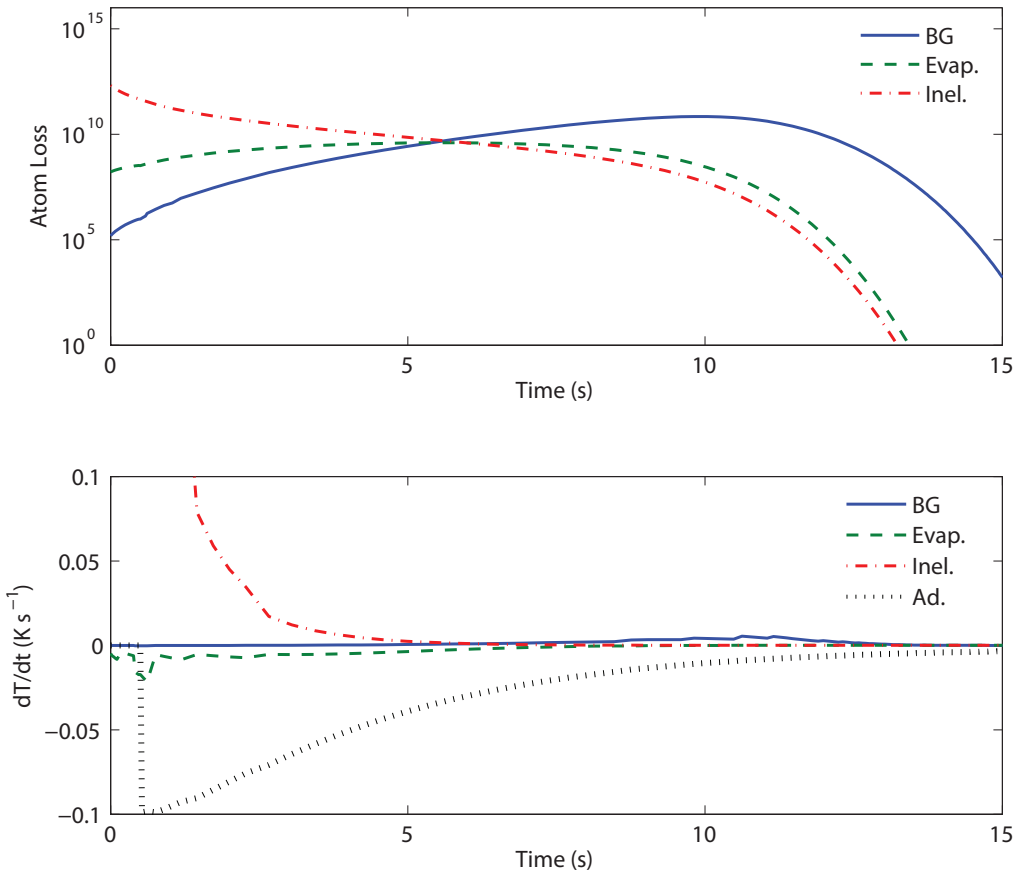

Figure 5-5: Contributions of different cooling and loss processes in the trap for a fast exponential ramp of both magnets. The curves are generated using the by the model using the results shown in Figure 5-4. The top plot shows the instantaneous atom loss rate due to collisions with the background gas (BG), elastic collisions with other atoms, (Evap.), and inelastic collisions with other atoms, (Inel.). The bottom plot shows the change in temperature due to different processes.

5.4 Prospects

The observed cooling of dysprosium atoms by lowering the trapping field is promising for further evaporative cooling of dysprosium atoms. If the model is correct, and the background gas is heating the atoms at the same rate as evaporation for most of this ramp, then further decreasing the background gas density by opening the valve could confirm this hypothesis.

A switch to ^{4}He as the buffer gas could also assist in lowering residual gas densities in the trap. To do this, the cell needs to be heated to about 600 mK for each load. The large magnetic dipole moment of the atoms should permit trapping at these higher temperatures. In the past, however, we have had problems getting large enough densities of ^{4}He in our cell for loading.

In addition, modifications are currently being made to allow for fast ramps onto a second power supply. This would enable us to control the end point of evaporation and stop it at various trap heights. Such experiments could result in an actual measurement of γ_{2b}.

Chapter 6

Conclusions and Prospects

We have isolated two rare earth atoms in a magnetic trap and measured the two-body collision rate coefficients. For dysprosium, $\mu = 9.94\mu_B$, we find, $g_{2b} = (1.8\pm0.2)\times 10^{-12}$ cm^{3}s^{-1}. For holmium, $\mu = 8.97\mu_B$, we find, $g_{2b} = (0.7\pm0.2)\times 10^{-12}$ cm^{3}s^{-1}. These measurements are consistent with dipolar relaxation as the dominant spin relaxation mechanism.

We have also demonstrated evaporative cooling of dysprosium atoms, from 300 mK to 50 mK, ending with 7×10^{10} atoms at the low temperature. Cooling efficiency is currently limited by collisions with background gas in the trapping region left by the ^{3}He buffer gas. We estimate the ratio of atom-atom elastic to inelastic collision rates, γ_{2b}, of 50, which may be sufficient for further evaporative cooling. Modifications of the apparatus are underway for better dynamic control of the magnetic trap depth to enhance evaporative cooling. In addition, better removal of the background gas will also be attempted.

This thesis also proposes an analytical model for predicting trap dynamics in the presence of finite background gas density. The model shows good agreement with the observations.

Further cooling of dysprosium could lead to the creation of a quantum degenerate gas of non-S state atoms, in which we may gain new insight into collisions and interactions of atoms with angular momentum. In addition, it could provide a guide for cooling molecules, with more complex electronic structure, to quantum degeneracy.

Cold samples of dysprosium and other large open shelled atoms could provide a new probe for making precision measurements of relativistic effects due to variations in the fine structure constant [37, 38, 40].

6.1 Future Directions

The experiments described in this thesis demonstrate the effectiveness of buffer gas loaded magnetic traps as a platform from which to begin evaporative cooling of multiple species. The results with holmium and dysprosium suggest that other atomic species which have been shown to have smaller inelastic collision rates because of suppressed anisotropies [18, 82] might be efficiently loaded and evaporatively cooled in a buffer gas cooling apparatus.

Historically, it has been the aim of the ultracold hydrogen group at MIT to do precision measurements using cold hydrogen. When the apparatus described in this thesis was originally designed it was intended to eventually be used to trap and possibly cool deuterium, which can not be trapped using the techniques used for trapping hydrogen [95]. We have demonstrated trapping of weakly magnetic species with $\mu = 1\mu_B$ [25]. Trapping these species requires buffer gas loading with ^{3}He . The demonstrated success of evaporative cooling in this thesis is the first in a ^{3}He buffer gas experiment and is an important step in extending these techniques to weakly trapped atoms.

Appendix A

Buffer Gas Removal

In order to achieve thermal isolation and be able to evaporatively cool a trapped atom sample, the buffer gas must be removed from the system. In order to load a magnetic trap in a cell 10 cm long, we need buffer gas densities on the order of $n_{bg} = 10^{16}$ cm^{-3}. However with buffer gas densities in this regime, the lifetime of the trapped atoms is essentially a diffusion problem with a small drift velocity toward the trap center. In order to do evaporative cooling, we need to remove as much buffer gas as possible from the trapping region.

There are two ways to reduce the buffer gas density in the cell. The first is to remove the bulk of the buffer gas through a valve. The second is to reduce the temperature of the cell walls so that the ^{3}He vapor pressure decreases. We attempt to use both of these methods in our experimental apparatus. Details of the experimental apparatus and achievable temperatures can be found in Chapter 1, and specifics of the fast cryogenic valve can be found in Brahms' thesis [25].

When the valve is opened not all of the buffer gas is removed from the cell. A film of helium is left on the cell walls. The vapor pressure of helium above this film determines the background gas density will be in the cell during evaporation. A paper by Huang *et al* , gives an numerical model of the ^{3}He vapor pressure at cold temperatures from empirical data [33]. This model predicts the vapor pressure to be significantly larger than the extrapolation of vapor pressure above the critical point use in previous buffer gas experiments [62, 91] (see Figure A-1). As we saw in chapters

3 and 4, the background gas can determine the success of evaporation. We will use the revised ^{3}He vapor pressure curve to predict background gas densities after the valve opens and as the cell cools after an ablation pulse.

A.1 Valve Conductance

The throughput, Q, of a valve can be defined as

$$Q = \dot{P} \cdot V = C \cdot P. \tag{A.1}$$

Here V is the volume of the chamber to be evacuated, P is the pressure inside the chamber, and C is the conductance of the valve. From Equation A.1, the pressure and the buffer gas density will decay with a time constant $\tau = V/C$. Assuming that the pressure in the chamber on the back of the valve is always low[1], Michniak [62] shows that the conductance of a valve, for ^{3}He, can be approximated by

$$C = 3.8 A_v \sqrt{T}. \tag{A.2}$$

This equation uses A_v in cm^2, T in Kelvin, and C in L s^{-1}. The lower chamber of our cell has a volume of $\sim$375 cm^3, and the valve time constant, τ_v, is approximately 14 ms for a cell temperature of 500 mK.

A.2 He Film

In addition to buffer gas leaving the cell, helium atoms are adsorbing and desorbing from the cell walls, changing background gas density at rates $\dot{n}_a$ and $\dot{n}_d$. The adsorption rate $\dot{n}_d$ is [62]

$$\dot{n_d} = P(d) \frac{A}{V} f \sqrt{\frac{1}{2\pi k_B T m}}. \tag{A.3}$$

[1]The chamber above the valve is lined with activated charcoal which acts as a pump in the upper chamber.

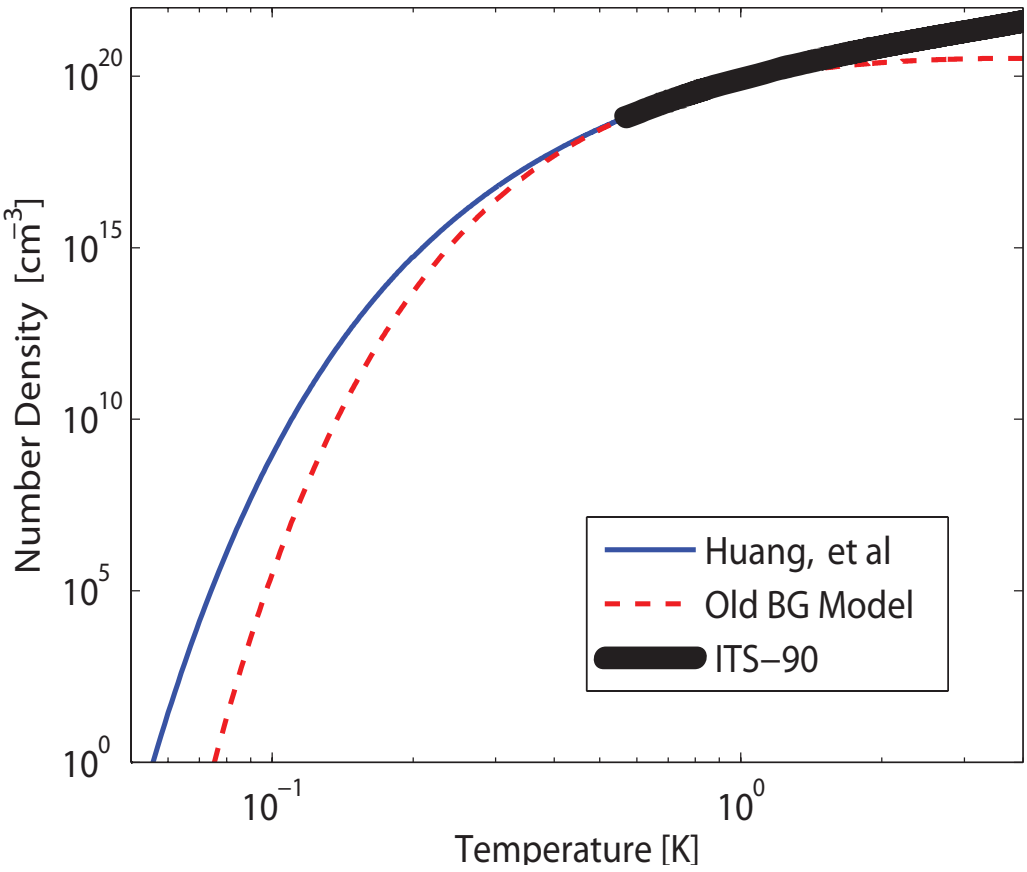

Figure A-1: Density as a function of temperature for ^{3}He below the critical point. The numerical model of empirical results developed in Huang *et al* [33] (solid lind) predicts that the vapor number density to be 100 times greater at 100 mK than the extrapolation used in previous buffer gas simulations [65] (dashed line). The new model is also in better agreement with the 1990 International Temperature Scale (shown by the thick solid line) for all temperature ranges. The ITS-90 is defined by the ^{3}He, ^{4}He vapor pressure relations for temperatures 0.65 K and 5 K [96]. For bulk ^{3}He, the cell temperature would need to be less than 120 mK to reach buffer gas densities less than $n_{bg} = 10^{11}$ cm^{-3}

Where A is the cell surface area, V is the cell volume, and f is the sticking probability ($\sim$0.75 for He on a solid surface) [97]. $P(d)$ is the pressure above the film as a function of thickness of the film. This is determined for thin films according to the classic equation [69]

$$P(d) = P_0 \exp\left(\frac{-\alpha}{Td^3}\right) \tag{A.4}$$

Here, d is the thickness of the film on the walls, P_0 is the vapor pressure of ^{3}He, α is the Van der Waals coefficient describing the strength of He-surface bond. For He on a G-10 surface, $\alpha = 1900$ K/Å[98]. Since the pressure scales as $e^{d^{-3}}$, the closer layers are bound much more tightly than the top layers. This leads to continuous desorption of background gas from the cell walls.

In equilibrium, $\dot{n}_d$ is equal to $\dot{n}_a$. However, because the valve is open, the helium will continue to be pumped out of the system at a rate $\dot{n}_v = n_{He}/\tau_v$ as described in the last section. We can write the adsorption equation as a function of the current buffer gas density in the cell.

$$\dot{n}_a = n_{He} k_B T \frac{A}{V} f \sqrt{\frac{1}{2\pi k_B T m}}. \tag{A.5}$$

Combining Equations A.3 - A.5 gives Equation A.6 for the time evolution of the buffer gas density as a function of temperature and film thickness.

$$\dot{n}_{He}(T,d) = \frac{-n_{He}}{\tau_v} + \frac{A}{V} f \sqrt{\frac{1}{2\pi m}} \left(P_0 \exp(\frac{-\alpha}{Td^3}) - k_B T n_{He}\right) \tag{A.6}$$

The film thickness varies as a result of the balance of adsorption and desorption from the cell walls.

$$\dot{d} = \frac{d_l}{N_l}\dot{N} = \frac{d_l}{N_l} V(\dot{n}_a - \dot{n}_d) \tag{A.7}$$

Here d_l is the thickness per layer and N_l is the number of atoms per layer. We can estimate the initial thickness of atoms in the film by finding d from Equation A.4. At 500 mK and initial buffer gas density of 10^{16} cc^{-}1, there is a film about 9 Å thick.

During the loading process, we heat the cell both with a heater and the ablation pulse to temperatures as high as 700mK. We can vary this peak temperature to achieve the most effective buffer gas removal. For our purposes I will assume an exponential decay of the temperature from some peak temperature with a time constant of about 20 seconds.

We can solve for this system of differential equations to find the buffer gas density, background pressure, and layer thickness as a function of time and temperature.

To first order, the goal is to reduce the buffer gas density in the shortest period of time. As can be seen in Figure A-2, we can decrease our buffer gas density faster by starting the pump out (i.e. opening the valve) at a higher temperature. However, while the buffer gas density decreases faster, the cell temperature will be higher. In effect, this will make the atoms equilibrate to a higher temperature and decrease the trap depth.

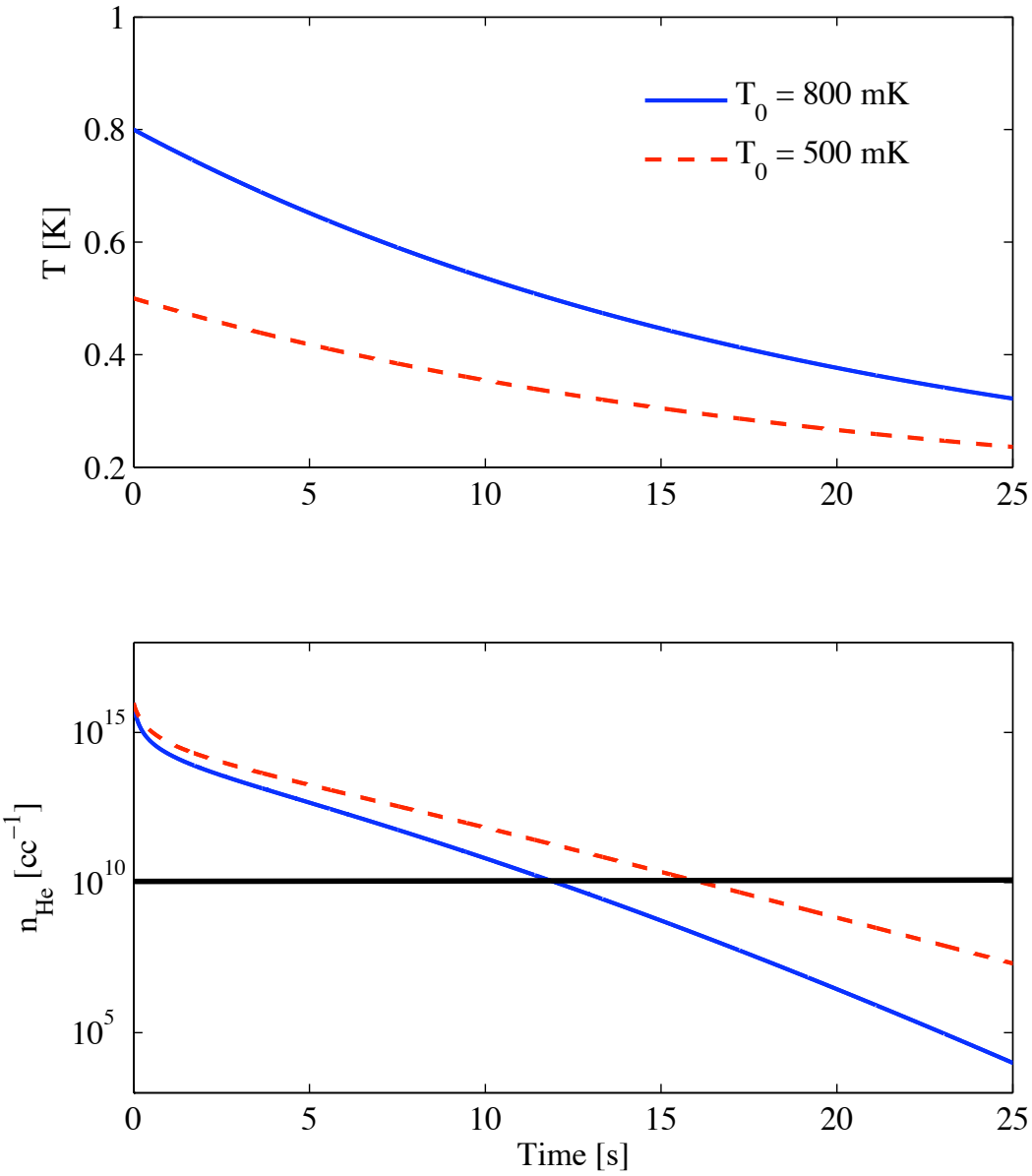

Figure A-2: Buffer gas density as a function of time after the valve is opened while the cell cools to base temperature of 150 mK. The initial buffer gas density is 10^{16} cm^{-3}. The solid blue line describes the trajectory starting where the cell starts at temperature 500 mK while the dashed red line starts at 800 mK. The removal of buffer gas is more efficient starting from a higher temperature.

Appendix B

Bucking Coil Design

In order to lower the magnetic field quickly without overly heating the cell and refrigerator, a number of modifications needed to be made to the apparatus. The rapidly changing magnetic flux through metal surfaces will cause eddy current heating. While not in the maximum of the magnetic field, the mixing chamber, cold plate, and heat link as well as the top of the cell all have significant surface area perpendicular to the magnetic field lines. Figure B-1 shows the magnitude of the field along the axis of the magnet at the distance of the mixing chamber, located around 38-40 cm above the trap minimum.

B.1 Design

We designed a bucking coil which bolts securely to the top of the larger magnet cask to cancel the magnetic field at critical points in the apparatus. This coil is run in series with the top coil but with the current in the opposite direction.

Biot-Savart simulations show that the bucking coil reduces the field near the mixing chamber to about 4 gauss as seen in Figure B-1 with both coils running 100A. In practice we see very little measurable heating of the mixing chamber when ramping both coil currents together at a fast rate.

However, when lowering the trap toward the window, the changing current in the lower coil does not change the current in the top and bucking coil. This results in

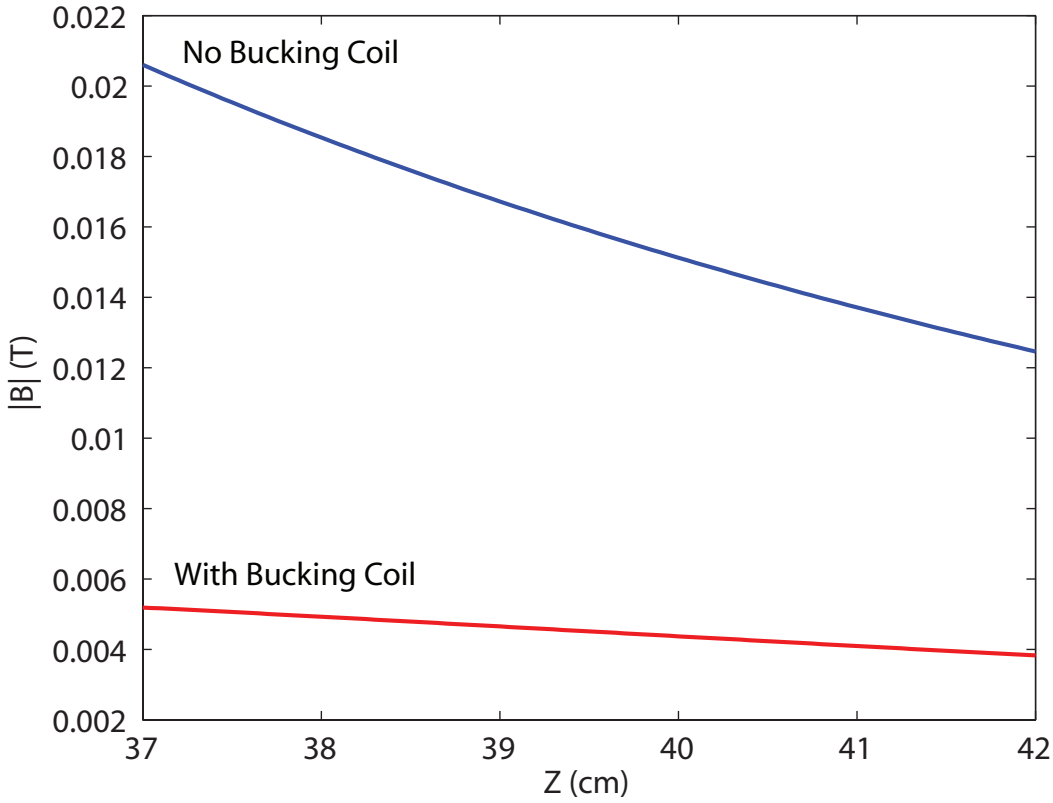

Figure B-1: Simulation of the magnetic field along the axis at the distance of the mixing chamber with and without the bucking coil. The magnitude field corresponds to 100 A in all three coils, but scales linearly with the current. When everything is aligned, the mixing chamber is about 38 cm above the magnetic field minimum.

a larger field at the mixing chamber and can cause more heating, which can in turn cause more buffer gas to be desorbed from the walls and destroy weakly trapped atom samples.

B.2 Construction

The bucking coil is wound onto a titanium form. A 5 mil thick piece of kapton tape was wrapped around the inner diameter of the form to insulate the wire from the form. A 5 mil thin piece of G-10 was inserted along the walls of the form on both sides to further protect the wire. Using a slow slow lathe turning at less than 1 rpm, a continuous strand of 0.7 mil diameter magnet wire was wrapped around the form. There are 23 layers with 28 turns per layer for a total of 644 turns. Each layer is separated by a thin layer of fiberglass coated with Stycast 1266 Epoxy. In addition, the wire was coated with epoxy as it was turned onto the form.

After wrapping, the wire was kept under tension and the epoxy was allowed to set overnight. The leads are protected with tubing and then soldered to lugs that screw into the and vapor cooled magnet leads.

Bibliography

[1] Alan L. Migdall, John V. Prodan, William D. Phillips, Thomas H. Bergeman, and Harold J. Metcalf. First observation of magnetically trapped neutral atoms. *Phys. Rev. Lett.*, 54(24):2596–2599, Jun 1985.

[2] M. H. Anderson, J. R. Ensher, M. R. Matthews, C. E. Wieman, and E. A. Cornell. Observation of Bose-Einstein Condensation in a Dilute Atomic Vapor. *Science*, 269(5221):198–201, 1995.

[3] K. B. Davis, M. O. Mewes, M. R. Andrews, N. J. van Druten, D. S. Durfee, D. M. Kurn, and W. Ketterle. Bose-einstein condensation in a gas of sodium atoms. *Phys. Rev. Lett.*, 75(22):3969–3973, Nov 1995.

[4] C. C. Bradley, C. A. Sackett, J. J. Tollett, and R. G. Hulet. Evidence of bose-einstein condensation in an atomic gas with attractive interactions. *Phys. Rev. Lett.*, 75(9):1687–1690, Aug 1995.

[5] Dale G. Fried, Thomas C. Killian, Lorenz Willmann, David Landhuis, Stephen C. Moss, Daniel Kleppner, and Thomas J. Greytak. Bose-einstein condensation of atomic hydrogen. *Phys. Rev. Lett.*, 81(18):3811–3814, Nov 1998.

[6] B. DeMarco and D. S. Jin. Onset of Fermi Degeneracy in a Trapped Atomic Gas. *Science*, 285(5434):1703–1706, 1999.

[7] R. Onofrio, C. Raman, J. M. Vogels, J. R. Abo-Shaeer, A. P. Chikkatur, and W. Ketterle. Observation of superfluid flow in a bose-einstein condensed gas. *Phys. Rev. Lett.*, 85(11):2228–2231, Sep 2000.

[8] S. Jochim, M. Bartenstein, A. Altmeyer, G. Hendl, S. Riedl, C. Chin, J. Hecker Denschlag, and R. Grimm. Bose-Einstein Condensation of Molecules. *Science*, 302(5653):2101–2103, 2003.

[9] M. W. Zwierlein, C. A. Stan, C. H. Schunck, S. M. F. Raupach, S. Gupta, Z. Hadzibabic, and W. Ketterle. Observation of bose-einstein condensation of molecules. *Phys. Rev. Lett.*, 91(25):250401, Dec 2003.

[10] M. Greiner, O. Mandel, T. Esslinger, T.W. Hansch, and I. Bloch. Quantum phase transition from a superfluid to a mott insulator in a gas of ultracold atoms. *Nature*, 415:39, 2002.

[11] D. Jaksch, C. Bruder, J. I. Cirac, C. W. Gardiner, and P. Zoller. Cold bosonic atoms in optical lattices. *Phys. Rev. Lett.*, 81(15):3108–3111, Oct 1998.

[12] David E. Pritchard. Cooling neutral atoms in a magnetic trap for precision spectroscopy. *Phys. Rev. Lett.*, 51(15):1336–1339, Oct 1983.

[13] Kendra Margaret Denny Vant. *Spectroscopy of ultracold metastable hydrogen: in pursuit of a precision measurement.* PhD thesis, Massachusetts Institute of Technology, 2005.

[14] R. deCarvalho, J.M. Doyle, B. Friedrich, T. Guillet, J. Kim, D. Patterson, and J.D. Weinstein. Buffer-gas loaded magnetic traps for atoms and molecules: A primer. *Eur. Phys. Jour. D*, 7(3):289–309, Oct 1999.

[15] John M. Doyle, Bretislav Friedrich, Jinha Kim, and David Patterson. Buffer-gas loading of atoms and molecules into a magnetic trap. *Phys. Rev. A*, 52(4):R2515–R2518, Oct 1995.

[16] R. deCarvalho, N. Brahms, B. Newman, J.M. Doyle, D. Kleppner, and T. Greytak. A new path to ultracold atomic hydrogen. *Can. Jour. of Phys.*, 83:293, 2005.

[17] Cindy I. Hancox, S. Charles Doret, Matthew Hummon, Linjiao T.Luo, and John M. Doyle. Magnetic trapping of rare-earth atoms at millikelvin temperatures. *Nature*, 431(7006):281, Sept 2004.

[18] Cindy I. Hancox, S. Charles Doret, Matthew T. Hummon, Roman V. Krems, and John M. Doyle. Suppression of angular momentum transfer in cold collisions of transition metal atoms in ground states with nonzero orbital angular momentum. *Physical Review Letters*, 94(1):013201, 2005.

[19] Wesley C. Campbell, Edem Tsikata, Hsin-I Lu, Laurens D. van Buuren, and John M. Doyle. Magnetic trapping and zeeman relaxation of NH ($x^3\sigma^1$). *Physical Review Letters*, 98(21):213001, 2007.

[20] Jonathan D. Weinstein, Robert deCarvalho, Cindy I. Hancox, and John M. Doyle. Evaporative cooling of atomic chromium. *Phys. Rev. A*, 65(2):021604, Jan 2002.

[21] J.D. Weinstein, R. deCarvalho, T. Guillet, B. Freidrich, and J.M. Doyle. Magnetic trapping of calcium monohydride molecules at millikelvin temperatures. *Nature*, 395:148, 1998.

[22] Jinha Kim, Bretislav Friedrich, Daniel P. Katz, David Patterson, Jonathan D. Weinstein, Robert DeCarvalho, and John M. Doyle. Buffer-gas loading and magnetic trapping of atomic europium. *Phys. Rev. Lett.*, 78(19):3665–3668, May 1997.

[23] Cindy I. Hancox, Matthew T. Hummon, Scott V. Nguyen, and John M. Doyle. Evaporative cooling of magnetically trapped atomic molybdenum. *Physical Review A (Atomic, Molecular, and Optical Physics)*, 71(3):031402, 2005.

[24] Nathan Brahms, Bonna Newman, Cort Johnson, Tom Greytak, Daniel Kleppner, and John Doyle. Magnetic trapping of silver and copper, and anomalous spin relaxation in the Ag-He system. *Physics Review Letters*, accepted for publication, 2008.

[25] Nathaniel C. Brahms. *Trapping of 1 μ_B atoms using buffer gas loading.* PhD thesis, Harvard University, 2008.

[26] M Baranov, L Dobrek, K Góral, L Santos, and M Lewenstein. Ultracold dipolar gases – a challenge for experiments and theory. *Physica Scripta*, T102:74–81, 2002.

[27] L. Santos, G. V. Shlyapnikov, P. Zoller, and M. Lewenstein. Bose-einstein condensation in trapped dipolar gases. *Phys. Rev. Lett.*, 85(9):1791–1794, Aug 2000.

[28] R.V. Krems, G.C. Groenenboom, and A. Dalgarno. Electronic interaction anisotropy between atoms in arbitrary angular momentum states. *Journal of Physical Chemistry A*, 108(41):8941–8948, 2004.

[29] J.G.E. Harris, W.C. Campbell, D. Ergov, S.E. Maxwell, R.A. Michniak, S.V. Nguyen, L.D. van Buuren, and J.M. Doyle. Deep superconducting magnetic traps for neutral atoms and moelcules. *Rev. of Sci. Inst.*, 75:17, 2004.

[30] Harold J. Metcalf and Peter van der Straten. *Laser Cooling and Trapping.* Springer, Inc., 1999.

[31] John Doyle. Private correspondance.

[32] F. Pobell. *Matter and Methods at Low Temperatures.* Springer, 2nd edition edition, 1996.

[33] Y. H. Huang and G. B. Chen. A practical vapor pressure equation for helium-3 from 0.01k to the critical point. *Cryogenics*, 46(12):833, Dec 2006.

[34] R.V. Krems and A.A. Buchachenko. Electronic interaction anisotropy between open-shell lanthanide atoms and helium from cold collision experiment. *Journal of Chemical Physics*, 123:101101, 2005.

[35] Harald F. Hess. Evaporative cooling of magnetically trapped and compressed spin-polarized hydrogen. *Phys. Rev. B*, 34(5):3476–3479, Sep 1986.

[36] R. V. Krems and A. Dalgarno. Disalignment transitions in cold collisions of $3p$ atoms with structureless targets in a magnetic field. *Phys. Rev. A*, 68(1):013406, Jul 2003.

[37] A. T. Nguyen, D. Budker, S. K. Lamoreaux, and J. R. Torgerson. Towards a sensitive search for variation of the fine-structure constant using radio-frequency $e1$ transitions in atomic dysprosium. *Phys. Rev. A*, 69(2):022105, Feb 2004.

[38] A. Cingoz, A. Lapierre, A.-T. Nguyen, N. Leefer, D. Budker, S. K. Lamoreaux, and J. R. Torgerson. Limit on the temporal variation of the fine-structure constant using atomic dysprosium. *Physical Review Letters*, 98(4):040801, 2007.

[39] V. A. Dzuba and V. V. Flambaum. Fine-structure anomalies and search for variation of the fine-structure constant in laboratory experiments. *Physical Review A (Atomic, Molecular, and Optical Physics)*, 72(5):052514, 2005.

[40] V. A. Dzuba and V. V. Flambaum. Relativistic corrections to transition frequencies of Ag I, Dy I, Ho I, Yb II, Yb III, Au I, and Hg II and search for variation of the fine-structure constant. *Physical Review A (Atomic, Molecular, and Optical Physics)*, 77(1):012515, 2008.

[41] Viatcheslav Kokoouline, Robin Santra, and Chris H. Greene. Multichannel cold collisions between metastable sr atoms. *Phys. Rev. Lett.*, 90(25):253201, Jun 2003.

[42] S. B. Nagel, C. E. Simien, S. Laha, P. Gupta, V. S. Ashoka, and T. C. Killian. Magnetic trapping of metastable $3p2$ atomic strontium. *Phys. Rev. A*, 67(1):011401, Jan 2003.

[43] N. Poli, R. E. Drullinger, G. Ferrari, J. Leonard, F. Sorrentino, and G. M. Tino. Cooling and trapping of ultracold strontium isotopic mixtures. *Physical Review A (Atomic, Molecular, and Optical Physics)*, 71(6):061403, 2005.

[44] Scott V. Nguyen, S. Charles Doret, Colin B. Connolly, Robert A. Michniak, Wolfgang Ketterle, and John M. Doyle. Evaporative cooling of metastable helium in the multi-partial-wave regime. *Physical Review A (Atomic, Molecular, and Optical Physics)*, 72(6):060703, 2005.

[45] Yu. Ralchenko, R.E. Kramida, J Reader, and NIST ASD Team. NIST atomic spectrum database. Online, July 2008. available at http://physics.nist.gov/asd3.

[46] Robert deCarvalho and John Doyle. Evaporative cooling at low trap depth. *Phys. Rev. A*, 70(5):053409, Nov 2004.

[47] Wolfgang Ketterle and N. J. Van Druten. Evaporative cooling of trapped atoms. *Advances in Atomic, Molecular, and Optical Physics*, 37:181–236, 1996.

[48] Cort N. Johnson. *Zeeman Relaxation of Cold Iron and Nickel in Collisions with ^3He.* PhD thesis, Massachusetts Institute of Technology, 2008.

[49] Oxford Instruments, 300 Baker Avenue, Suite 150, Concord, MA 01742, http://www.oxford-instruments.com.

[50] American Magnetics, Inc., Oak Ridge, TN 37830, http://www.americanmagnetics.com.

[51] Cirrus Software Inc., 4794 Fernglen Dr., Burnaby BC, Canada V5G 3V7.

[52] Southern Spring Mfg., Inc., 915 Pinemont, Houston, TX 77018, http://www.southernspring.net/.

[53] Janis Research Co., 2 Jewel Drive, Wilmington, MA 01887, http://www.janis.com.

[54] Stanford Research Systems, 1290-D Reamwood Ave., Sunnyvale, CA 94089, http://www.thinksrs.com/.

[55] K. B. Blagoev and V. A. Komarovskii. Lifetimes of levels of neutral and singly ionized lanthanide atoms. *Atomic Data and Nuclear Data Tables*, 56:1–40, 1994.

[56] G. Nave. Atomic transition rates for neutral holmium (HoI). *J. Opt. Soc. Am. B*, 20:2193–2202, 2003.

[57] E.A. Den Hartog, L.M. Wiese, and J.E. Lawler. Radiative lifetimes of HoI and HoII. *J. Opt. Soc. Am. B*, 16:2278–2284, 1999.

[58] Coherent, Inc., 5100 Patrick Henry Drive, Santa Clara, CA 95054, http://www.coherent.com.

[59] Hamamatsu Corp., 360 Foothill Rd, Bridgewater, NJ 08807, http://sales.hamamatsu.com.

[60] National Instruments, Inc., 11500 N. Mopak Expwy., Austin, TX 78759, http://www.ni.com/.

[61] 3150 Central Expressway, Santa Clara, CA 95051, http://www.continuumlasers.com.

[62] Robert Michniak. *Enhanced Buffer Gas Loading: Cooling and Trapping of Atoms with Low Effective Magnetic Moments*. PhD thesis, Harvard University, 2004.

[63] Cryomagnetics, Inc., http://www.cryomagnetics.com/.

[64] Lakeshore, Inc., 575 McCorkle Blvd, Westerville, OH 43082, http://www.lakeshore.com.

[65] Robert deCarvalho. *Inealstic Scattering of Magnetically Trapped Atomic Chromium*. PhD thesis, Harvard University, 2003.

[66] J.B. Hasted. *Physics of Atomic Collisions*. American Elsevier, 2 edition, 1972.

[67] Claude Cohen-Tannoudji, Bernard Diu, and Franck Laloë. *Quantum Mechanics*, volume 2. John Wiley and Sons, 1977.

[68] D.J. Griffiths. *Introduction to Quantum Mechanics*. Prentice Hall, 1995.

[69] A. Roth. *Vacuum Technologies*. Elsevier Science, Third, updated and enlarged edition. edition, 1990.

[70] Thad Walker and Paul Feng. *Advances in Atomic, Molecular, and Optical Physics*, chapter Measurements of Collisions between Laser-Cooled Atoms, pages 125–170. Academic Press, 1994.

[71] B.J. Verhaar. *Atomic Physics*, volume 14, chapter Cold Collision Phenomena, pages 351–367. American Inst. of Physics, 1995.

[72] M. J. Jamieson, A. Dalgarno, and M. Kimura. Scattering lengths and effective ranges for He-He and spin-polarized H-H and D-D scattering. *Phys. Rev. A*, 51(3):2626–2629, Mar 1995.

[73] E. R. I. Abraham, W. I. McAlexander, C. A. Sackett, and Randall G. Hulet. Spectroscopic determination of the s-wave scattering length of lithium. *Phys. Rev. Lett.*, 74(8):1315–1318, Feb 1995.

[74] Kendall B. Davis, Marc-Oliver Mewes, Michael A. Joffe, Michael R. Andrews, and Wolfgang Ketterle. Evaporative cooling of sodium atoms. *Phys. Rev. Lett.*, 74(26):5202–5205, Jun 1995.

[75] John L. Bohn, James P. Burke, Chris H. Greene, H. Wang, P. L. Gould, and W. C. Stwalley. Collisional properties of ultracold potassium: Consequences for degenerate bose and fermi gases. *Phys. Rev. A*, 59(5):3660–3664, May 1999.

[76] N. R. Newbury, C. J. Myatt, and C. E. Wieman. s-wave elastic collisions between cold ground-state $rb87$ atoms. *Phys. Rev. A*, 51(4):R2680–R2683, Apr 1995.

[77] A. J. Moerdijk, H. M. J. M. Boesten, and B. J. Verhaar. Decay of trapped ultracold alkali atoms by recombination. *Phys. Rev. A*, 53(2):916–920, Feb 1996.

[78] H. T. C. Stoof, J. M. V. A. Koelman, and B. J. Verhaar. Spin-exchange and dipole relaxation rates in atomic hydrogen: Rigorous and simplified calculations. *Phys. Rev. B*, 38(7):4688–4697, Sep 1988.

[79] Jonathan Weinstein. *Magnetic Trapping of Atomic Chromium and Molecular Calcium Monohydride*. PhD thesis, Harvard University, 2001.

[80] Dimitry Budker, Derek F. Kimball, and David DeMille. *Atomic Physics: an exploration through problems and solutions*. Oxford University Press, 2004.

[81] P. O. Fedichev, M. W. Reynolds, U. M. Rahmanov, and G. V. Shlyapnikov. Inelastic decay processes in a gas of spin-polarized triplet helium. *Phys. Rev. A*, 53(3):1447–1453, Mar 1996.

[82] R. V. Krems, J. Kłos, M. F. Rode, M. M. Szcześniak, G. Chałasiński, and A. Dalgarno. Suppression of angular forces in collisions of non-s-state transition metal atoms. *Physical Review Letters*, 94(1):013202, 2005.

[83] Roman Krems. Private communications.

[84] Toptica Photonics, 1286 Blossom Drive, Victor, NY 14564, http://www.toptica.com/.

[85] Charlotte E. Moore. *Atomic Energy Levels As Derived From the Analyses of Optical Spectra*, volume 2 of *NSRDS-NBS*. National Bureau of Standards, 35 edition, 1971.

[86] Cindy Hancox. *Magnetic Trapping of transition-metals and rare-earth atoms using buffer-gas loading*. PhD thesis, Harvard University, 2005.

[87] Naoto Masuhara, John M. Doyle, Jon C. Sandberg, Daniel Kleppner, Thomas J. Greytak, Harald F. Hess, and Greg P. Kochanski. Evaporative cooling of spin-polarized atomic hydrogen. *Phys. Rev. Lett.*, 61(8):935–938, Aug 1988.

[88] H.F. Hess, G.P. Kochanski, J.M. Doyle, N. Masuhara, T.J. Greytak, and D. Kleppner. Magnetic trapping of spin-polarized atomic hydrogen. In *Proc. 18th Conf. on Low Temp. Physics, Kyoto*, volume 26. Japanese Journal of Applied Physics, 1987. Supplement 26-3.

[89] Ad Lagendijk, Isaac F. Silvera, and Boudewijn J. Verhaar. Spin exchange and dipolar relaxation rates in atomic hydrogen: Lifetimes in magnetic traps. *Phys. Rev. B*, 33(1):626–628, Jan 1986.

[90] J.M. Doyle, J.C. Sandberg, I.A. Yu, C.L. Cesar, D. Kleppner, and T.J. Greytak. Evaporative cooling of atomic hydrogen: Theory of cooling and progress towards the bose-einstein transition. *Physica B*, 13:194–196, 1994.

[91] Scott Nguyen. *Buffer Gas Loading and Evaporative Cooling in the multi-partial-wave regime*. PhD thesis, Harvard University, 2006.

[92] Jinha Kim. *Buffer-Gas Loading and Magnetic Trapping of Atomic Europium*. PhD thesis, Harvard University, 1997.

[93] Wolfgang Petrich, Michael H. Anderson, Jason R. Ensher, and Eric A. Cornell. Stable, tightly confining magnetic trap for evaporative cooling of neutral atoms. *Phys. Rev. Lett.*, 74(17):3352–3355, Apr 1995.

[94] The MathWorks, Inc., 3 Apple Hill Drive, Natick, MA 01760, http://www.mathworks.com.

[95] Julia Steinberger. *Progress Towards High Precision Measurements on Ultracold Metastable Hydrogen and Trapping Deuterium*. PhD thesis, mite, 2004.

[96] H Preston-Thomas. The international temperature scale of 1990 (ITS-90). *Metrologia*, 27(1):3–10, 1990.

[97] M. Sivani, M.W. Cole, and D.L. Goodstein. Sticking probability of ^{4}He on solid surfaces at low temperature. *Physical Review Letters*, 51:188–192, 1983.

[98] G. Vidali, G. Ihm, H-Y. Kim, and M.W. Cole. Potentials of physical adsorption. Technical report, Surface Science Reports, 1991.